Charles University

Faculty of Science

Study programme: Animal Physiology

Mgr. Zuzana Čočková

The role of RNA demethylase FTO in differentiation, regulation of energy metabolism and sensitivity to streptozotocin of neuronal and glial cell models

Funkce RNA demetylázy FTO v diferenciaci, regulaci energetického metabolismu a citlivosti k streprozotocinu modelových neuronálních a gliových buněk

Doctoral thesis

Supervisor: doc. RNDr. Jiří Novotný, DSc.

Prague, 2022

Declaration

I hereby declare that this PhD dissertation is entirely my own original work, and that neither the whole thesis nor any part of it has been submitted anywhere else in order to obtain any academic degree. I have clearly stated the extent of my contribution to the research presented in the thesis. All publications and other information sources used in this thesis have been duly referenced.

Prague, 3.1. 2022 ……..

Zuzana Čočková

Acknowledgment

First of all, I would like to express my deep gratitude to my supervisor, doc. RNDr. Jiří Novotný, DSc., for his guidance, continuous support and assitance throughout my research journey. I am also grateful to my consultant, Mgr. Petr Telenský, Ph.D., for his insights and stimulating discussions that have been of great importance in the development of this thesis. His enthusiasm and encouragement has been a source of great motivation and inspiration.

I was fortunate to have a wonderful team of colleagues who were always willing to help and provided me with friendly work environment. Althought I do not wish them to struggle, it was comforting not to struggle alone. A special thank you goes to Eva Filipovska from the lab next door for not only being a great colleague, but also a great friend.

Furthermore, I am thankful to Mgr. Olga Horáková, Ph.D., RNDr. Alena Pecinová, Ph.D., RNDr. Tomáš Mráček, Ph.D., doc. RNDr. Martin Kalous, CSc., and RNDr. Jitka Žurmanová, Ph.D. for their advice and granting me access to their machines that enriched my life with mitochondria.

Last but not least, I would like to thank my family and friends for their unconditional support and encouragement.

List of publications related to this thesis

Statement about the extent of participation

1. **Cockova Z**, Ujcikova H, Telensky P, Novotny J. (2019) Protein profiling of SH-SY5Y neuroblastoma cells: The effect of rhein. J Biosci. 44(4):88 IF 1.823

   My contribution: I performed differentiation and assessed the neurite outgrowth. I also conducted the enzymatic assays and ran Western blotting procedures. In addition, I prepared samples for 2D electrophoresis and drafted the manuscript.

2. **Cockova Z**, Honc O, Telensky P, Olsen MJ, Novotny J. (2021) Streptozotocin-Induced Astrocyte Mitochondrial Dysfunction Is Ameliorated by FTO Inhibitor MO-I-500. ACS Chem Neurosci. 12(20):3818-3828 IF 4.418

   My contribution: I did sample preparations, carried out RNA silencing, RNA isolation, viability and cytotoxicity tests, respirometry, Western blotting assays, and determined the levels of ATP, ROS, and m6A. I performed flow cytometry experiments with assistance of Ondřej Honc. I also did the data analysis and manuscript writing.

I confirm, on behalf of all co-authors, that the above stated information about contribution of Zuzana Čočková to all articles is correct.

Doc. RNDr. Jiří Novotný, DSc.

Abstract

Fat mass and obesity associated (FTO) demethylase is responsible for erasure of the most abundant epitranscriptomic mark in eukaryotic mRNA, the N6-methyladenosine (m6A) residue. Together with other m6A erasers, writers (methyltransferases) and readers it forms an m6A regulatory pathway that controls the amount, location and biological effect of m6A. The dynamic regulation of the brain's m6A methylome during neurodevelopment is essential for maintaining cerebral functions. In addition, preclinical research suggests that the m6A regulatory pathway regulates energy balance in a tissue- and cell type-specific manner. The *FTO* gene has been associated with lifelong risks of obesity and metabolic syndrome as well as regulation of total body energy intake and expenditure. However, little is understood about the function of the m6A pathway in control of brain energy metabolism. That is of interest in pursuit of understanding Alzheimer's disease, as this illness is characterized by profound disruptions in cerebral energy metabolism and mounting evidence suggests that disrupted brain bioenergetics may play a role in the disease's early genesis, before the appearance of clinical symptoms.

In the present thesis we aimed to investigate the role of FTO in models of two brain cell types, neurons and astrocytes. Using neuronal SH-SY5Y cells, we wanted to find out whether FTO plays a role in the differentiation process of neurons. Furthermore, we examined both astrocytic CCF-STTG1 cells and SH-SY5Y in order to investigate if and how FTO affects bioenergetics and expression profile of proteins essential for proper function of these cells. Finally, with more focus on CCF-STTG1 cells, we studied the function of FTO in resilience of cells towards streptozotocin, an *in vitro* model of Alzheimer's disease pathogenesis.

Here, we demonstrate that FTO inhibition can impair normal differentiation of SH-SY5Y cells. Inhibition of FTO during the differentiation process results in insufficient morphological changes of cells as well as altered expression profile of neuronal markers. Further we show that FTO inhibition alters proteomes of SH-SY5Y and CCF-STTG1 cells. Proteins affecting the function of mitochondria were detected among differentially regulated proteins. We discovered that FTO inhibition affects the mitochondrial respiration and causes diverse effects in neurons and astrocytes. Additionally, we demonstrate that the FTO inhibition induces stimulation of mitochondrial biogenesis in astrocytes as evidenced by elevated mitochondrial mass in cells and increased levels of peroxisome proliferator-activated receptor gamma coactivator 1-alpha (PGC-1α) and intracellular ATP content. Last but not least, we found that astrocytes treated with streptozotocin overexpress FTO. The FTO inhibitor treatment of astrocytes improved cell viability, and decreased oxidative stress, apoptosis, reactivity, and mitochondrial aberrations induced by streptozotocin.

Abstrakt

Demetyláza FTO (z angl. Fat mass and obesity associated) je zodpovědná za odstraňování nejrozšířenější epitranskriptomické modifikace v eukaryotické mRNA, N6-methyladenosinu (m6A). FTO spolu s dalšími demetylázami, metyltransferázami a m6A-čtecími proteiny tvoří regulační dráhu, která řídí množství, lokalizaci a biologický účinek m6A. Dynamická regulace metylomu m6A v mozku během vývoje je nezbytná pro zachování mozkových funkcí. Předklinický výzkum navíc ukázal, že způsob regulace energetické rovnováhy pomocí m6A dráhy může být rozdílný v odlišných tkáních či buněčných typech. Gen *FTO* je spojován s celoživotním rizikem obezity a rozvojem metabolického syndromu, a také s regulací celkového příjmu a výdeje energie v těle. O funkci dráhy m6A při řízení energetického metabolismu v mozku je však známo jen málo. Studium tohoto fenoménu je žádoucí mimo jiné pro lepší porozumění Alzheimerově chorobě, protože toto onemocnění je charakteristické poruchami energetického metabolismu mozku a stále více důkazů naznačuje, že narušená bioenergetika mozku může hrát roli v ranných fázích onemocnění, ještě před objevením klinických příznaků.

V této práci jsme se zaměřili na zkoumání role FTO v modelech dvou typů mozkových buněk, neuronů a astrocytů. Pomocí neuronálních buněk SH-SY5Y jsme chtěli zjistit, zda FTO hraje roli v procesu jejich diferenciace. Dále jsme zkoumali jak SH-SY5Y, tak astrocytární buňky CCF-STTG1, abychom zjistili, zda a jak FTO ovlivňuje bioenergetiku a expresní profil proteinů nezbytných pro správnou funkci těchto buněk. Nakonec jsme se více zaměřili na buňky CCF-STTG1 a zkoumali roli FTO v odolnosti buněk vůči streptozotocinu, *in vitro* modelu patogeneze Alzheimerovi choroby.

Zjistili jsme, že inhibice FTO může narušit normální diferenciaci buněk SH-SY5Y. Při inhibici FTO během procesu diferenciace jsme pozorovali nedostatečné morfologické změny buněk a rovněž změněný expresní profil neuronálních markerů. Dále ukazujeme, že modulace FTO mění proteom buněk SH-SY5Y a CCF-STTG1. Mezi odlišně regulovanými proteiny byly zjištěny proteiny ovlivňující funkci mitochondrií. V návaznosti na tento efekt bylo zjištěno, že inhibice FTO ovlivňuje mitochondriální respiraci a tento effekt je různý v neuronech a astrocytech. Dále jsme pozorovali, že inhibice FTO stimuluje biogenezi mitochondrií v astrocytech, což se projevilo nárůstem mitochondriální masy v buňkách, zvýšenou hladinou koaktivátoru 1 alfa receptorů aktivovaných peroxizomovými proliferátory typu gama (PGC-1α) a vyšším obsahem intracelulárního ATP. V neposlední řadě jsme zjistili, že astrocyty ovlivněné streptozotocinem nadměrně exprimují FTO. Naše výsledky ukazují, že inhibice FTO v astrocytech zlepšila životaschopnost buněk a snížila oxidační stres, apoptózu, reaktivitu a mitochondriální aberace vyvolané poškozujícím účinkem streptozotocinu.

List of abbreviations

70S6K	ribosomal protein S6 kinase beta-1
2-DE	2-dimensional electrophoresis
2-DG	2-deoxygluocose
AA	antimycin A
ABCF1	ATP Binding Cassette Subfamily F Member 1
AD	Alzheimer's disease
ADAM19	the disintegrin and metalloproteinase domain-containing protein 19
ADAR	adenosine deaminase acting on RNA
ADAT	adenosine deaminase acting on tRNA
ADP	adenosine diphosphate
AID	activation-induced cytidine deaminase
ALKBH	AlkB homolog
AMP	adenosine monophosphate
AMPK	AMP-activated protein kinase
APOBEC	apolipoprotein B mRNA-editing enzyme catalytic polypeptide-like
APOE	apolipoprotein E
APP	amyloid-beta precursor protein
ARC	activity-regulated cytoskeleton-associated protein
ATCC	American Tissue Culture Collection
ATF4	activating transcription factor 4
ATP	adenosine triphosphate
ATP5A	ATP synthase F1 subunit alpha
BAX	apoptosis regulator BAX
BCA	bicinchoninic acid
BCL-2	apoptosis regulator BCL-2
BDNF	brain-derived neurotrophic factor
C1QBP	complement component 1 Q subcomponent-binding protein
CA1	cornu ammonis 1
CAMK2	calcium/calmodulin dependent protein kinase II
CASP3	caspase 3
CBB	coomassie brilliant blue
CNS	central nervous system
CREB	cAMP-response element binding protein
DHE	dihydroethidium
DMSO	dimethyl sulfoxide
DTT	dithiothreitol
ECACC	European Collection of Authenticated Cell Cultures
ECAR	extracellular acidification rate
EDTA	ethylene diamine tetraacetic acid
EGTA	ethylene glycol-bis(β-aminoethyl ether)-N,N,N′,N′-tetraacetic acid
eIF	eukaryotic initiation factor
ENO1	alpha-enolase
ERK	mitogen-activated protein kinase
ETC	electron transport chain

FBS	fetal bovine serum
FC	fold change
FCCP	carbonyl cyanide-4-(trifluoromethoxy)phenylhydrazone
FDR	false discovery rate
FMRP	fragile X mental retardation protein
FOX(M1/O1)	forkhead box protein (M1/O1)
FTO	fat mass and obesity associated protein
G3BP	Ras GTPase-activating protein-binding protein
GAP43	growth associated protein 43
GAPDH	glyceraldehyde 3-phosphate dehydrogenase
GFAP	glial fibrillary acidic protein
GO	gene ontology
GRP75	75-kDa glucose-regulated protein (mortalin)
GTP	guanosine triphosphate
HCD	higher-energy C-trap dissociation
HEPES	hydroxyethyl-piperazineethane-sulfonic acid buffer
hnRNP(A/AB/C/H/L)	heterogeneous nuclear ribonucleoprotein (A/AB/C/H/L)
IAA	iodoacetamide
ICV	intracerebroventricular
IGF2BP	insulin-like growth factor 2 mRNA-binding protein
IL	interleukin
IRS	insulin receptor substrate
IRβ	insulin receptor beta
LC	liquid chromatography
LDH	lactate dehydrogenase
LPS	lipopolysaccharide
m6A	N6-methyladenosine
MALDI	matrix assisted laser desorption/ionization
MAP2	microtubule associated protein 2
MAT2A	methionine adenosyltransferase 2A
METTL	methyltransferase-like
MMP	mitochondrial membrane potential
MS	mass spectrometry
MT-CO1	cytochrome c oxidase subunit 1
mTOR	mammalian target of rapamycin
mTORC1	mTOR complex 1
MTT	3-(4,5-dimethyl-2-thiazolyl)-2,5-diphenyl-2H-tetrazolium bromide
MYD88	myeloid differentiation primary response 88
NAD	nicotinamide adenine dinucleotide
NADP	nicotinamide adenine dinucleotide phosphate
NDUFB8	NADH dehydrogenase 1 beta subcomplex subunit 8
NMDAR	N-methyl-D-aspartate receptor
NPY1R	neuropeptide Y receptor 1
NRF2	nuclear factor erythroid 2–related factor 2
NSE	neuron-specific enolase
OCR	oxygen consumption rate

OXPHOS	oxidative phosphorylation
PAGE	polyacrylamide gel electrophoresis
PARP1	poly [ADP-ribose] polymerase 1
PBS	phosphate-buffered saline
PGC-1α	proliferator-activated receptor gamma coactivator 1-alpha
PRRC2A	proline-rich and coiled-coil-containing protein 2A
PRX	peroxiredoxin
PSEN1	presenilin
RA	retinoic acid
RBM15	RNA-binding motif protein 15
ROS	reactive oxygen species
SAH	S-adenosylhomocysteine
SAM	S-adenosylmethionine
SDHA	succinate dehydrogenase subunit A
SDS	sodium dodecyl sulphate
SIRT1	sirtuin-1
SRSF	serine and arginine/rich splicing factor
STAT3	signal transmitter and transcription activator 3
SYP	synaptophysin
TH	tyrosine hydroxylase
TMPD	N,N,N′,N′-tetramethyl-p-phenylenediamine
TNF-α	tumor necrosis factor alpha
TOF	time of flight
TRAF6	tumor necrosis factor receptor associated factor 6
TUBA	tubulin alpha
TUBB3	beta-3 tubulin
UCP1	uncoupling protein 1
UQCRC2	ubiquinol-cytochrome C reductase core protein 2
UTR	untranslated region
WTAP	Wilms tumor 1-associated protein
XIST	X-inactive specific transcript
YTH	YT521-B homology
YTHDC	YTH domain-containing protein
YTHDF	YTH domain-containing family protein
αKG	alpha-ketoglutarate

Table of contents

1 Introduction

Aside from DNA methylation and chromatin modification, research over the last decade has shown huge regulatory significance of RNA modifications, forming the area of "RNA epitranscriptomics". Epitranscriptomics involves changes to the RNA structure that are functional and do not affect the nucleotide sequence. It has been demonstrated that this collection of RNA alterations has a significant regulatory impact on gene expression (Kumar and Mohapatra, 2021; Seo and Kleiner, 2021). N6-methyladenosine (m6A) is one of many naturally occurring biological RNA modifications that have been discovered, and it has recently received the most attention. It is the most prevalent reversible alteration of messenger RNA and its levels are controlled by specific methyltransferases and demethylases.

The functions of fat mass and obesity-associated (FTO) demethylase, an enzyme responsible for deleting the m6A RNA modification, which is particularly abundant in the brain, are subjects of this study. The possible role of an epitranscriptomic mark m6A in the control of many nervous system functions has recently been revealed (Widagdo et al., 2022; Yu et al., 2021). Changes in the m6A profile or its machinery enzymes have been linked to neurodevelopment, energy metabolism, and neuroplasticity, all of which are linked to Alzheimer's disease (AD) risk and progression (Arendt and Bullmann, 2013; Demetrius et al., 2015; Janelidze et al., 2018).

Changes in FTO functioning have been found to trigger mitochondrial-driven oxidative stress and increase tau phosphorylation in neurons (H. Li et al., 2018; Pitman et al., 2013). FTO demethylase has been found to alter energy balance in a variety of metabolically active tissues (Pitman et al., 2012; Y. Wang et al., 2012). Accumulated evidence suggests a potent regulatory role of FTO in glucose metabolism and mitochondrial biogenesis. Because FTO's influence on bioenergetics appears to be tissue-specific (Pitman et al., 2012), it's vital to look into the function of FTO in different cell types. While considerable research has focused on the role of FTO in neuronal cells, there have been a very few investigations on the role of FTO in astrocytes. Therefore, both neuronal and astrocytic cells were used for investigation in this study.

The fundamental etiology of AD is now widely acknowledged to be significantly more complex than the standard amyloid cascade theory, which focuses on the abnormal deposition of amyloid-beta peptide (Hardy and Higgins, 1992). Neuroinflammation and disrupted brain bioenergetics are emerging as potential contributors in the early genesis of this neurodegenerative illness (Arendt and Bullmann, 2013; Demetrius et al., 2015; Janelidze et al., 2018). In this sense, non-neuronal cell changes during AD pathogenesis are receiving increasing attention. Several investigations have found that the inflammatory

processes that occur in the brain burdened by AD are associated with neuroglia activation (Cagnin et al., 2001; Furman et al., 2012; Heneka et al., 2015). Astrocytes are the primary glial cell type in the central nervous system and play a critical role in maintaining neuronal homeostasis. Insulin resistance, mitochondrial dysfunction followed by oxidative stress, and signaling pathway dysregulation are all symptoms of astrocyte dysfunction. Furthermore, inflammatory and neurotoxic substances are released in response to abnormal glial activation (Lian et al., 2015; Sami Saribas et al., 2017).

To mimic the harmful circumstances seen in cells of Alzheimer's patients, we chose to use the streptozotocin (STZ) compound to disrupt the cells. STZ, unlike some other cellular AD-like models, is generally employed as an experimental model of the early pathophysiological changes in AD illness, due to its capacity to cause metabolic abnormalities, oxidative stress, and neuroinflammation (Grieb, 2016). *In vitro* STZ treatment was shown to promote several hallmarks of AD like beta-amyloid accumulation, tau hyperphosphorylation, as well as to impair neurotransmission, glucose metabolism, mitochondrial function and survival of mouse neuronal N2A cells (Biswas et al., 2016). Furthermore it caused cellular stress and increased apoptosis in the astrocytic C6 cell line (Biswas et al., 2017). In this work, investigations of the role of FTO in STZ-induced harmful effects resembling AD-like pathophysiology were mainly focused on the astrocytic model.

2 Literature review

2.1 Epitranscriptomics

A relatively short time ago, a long-understudied field of RNA modifications has reemerged into the spotlight. Similarly to what epigenetics represents to DNA, epitranscriptomics entail functional alterations to the RNA structure, which does not result in change of nucleotide sequence. The ensemble of known naturally occurring biochemical RNA modifications now contains more than 100 distinct items. Many forms of cellular RNA undergo these modifications, including ribosomal RNA (rRNA), transfer RNA (tRNA), messenger RNA (mRNA), and small nuclear RNA (snRNA). Epitranscriptomic mechanisms play important roles in bridging environmental stimuli, RNA functionality, and biological processes. Among the best characterized post-transcriptional modifications till today are isomerization of uridine bases (pseudouridine), methylation of cytosine or adenine, and RNA editing.

Conversion of uridine nucleotides to pseudouridine is occurring on both mRNAs and non-coding RNAs (ncRNAs) and it is catalyzed by pseudouridine synthases. Of all RNA modifications, pseudouridine is the most prevalent (Ofengand, 2002), and its accumulation is expected to contribute to the stability of regional RNA structure, mRNA translation, and accessibility to RNA binding proteins (Yu and Meier, 2014).

During RNA editing, canonical bases are converted into alternative nucleobases. Adenosine and cytidine deaminases are the two main types of enzymes that primarily mediate RNA editing. Apart from mRNAs, these enzymes also change other RNA molecules such as miRNAs and tRNAs. Members of the ADAR and ADAT (adenosine deaminase acting on RNA/tRNA) protein families, known as adenosine to inosine (A-to-I) editors, play a crucial role in alternative splicing and transcriptional regulation. According to studies, post-transcriptional regulation of circadian rhythm, sleep, neurodevelopment, and neurotransmission involves ADARs and A-to-I editing. On the other hand, the cytidine to uridine (C-to-U) editors which are part of the AID/APOBEC (activation-induced cytidine deaminase/apolipoprotein B mRNA-editing enzyme catalytic polypeptide-like) protein family play a significant role in both innate and adaptive immunity (Christofi and Zaravinos, 2019).

Methylation of RNA involves attachment of a methyl group to a specific site on either the base of an RNA molecule (e.g., N6-methyladenosine (m6A), N1-methyladenosine (m1A), 5-methylcytidine (m5C), 3-methylcytidine (m3C), 1-methylguanosine (m1G) and N7-methylguanosine (m7G)), or ribose sugar (e.g., 2′-O-methyladenosine, N6,2′-O-dimethyladenosine (m6Am)). RNA methylations have been

linked to the regulation of distinct processes of RNA metabolism, including nuclear export, processing, stability, and translation (Seo and Kleiner, 2021). The most common post-transcriptional modification of both plant and animal mRNAs is the m6A (Desrosiers et al., 1974; Meyer et al., 2012).

2.2 N6-methyladenosine (m6A)

N6-methyladenosine (m6A) is the most common mRNA modification, appearing on 0.1-0.4% of adenosines and on average three times in every mRNA molecule (Wei et al., 1975). m6A was initially discovered in polyA RNA fractions in 1974 (Desrosiers et al., 1974; Perry and Kelley, 1974), but it wasn't until more recent technological advancements that made it feasible to explore specific m6A sites inside mRNAs. These studies have shown that the distribution of m6A within mRNA is not random (Fig. 1). The presence of m6A modifications has been found to be enriched in 3 prime untranslated regions (UTR), coding sequences, and the vicinity of stop codons (Dominissini et al., 2012; Meyer et al., 2012; Schwartz et al., 2013). Besides mRNA, long non-coding RNAs have also been reported to contain m6A (Liu et al., 2013; Meyer et al., 2012).

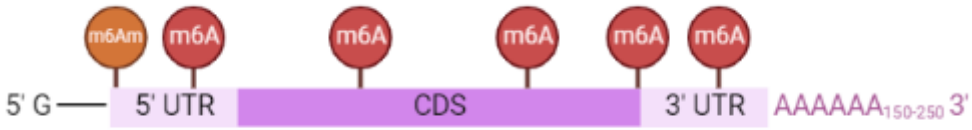

Fig. 1. Schematic structure of messenger RNA with N6-methyladenosine (m6A) modifications sites. The m6A is enriched mainly in coding sequences (CDS), in proximity to stop codons, in 3 prime untranslated regions (3' UTRs), and also occurs in 5 prime untranslated regions (5' UTRs). N6,2′-O-dimethyladenosine (m6Am) modification, which shares some common regulatory mechanisms as m6A, is predominantly localized near the 7-methylguanosine cap. Adapted from (Dermentzaki and Lotti, 2020).

Importantly, m6A modification is reversible and has been found to dynamically change in response to various conditions, e.g. due to cellular stress or in development (Anders et al., 2018; Engel et al., 2018; Shafik et al., 2021). Consequently, it appeared likely that m6A might be functionally involved in the regulation of mRNA fate in response to environmental cues. Multiple proteins responsible for the regulation and recognition of m6A have been identified so far. They can be classified into three groups based on their activity: writers that produce m6A, erasers that remove m6A, and readers that can identify m6A sites and exert functional effects.

2.2.1 Mechanisms of m6A regulation

N6-methyladenosine is a reversible modification of the nitrogen-6 position of the adenosine base. Two groups of inversely working enzymes are responsible for the control of m6A levels: methyltransferases and demethylases. Another class of proteins promoting the biological activity of m6A through the recognition of m6A sites is called readers (Fig. 2).

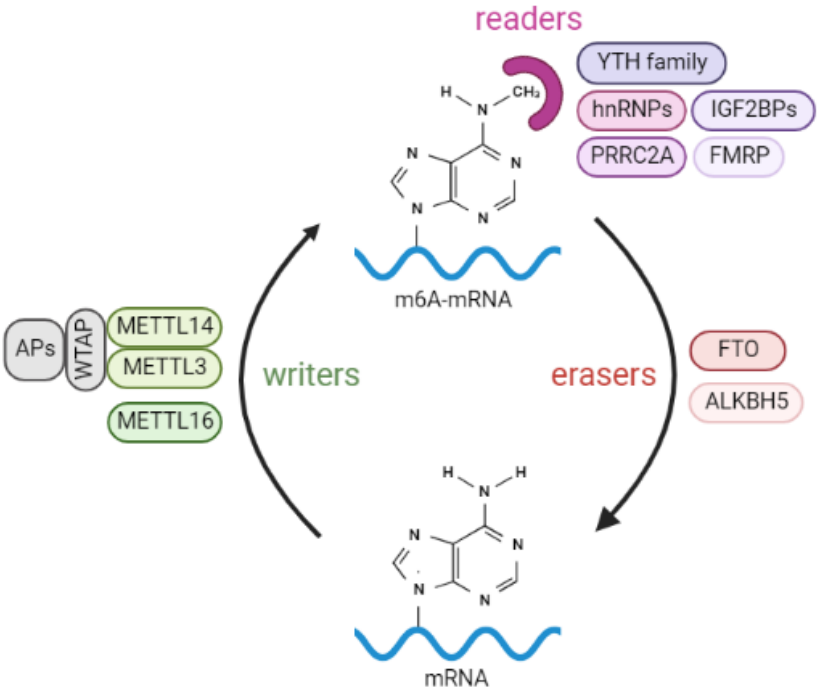

Fig. 2. Scheme of m6A regulation machinery. Methyltransferases called writers are in charge of the methylation of adenosine in mRNA. A methyltransferase complex, which is a major source of m6A formation, is formed by methyltransferase-like 3 (METTL3), methyltransferase-like 14 (METTL14), Wilms tumor 1-associated protein (WTAP), and adaptor proteins (AP). Another writer, methyltransferase-like 16 (METTL16) operates independently of the methyltransferase complex. Eraser proteins carry out the removal of m6A. Fat mass and obesity-associated protein (FTO) and AlkB homolog 5 (ALKBH5) are the two primary m6A demethylases. The biological consequence of m6A decoration is ultimately mediated by reader proteins that recognize m6A sites. Reader proteins including the YTH domain-containing family and insulin-like growth factor 2 mRNA-binding proteins 1-3 (IGF2BP1-3) operate by directly binding to m6A-modified mRNA. Other reader proteins, such as heterogeneous nuclear ribonucleoproteins (hnRNPs), fragile X mental retardation protein (FMRP), or proline-rich and coiled-coil-containing protein 2A (PRRC2A), function via an indirect mechanism. Created with BioRender.

The m6A methyltransferases complex is necessary for the formation of m6A. Localized mainly in the nucleoplasm (Arcidiacono et al., 2020), two main proteins are critical for the establishment of the methyltransferases complex: methyltransferase-like 3

(METTL3) and methyltransferase-like 14 (METTL14). While METTL3 is responsible for the binding of the methyl donor S-Adenosyl methionine (SAM), METTL14 serves for substrate recognition. An adapter protein is occasionally required by the METTL3–METTL14 heterodimer. The first adaptor shown to bind with both METTL3 and METTL14 is Wilms tumor 1-associated protein (WTAP). WTAP also interacts with a variety of proteins and long-non-coding RNAs, suggesting that it may recruit other components to the methyltransferase complex. Other adaptor proteins, including KIAA142929, RNA-binding motif protein 15 (RBM15), and its paralogue RBM15B30, were shown to interact with the METTL3 complex, and the removal of these adaptors reduced cellular m6A levels. In mRNAs, the methyltransferases complex-mediated installation of m6A occurs at the conserved DRA*CH motif (D = A/G/U; R = A/G; and H = U/A/C; A* = N6-methylated adenosine) (Zhou and Pan, 2016).

In addition, methyltransferase-like 16 (METTL16) has been recently discovered as methyltransferase complex-independent m6A methyltransferase (Warda et al., 2017). METTL16 was found to methylate m6A sites mostly in 3 prime untranslated regions, and its deletion is associated with a partial reduction in m6A levels (Koh et al., 2019).

The m6A writer-mediated methylation is dynamically controlled by substrates and products. S-adenosylhomocysteine (SAH), an intermediate of methionine metabolism, is a potent allosteric inhibitor of METTL3. Also, it has been revealed that the activity of METTL16 influences the stability of the methionine adenosyltransferase 2A (MAT2A) mRNA, which encodes the SAM synthase, hence exerting a negative feedback regulation of de novo SAM synthesis (Kim and Lee, 2021; Pendleton et al., 2017).

For the removal of m6A are responsible eraser proteins with demethylation activity. The two main m6A demethylases identified so far are fat mass and obesity-associated protein (FTO) and AlkB homolog 5 (ALKBH5) (Gerken et al., 2007; Zheng et al., 2013). Both enzymes oxidize the N-methyl group of the m6A site to a hydroxymethyl group using ferrous iron as a cofactor and alpha-ketoglutarate (αKG) as a co-substrate. While FTO removes methyl residue from adenosine through the formation of intermediates N6-hydroxymethyladenosine (hm6A) and N6-formyladenosine (f6A) (Fu et al., 2014), ALKBH5 catalyzes direct m6A-to-A conversion (Toh et al., 2020).

Several metabolites were shown to have an impact on m6A RNA demethylation caused by FTO and ALKBH5. FTO and ALKBH5 are members of the KG-dependent dioxygenase family of proteins, which depend on αKG, non-heme iron, and O_2 for complete enzymatic activity. As a result, demethylation activities of FTO and ALKBH5 are abolished when αKG and iron binding sites in the Fe(II)/αKG oxygenase domain are altered. Along with αKG, the molecularly similar citric acid cycle products succinate and fumarate also have an impact on the activity of m6A demethylase, but only exceptionally high levels of

succinate and fumarate may prevent αKG binding. Additionally, nicotinamide adenine dinucleotide (NAD) and nicotinamide adenine dinucleotide phosphate (NADP) were discovered to increase the FTO activity (Kim and Lee, 2021).

Ultimately, for the translation of m6A marks into biological effects are responsible proteins called readers. Different readers recognize different m6A-modified RNA sites and exert different functions. Several nuclear and cytoplasmic readers have been identified so far. The two basic methods that m6A readers connect to RNAs are direct reading and indirect reading.

Direct reading is the interaction of specific m6A readers with m6A sites in RNA. Among proteins with the capacity to bind m6A-containing RNA in a direct manner are the members of the YTH (YT521-B homology) domain-containing protein family. While YTHDC1 operates in the nucleus, YTHDC2 and highly similar YTHDF1, YTHDF2, and YTHDF3 are localized in the cytoplasm. Among other cytoplasmic direct readers that do not contain the YTH domain are insulin-like growth factor 2 mRNA-binding proteins 1-3 (IGF2BP1-3) (Yang et al., 2018).

The m6A decoration on RNA can cause structural changes in RNA molecules, ultimately exposing or blocking certain regions to RNA-binding protein interaction. The process of changing secondary RNA structure by the m6A to facilitate indirect reading by RNA-binding proteins is known as the "m6A switch". Numerous members of the heterogeneous nuclear ribonucleoprotein (hnRNPs) family (including hnRNPA2B1, hnRNPC, and hnRNPG) have been identified as nuclear indirect readers (Yang et al., 2018). However, there is uncertainty on this subject as different study has demonstrated that hnRNPA2B1 directly binds to the m6A region of miRNA (Alarcón et al., 2015). So far, an m6A binding ability has also been identified in a few additional proteins including eukaryotic initiation factor 3 (eIF3) (Meyer et al., 2015), ATP Binding Cassette Subfamily F Member 1 (ABCF1) (Coots et al., 2017), fragile X mental retardation protein (FMRP) (F. Zhang et al., 2018), and proline-rich and coiled-coil-containing protein 2A (PRRC2A) (Wu et al., 2019). On the other hand, Ras GTPase-activating protein-binding proteins (G3BPs) were identified as proteins that are repelled by m6A (Edupuganti et al., 2017). It is intriguing that altering m6A readers can also change overall m6A levels. This is likely because of their ability to regulate RNA metabolism. For example, YTHDF1 overexpression or YTHDF1-3 knockdown raised the m6A/A ratio most likely by influencing the stability of mRNAs decorated with the m6A (Shi et al., 2017; Xiao Wang et al., 2015).

2.2.2 m6A in RNA metabolism

The whole life cycle of an RNA molecule is encompassed by RNA metabolism, a set of intricate and highly regulated processes that includes transcription, processing, nuclear export, translation, and degradation. Post-transcriptional modification m6A has been associated with various aspects of RNA metabolism (Fig. 3) as well as with modulation of the epigenetic effect of noncoding RNAs like microRNA (Yang et al., 2018).

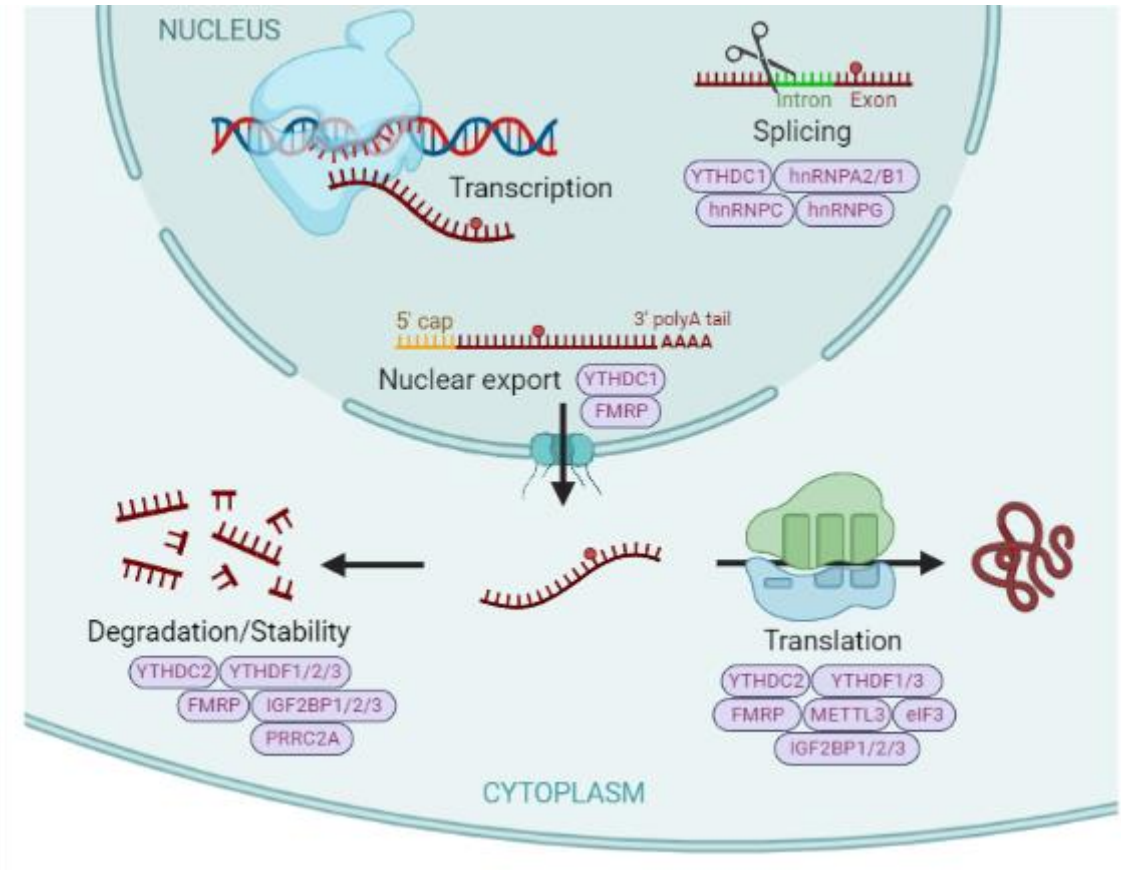

Fig. 3. Roles of m6A in the regulation of mRNA fate. Various aspects of mRNA metabolism including mRNA maturation, nuclear export, translation, and turnover have all been observed to be affected by m6A modification. The effect is mediated usually by m6A reader proteins. Different readers are able to recognize distinct m6A-modified RNA sites and execute different functions. Created with BioRender.

RNA processing covers nuclear steps of maturation of mRNA from precursor pre-mRNA, including 5' capping, 3' polyadenylation, and removal of introns (splicing). Many m6A regulating proteins have been shown to be localized within nuclear speckles, nuclear domains enriched in pre-mRNA splicing factors (Ping et al., 2014). According to a study by Salditt-Georgieff, m6A levels are higher in pre-mRNA than in maturated mRNA (Salditt-Georgieff et al., 1976). Additionally, it was observed that m6A methylation is deposited on chromatin-associated nascent pre-mRNA and remains relatively preserved until the mRNA

decay (Ke et al., 2017). Intronic m6A was shown to affect alternative splicing of Sex lethal gene in Drosophila (Haussmann et al., 2016). According to Wei's group, introns have binding sites for m6A methyltransferase METTL3. Depletion of METTL3 was followed by intron retention and disrupted mRNA maturation (Wei et al., 2021). Enhanced m6A levels by higher levels of METTL3, or down-regulated FTO promoted the binding of serine and arginine-rich splicing factor (SRSF) 2 to RNA. In spermatogenic cells, ALKBH5-mediated m6A reduction seems to be necessary for the proper splicing of mRNA (Tang et al., 2017). MAT2A mRNA and snRNA, both of which participate in mRNA splicing, were shown to be methylated by METTL16 (Pendleton et al., 2017). Several m6A readers were also suggested to be involved in RNA processing. YTHDC1 bound to m6A sites can apparently recruit SRSF3 to mRNA (Xiao et al., 2016). An m6A binding hnRNPs were repeatedly shown to play a role in both, pre-mRNA and pre-miRNA processing (Geuens et al., 2016).

Once maturated, mRNA leaves the nucleus through nuclear pore complexes. It appears that m6A promotes the nuclear export of mRNA to the cytoplasm. Delayed mRNA export was seen after the knockdown of METTL3 or YTHDC1 (Fustin et al., 2013; Roundtree et al., 2017). An inhibition of ALKBH5, on the other hand, stimulated the export (Zheng et al., 2013) .

In cytoplasm, mRNA enters the process of translation in order to produce protein. Most commonly, the small (40S) ribosomal subunit associates with several eukaryotic initiation factors (eIF3, eIF1, eIF1A, eIF5, and eIF2-GTP-met-tRNA) to form the 43S pre-initiation complex, which then connects to mRNA via the eIF4 initiation factor complex (composed of eIF4E, eIF4A, eIF4G, and eIF4B) to start translation in mammals. Interestingly, the eIF3 can presumably directly bind to m6A sites at 5' UTR of transcripts and recruit the ribosomal complex even in absence of eIF4E (Meyer et al., 2015). Additionally, it was reported that eIF3 and YTHDF1 interact to facilitate the translation of m6A mutated transcripts (Liu et al., 2020). Lower translation efficiency was seen in relation with the down-regulation of YTHDF1 or YTHDF3 which reportedly facilitates the binding of m6A-tagged mRNAs to ribosomes (A. Li et al., 2017). Independent of its methyltransferase activity, cytoplasmic METTL3 can also recruit eIF3 to engage with the translation initiation machinery and advance translation (Jin et al., 2019). It has been demonstrated that m6A stimulates cap-independent translation, which usually occurs in cells in response to stress (Meyer et al., 2015). Adenosine that has been methylated can also interfere with base pairing, which affects tRNA docking and elongation (Choi et al., 2016).

The turnover of RNAs is an important step in the regulation of gene expression. Overall, the half-life of m6A-decorated mRNAs was detected to be shorter than that of m6A-free mRNAs. That was demonstrated for example when inhibition of either METTL3 or METTL14 was associated with altered half-lives of target mRNAs (Sang et al., 2022; Y.

Xu et al., 2022). RNA degradation that is dependent on the deadenylation was found to be modulated by m6A. YTHDF2 allegedly directly interacts with a subunit of deadenylation complex which mediates RNA degradation by shortening of polyA tail. Furthermore, the lifetime of YTHDF2's mRNA targets lengthened as YTHDF2 protein levels dropped (Du et al., 2016). Increased mRNA stability was also associated with IGF2BP, a distinct m6A-binding protein (Huang et al., 2018).

2.2.3 m6A demethylase FTO

The fat mass and obesity-associated (FTO) protein is an Fe(II) and αKG dependent demethylase of m6A in mRNA that removes methyl residue from adenosine through hm6A and f6A intermediates (Fu et al., 2014). FTO was also shown to be capable of demethylating N6-2-O-dimethyladenosine (m6Am) (Mauer et al., 2017) and loss of FTO was seen to affect levels of other epitranstriptomic modifications such as pseudouridine or 3-methyluridine (Berulava et al., 2013). Wei showed that FTO binds multiple RNA species with main targets being m6A in mRNA and snRNA, m6Am near mRNA cap, and m1A in tRNA (Wei et al., 2018).

To some extent, the function of FTO is affected by its localization. FTO was found to be typically localized in the cell nucleus (Berulava et al., 2013; Gerken et al., 2007). Some authors observed the localization of FTO within nuclear speckles (Berulava et al., 2013; Jia et al., 2011). However, FTO protein was detected also in the cytoplasm, and it appears that the cellular distribution of FTO is distinct among different cell lines (Wei et al., 2018), or it is changing upon stimulus (Vujovic et al., 2013; Walters et al., 2017) or during the cell cycle (Hirayama et al., 2020) and development (Y. Wang et al., 2012). In addition, evidence showed that FTO can shuttle between cytoplasm and nucleus possibly thanks to the interaction with exportin 2 (Aas et al., 2017; Gulati et al., 2014). While nuclear FTO is suggested to preferentially demethylate m6A, cytoplasmic FTO participates in the regulation of both m6A and m6Am levels (Relier et al., 2021; Wei et al., 2018).

The beginnings of FTO research are linked to the so-called fused toes mutation in mice. Heterozygous mutants had severe developmental deformities such as aberrant craniofacial features, damaged hypothalamus, or fused digits as a result of a disrupted mechanism of programmed cell death. The fundamental change causing the observed phenotype was a loss of six consecutive genes in a specific chromosomal sequence, including the previously unknown *Fto* gene (Peters et al., 1999; van der Hoeven et al., 1994). Later, targeted *Fto* knockout mice manifested growth retardation, changes in body weight and food intake, and a rise in postnatal mortality (Gao et al., 2010; McMurray et al., 2013). Similar symptoms were seen after the deletion of *Fto* in the central nervous system,

indicating a crucial function for brain-localized FTO (Gao et al., 2010). The deletion of the *FTO* gene in humans is linked to several severe conditions, including microcephaly, disturbance of cognitive performance, growth retardation, and, less often, structural alterations to the brain and heart (Boissel et al., 2009).

A genome-wide search for type 2 diabetes genetic risk factors discovered a point polymorphism in *FTO* that predisposes to obesity via affecting body mass index (Frayling et al., 2007). Intensive research was then carried out in purpose to elucidate the role of FTO in obesity. Manipulations of FTO function in animals were often accompanied by alterations in food intake, fat mass, and body weight (Church et al., 2010). The actual role of FTO in obesity is still unclear, though. Some authors pointed out that risk variants of the *FTO* gene which are associated with obesity were not affecting the FTO protein levels, but the expression of neighboring genes (Smemo et al., 2014; Stratigopoulos et al., 2016). Others, however, observed that *FTO* single nucleotide polymorphisms boost *FTO* expression (Berulava et al., 2013; Karra et al., 2013). Nevertheless, genetic variations in the *FTO* gene have been linked to a number of illnesses, including cancer, hypertension, neurological diseases, and metabolic disorders (Bego et al., 2019; Hernández-Caballero and Sierra-Ramírez, 2015; Keller et al., 2011; Timpson et al., 2009; H. Wang et al., 2012).

A pivotal moment in FTO research was a study showing for the first time that m6A can be demethylated and that FTO is responsible for the removal of this epitranscriptomic mark. Cells that either overexpressed or were deprived of FTO displayed changes in m6A levels within the polyA tail of mRNA (Jia et al., 2011).

Since FTO is an epitranscriptome regulator capable of affecting gene expression, it is not surprising that the alterations of FTO demethylase activity or expression levels have been linked to numerous biological processes, as well as many pathophysiological states. FTO appears to be critically involved in energy homeostasis (Chen et al., 2022; Liu et al., 2017; Yang et al., 2019), brain development (L. Li et al., 2017), and cognitive functions (Bai et al., 2018; Liu et al., 2022). Dysfunctions in FTO m6A demethylase activity have been implicated in diabetes (Yang et al., 2019), cancer (Li et al., 2022), and neurodegenerative diseases (Han et al., 2020; H. Li et al., 2018). The participation of m6A and FTO in energy metabolism, cell fate determination, and AD will be discussed in later sections.

2.2.3.1 FTO inhibitors

The search for compounds that target the m6A modification regulators is thought to be a promising therapeutic strategy for treating cancer because of the overwhelming evidence demonstrating the presence of m6A modification in many types of cancers and

its involvement in regulating the expression of oncogenes and tumor suppressor genes (Li et al., 2022). Until now, a number of FTO inhibitors have been reported to block the demethylation activities of FTO, including rhein, MO-I-500, meclofenamic acid, R-2HG, fluorescein derivatives, FB23-2, entacapone, CS1, CS2, FTO-02, and FTO-04 (Chen et al., 2012; Huang et al., 2015; Y. Huang et al., 2019; Huff et al., 2021; Peng et al., 2019; Su et al., 2020, 2018; T. Wang et al., 2015; Zheng et al., 2014). The aforementioned FTO inhibitors offer an useful instrument for the investigation of m6A modification and the biological impact of FTO. Two well-known FTO inhibitors have been employed in this study: MO-I-500 (Fig. 4B), a synthetic FTO inhibitor, and rhein (Fig. 4A), a naturally occurring rhubarb component.

- Rhein: In a 2012 research, rhein was shown to be the most effective FTO inhibitor among the investigated drugs. Rhein inhibits FTO either by competitively binding to the αKG cofactor at the active site or by directly binding to nucleic acids. *In vitro* cells treated with rhein showed an increase in m6A mRNA, which was demonstrated to depend on the concentration of rhein applied. Rhein's IC50 was found to be 1,2–21 μM (Chen et al., 2012). However, it was also shown that rhein inhibited the activity of the AlkB repair enzymes ALKBH2, and ALKBH3 (Li et al., 2016).

- MO-I-500: MO-I-500, a dihydroxyfuran sulfonamide compound, was proven to inhibit FTO demethylation *in vitro* with an IC50 of 8.7 μM. After Hela cells were treated with MO-I-500, m6A levels increased in a manner similar to those affected by FTO siRNA (Zheng et al., 2014). Despite being an αKG and ascorbic acid mimic, MO-I-500 exhibits considerable FTO selectivity over some αKG-dependent dioxygenases. The selectivity for AlkB proteins is unfortunately unknown. The inhibition of FTO by MO-I-500 was shown to be accompanied by reduced proliferation, altered production of specific microRNAs, and anticonvulsant activity (Singh et al., 2016; Zheng et al., 2014).

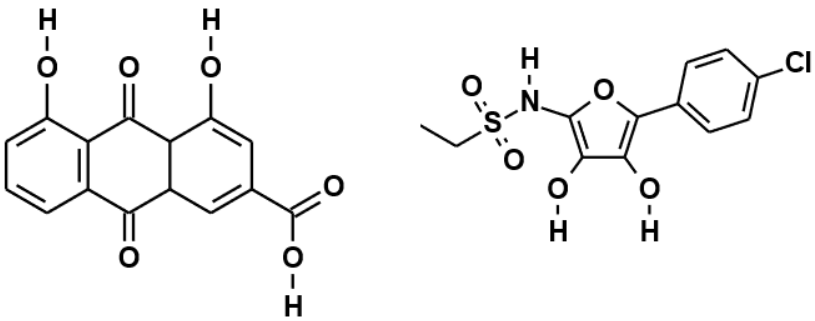

Fig. 4. Chemical structure of FTO inhibitors rhein (left) and MO-I-500 (right).

2.3 Physiological roles of m6A neuroepitranscriptome

m6A modification was shown to be highly conserved at gene and base level throughout different tissues from humans, mice and rats (Schwartz et al., 2013; Z. Zhang et al., 2019). Because of its potential to regulate gene expression, practically every biological process can be affected by m6A. In recent years, studies have shown the essential role of m6A RNA modification in both physiological and pathophysiological conditions. Disruptions of proteins involved in m6A regulation were linked to obesity (Krüger et al., 2020; Zhao et al., 2014b), developmental defects (Peters et al., 1999; van der Hoeven et al., 1994), or impaired spermatogenesis (T. Huang et al., 2019). The role of m6A appears to depend on cellular and environmental context. Following the same modulation of the m6A pathway, various tissues exhibit different phenotypes (Pitman et al., 2012). Additionally, it was shown that changes in environmental circumstances can cause shifts in expression of m6A machinery proteins. For example, altered expression of mammalian YTHDF1, but not YTHDF2 or YTHDF3 seems to be involved with adaptation to conditions of low oxygen (Shi et al., 2019).

Emerging evidence is showing that m6A modification is critical for the proper function and development of the nervous system. In 2012, Meyer's group found that m6A is vastly localized within the brain and its levels increase throughout the life span (Meyer et al., 2012). Similarly, levels of m6A demethylase FTO were shown to be highly abundant in the brain (McTaggart et al., 2011). Furthermore, both FTO deficiency or *FTO* risk variants are associated with reduced brain volume (L. Li et al., 2017; Melka et al., 2013). FTO was found to affect fear memory retention (Walters et al., 2017), dopaminergic pathway (Hess et al., 2013; Sevgi et al., 2015), or locomotion (Hess et al., 2013; Ruud et al., 2019). YTHDF1 is increased in the hippocampus, where it participates in m6A accumulation during learning and memory (Shi et al., 2018). Knockdown of either YTHDF1 or YTHDF3 decreased the volume of dendritic spines of primary hippocampal neurons (Shi et al., 2018).

m6A functions have been described in a wide range of nervous system cell types. Although the majority of studies were carried out on neurons, m6A has been identified to contribute to the functioning of glial cells. For example, m6A was linked with oligodendrocyte differentiation (Wu et al., 2019; H. Xu et al., 2020), inflammation processes in microglia (Ding et al., 2022; Wen et al., 2022), and morphology of Purkinje cells and astrocytes (Ma et al., 2018; Yang et al., 2022). It also appears that the m6A pathway is implicated in the regulation of gliogenesis. Astrocyte numbers were decreased as a result of *Mettl3* or *Mettl14* knockdown (J. Chen et al., 2019; Yoon et al., 2017). In one study by Frederikson, the authors speculated that the m6A demethylase FTO is missing

in astrocytes, because they did not detect FTO in glial fibrillary acidic protein (GFAP)-positive cells by immunofluorescence staining (Fredriksson et al., 2008). Different studies have nevertheless contradicted this observation (Cockova et al., 2021; Walters et al., 2017; Yi et al., 2021).

2.3.1 m6a in cell differentiation and brain development

Stem cells possess the self-renewal capacity and potency to differentiate into multiple cell types. Increasing evidence has demonstrated that m6A machinery proteins are associated with cancer and healthy stem cell self-renewal. For example, the knockdown of methyltransferases METTL3 or METTL14 promotes glioblastoma stem cells' self-renewal while overexpression of METTL3 or inhibition of m6A demethylase FTO have the opposite effect (Cui et al., 2017). In embryonic mouse stem cells, the knockdown of either METTL3 or METTL14 results in a loss of self-renewal capacity and down-regulation of pluripotent factors of these cells (Wang et al., 2014). Interestingly, m6A methylome mapping showed thousands of mRNAs including transcripts for pluripotent genes to have conserved m6A motifs (Batista et al., 2014).

During development, distinct cell types are generated and this event is regulated by epigenetic, transcriptional, and epitranscriptomic mechanisms. Several lines of evidence suggest that m6A is involved in the differentiation process. The expression pattern of m6A as well as the expression of m6A machinery proteins differs across various developmental stages of the cerebellum (Ma et al., 2018). Prenatally, m6A is markedly increased throughout brain development (Meyer et al., 2012). Increased m6A levels were seen to promote the degradation of transcripts encoding proteins with known functions in neuron differentiation and cell cycle (Yoon et al., 2017). Modulation of levels of m6A writers or erasers leads to defects in brain development (M. Li et al., 2018; Wang et al., 2018; Yoon et al., 2017). Loss of FTO was followed by reduced brain size in mice (L. Li et al., 2017). Similar outcomes were observed in *FTO* risk allele carriers that had overall reduced brain sizes as well as decreased volumes of specific brain regions (Ho et al., 2010). Cerebellar atrophy occurred in Purkinje cell-specific *Wtap*-depleted mice as a result of severe cell degeneration and apoptosis. Synapses of Purkinje cells experienced excessive deterioration as a result of *Wtap* loss (Yang et al., 2022). m6A modification has been observed to modulate both embryonic and adult neurogenesis. m6A methyltransferases METTL3 and METTL14 extended cortical neurogenesis into postnatal stages likely by prolonging the cell cycle of radial glia (Yoon et al., 2017). Knockdown of FTO in adult neural stem cells reduced proliferation and neuronal differentiation (Cao et al., 2020). YTHDF2 inhibited the self-renewal of neural stem cells and the spatio-temporal generation

of neurons in the embryonic neocortex (M. Li et al., 2018). In hypoxic conditions, the knockdown of ALKBH5 disrupted the m6A methylation pattern in mRNAs of cell fate determination genes, which was accompanied by increased proliferation and differentiation in the cerebellum (Ma et al., 2018). FTO deficiency resulted in altered expression of key m6A-tagged components of the brain-derived neurotrophic factor (BDNF) pathway (L. Li et al., 2017).

Several m6A machinery proteins (METTL3/14/16, FTO, ALKBH5, YTHDF1/2/3) were shown to be present in extrasomatic regions of neurons, suggesting subcellular-specific functions. FTO was found to be localized within axons and it is presumably locally translated there. Axon-specific FTO siRNA or inhibition by rhein caused a raise in m6A levels and was followed by repressed axon elongation, likely due to decreased local translation of growth associated protein 43 (GAP43) (Yu et al., 2018). Similarly, down-regulation of FTO led to shorter axonal length in mice dorsal root ganglia neurons (Weng et al., 2018). Furthermore, research has shown that FTO influences axon guidance components (Qi et al., 2022). In neurons, methylation of N6-adenosine can play a role in the localization of specific mRNAs to neurites. Knockdown of either YTHDF2 or YTHDF3 impaired localization of two transcripts essential for synaptic plasticity to axons and dendrites, calcium/calmodulin-dependent protein kinase 2 (*Camk2a*) and microtubule associated protein 2 (*Map2*) (Flamand and Meyer, 2022).

METTL14 depletion was associated with disturbed oligodendrocyte maturation (H. Xu et al., 2020). The proliferation and differentiation of oligodendrocyte progenitor cells were additionally shown to be regulated by PRRC2A, an m6A reader. A deficiency of PRRC2A in the brain led to hypomyelination (Wu et al., 2019).

2.3.2 m6A in control of energy metabolism

The findings of studies indicate a strong relationship between m6A and energy metabolism. An m6A demethylase *FTO* is expressed in many highly metabolically active tissues such as CNS, skeletal muscle, heart, liver, pancreas, and adipose tissue (Dominissini et al., 2012). Human metabolic illnesses including obesity, metabolic syndrome, and cancer have all been linked to m6A. In numerous populations, the *FTO* risk variants are strongly associated with hyperglycemia, insulin resistance, and diabetes mellitus (Frayling et al., 2007; Krüger et al., 2020; Yang et al., 2019). Elevated levels of FTO, METTL3, METTL14, and WTAP were seen in patients with type 2 diabetes (Shen et al., 2015; Yang et al., 2019).

A particularly high abundance of FTO in the brain and especially in the hypothalamic nuclei which regulate feeding (nucleus arcuatus, paraventricularis,

dorsomedialis, ventromedialis) suggested that FTO can be linked to appetitive behavior and food intake (Fredriksson et al., 2008). Mice lacking *Fto* have shown increased food consumption as well as increased energy expenditure (Fischer et al., 2009; Tung et al., 2010). Variations in hypothalamic *FTO* expression were observed to occur as a result of feeding for calories but did not appear during rewarding eating (Olszewski et al., 2009). However, m6A also has a substantial impact on reward learning by controlling the expression of relevant proteins in the dopaminergic signaling pathway. Dopamine receptor type 2 and type 3 signaling was impaired in the midbrain of mice by FTO depletion due to the disruption of demethylation on certain mRNAs involved in dopaminergic transmission (Hess et al., 2013). It has been demonstrated that gene variations of the FTO protein have an impact on dopamine-dependent midbrain responses to reward learning in humans (Sevgi et al., 2015).

Conversely, nutritional status and diet were observed to modulate m6A patterns. The arcuate nucleus and the whole hypothalamus both underwent changes in *FTO* mRNA levels as a result of starvation (Cheung et al., 2013; Gerken et al., 2007; Vujovic et al., 2013). Given that both up- and down-regulation have been shown, *FTO* expression fluctuations may be influenced by the degree of fasting or other circumstances. Glucose intracerebroventricular (ICV) administration was observed to increase hypothalamic *Fto* mRNA levels in fasted mice (Poritsanos et al., 2011). Hypothalamic *Fto* expression is similarly modulated by exposure to a high-fat diet, with down-regulation observed after short exposure and elevation after longer exposure (Tung et al., 2010).

On the tissue and cellular level, the metabolism of amino acids, glucose, lipids, and other metabolites, or components of cells, was shown to be regulated by m6A. In human lung adenocarcinoma cells, an altered m6A pattern was associated with stimulated glycolysis. Methylation of a transcript for a key glycolytic enzyme, alpha-enolase, was observed to promote its translation thanks to the facilitated binding of YTHDF1 (Ma et al., 2022). Through m6A-dependent mechanisms, FTO can influence the metabolism of glucose. According to research, FTO-mediated m6A mRNA demethylation controls glucose metabolism during hepatic gluconeogenesis (Mizuno and Lew, 2021). It has been established that forkhead box protein O1 (FOXO1) is a direct substrate of FTO and a crucial transcription factor for modulating gluconeogenesis. Entacapone, a proposed FTO inhibitor, lowers blood sugar via the FTO-FOXO1 pathway (Peng et al., 2019). Regulation of *FTO* mRNA was associated with the expression of genes involved in glucose homeostasis processes, e.g. genes encoding neurotrophic factors (tumor necrosis factor alpha (TNF-α), nuclear factor-kappa B (NFκB)), the ATP-sensitive inward rectifying potassium channel, insulin gene, AMP-activated protein kinase (AMPK), or activating transcription factor 4 (ATF4) (Mizuno and Lew, 2021; Pitman et al., 2012; Zhao et al.,

2014a; Zhou et al., 2018). Knockdown of FTO is accompanied by changes in ATP levels and glucose uptake rates in cells, and the course of these changes is dependent on the cell type (Pitman et al., 2012).

FTO expression changes were linked to insulin sensitivity regulation in muscle and pancreatic cells (Bravard et al., 2011; Fan et al., 2015). Hepatocyte-specific *Mettl3* knock-out mice fed a high-fat diet displayed improved insulin sensitivity due to m6A-dependent control of fatty acid synthase (Xie et al., 2019). It has been demonstrated that suppression of FTO increases the phosphorylation of protein kinase B (Akt) in skeletal muscle and endotheliocytes, which in turn reduces insulin resistance and glucose intolerance imposed on by a high-fat diet (Krüger et al., 2020). In liver tissue, FTO interacts with leptin and the signaling pathways of the signal transmitter and transcription activator 3 (STAT3), an important regulator of both mitochondrial and glucose metabolism (Bravard et al., 2011). Through controlling *FTO* expression and FTO-dependent demethylation of m6A, the energy sensor AMPK increased lipid accumulation in skeletal muscle cells (Wu et al., 2017). FTO deficiency in adipocytes leads to the uncoupling of the respiratory chain and increased production of the uncoupling protein 1 (UCP1) (Tews et al., 2013). Overall, the m6A pathway was found to be a key regulator of adipogenic processes.

In SH-SY5Y neuronal cells, siRNA-mediated suppression of *FTO* expression increased ATP concentrations while lowering glucose absorption and decreasing neuropeptide Y mRNA expression through activation of STAT3. Furthermore, phosphorylation of AMPK and Akt was reduced by FTO siRNA (Pitman et al., 2012). Overexpression of functional FTO in neuronal SK-N-SH cells caused FTO to interact with CAMK2, which delayed cAMP-response element binding protein (CREB) dephosphorylation and increased the levels of BDNF and neuropeptide Y receptor 1 (NPY1R) (Lin et al., 2014). Both of these proteins have been previously identified in relation to energy homeostasis (Thorsell and Heilig, 2002; Yang et al., 2016).

Studies investigating the role of m6A in energy metabolism of glial cells are still very scarce. So far, most of the work with respect to glial metabolism has focused on cancer research and the role of m6A in the metabolic reprogramming of tumor cells. By targeting the long non-coding RNA X-inactive specific transcript (XIST), m6A can contribute to the regulation of glucose metabolism in glioma cells, the most common adult brain tumor (Cheng et al., 2020; Patil et al., 2016). In comparison to neural progenitor cells, glioma stem cells exhibited more frequent m6A modification peaks at transcripts relevant to metabolic pathways (Li et al., 2019). Zhang and colleagues showed that the m6A demethylase *ALKBH5* is abundantly expressed in glioblastoma stem cells. Furthermore, the authors observed that ALKBH5 demethylates the nascent transcripts of forkhead box protein M1 (FOXM1) and boosts its expression (Zhang et al., 2017). Transcription factor

FOXM1 is associated with control of the cell cycle and the proliferation of tumor cells. In addition, FOXM1 exerts a significant regulatory influence over the metabolic reprogramming of tumor cells. When *FOXM1* expression is inhibited, expression of glucose transporter 1 and hexokinase 2 are markedly reduced (Shang et al., 2017; Wang et al., 2016). In addition, FOXM1-deficient cells display lower oxygen consumption rates under basal conditions and reduced mitochondrial reserve respiratory capacity.

Various data support a connection between mitochondrial metabolism and m6A alteration. Roles of m6A in mitochondrial function will be reviewed further in the chapter *Mitochondrial impairment*.

2.4 Role of m6A in Alzheimer's disease

The most common form of dementia, Alzheimer's disease (AD), is brought on by abnormal changes in the brain. AD results in memory loss, confusion, behavioral abnormalities, and a progressive loss of mental capabilities. The early-onset (familiar) AD is believed to be primarily caused by the altered genetic background of three genes: amyloid-beta precursor protein (*APP*), presenilin 1 and 2 (*PSEN1, PSEN2*). However, the majority of AD cases (about 95%) are late-onset (also known as sporadic AD), for which the origin is still unclear, despite the numerous risk factors connected to this illness (Piaceri et al., 2013). The traditional amyloid cascade hypothesis centered on the abnormal buildup of the amyloid-beta peptide as the main starting component involved in AD pathogenesis. Deposition of the amyloid-beta peptide into plaques, which eventually results in the generation of neurofibrillary tangles, cell death, and dementia was hypothesized to be the primary event in the pathogenesis of AD (Hardy and Higgins, 1992). However, a great deal of evidence has been accumulated over the past several years that opposes the idea that the amyloid cascade is the key factor in disease pathogenesis, especially in the case of sporadic AD. First of all, neuritic plaques have been frequently demonstrated to be present in the brains of individuals with normal cognitive function. Also, the density of plaques and the severity of dementia have a low correlation (Demetrius et al., 2015). Although it may contribute to the development of the illness, it appears that cerebral amyloid-beta peptide is not the primary pathogenetic component for the onset of AD.

Thus, new elements have begun to be identified as potential contributions to the early etiology of this neurodegenerative illness, including neuroinflammation and altered brain bioenergetics. Various investigations have found that the inflammatory processes that occur in the brain during AD are associated with neuroglia activation (Hashioka et al., 2021). The mitochondrial cascade hypothesis, on the other hand, is linking the decline in mitochondrial function with faster brain aging and development of AD symptoms

(Swerdlow and Khan, 2004). The Inverse Warburg hypothesis is another bioenergetic model that is based on metabolic reprogramming towards up-regulated oxidative phosphorylation (OXPHOS) in neurons with inefficient energy utilization, resulting in oxidative stress and further mitochondrial damage (Demetrius et al., 2015).

Recently, the significance of m6A alteration in AD has been the subject of an increasing number of studies. Changes in the *FTO* gene have been linked to an increased risk of developing a variety of neuropathological disorders, including stroke, epilepsy, depression, poor cognitive function, and Alzheimer's dementia (Ho et al., 2010; Keller et al., 2011; Rivera et al., 2012; Rowles et al., 2012; Timpson et al., 2009). Furthermore, m6A has been discovered to be a conserved epitranscriptomic alteration in a variety of neurodegenerative disorders, including AD (Engel et al., 2018; Hess et al., 2013; Shafik et al., 2021). Memory deficits, neurotoxic compound buildup, oxidative stress, neuroinflammatory response, and mitochondrial malfunction are just a few of the disorders associated with AD that have been connected to RNA m6A methylation.

2.4.1 Amyloid-beta and tau pathology

One of the main pathological characteristics of AD is the buildup of insoluble neurotoxic aggregates, such as extracellular amyloid-beta plaques and intracellular tau neurofibrillary tangles. Their accumulation can contribute to neuronal degeneration and synaptic dysfunction (Lane et al., 2018). In human postmortem AD samples, Huang discovered METTL3 accumulation in the insoluble fractions, which was positively correlated with the amount of insoluble tau neurofibrillary tangles. This was accompanied by an altered distribution pattern and increased levels of METTL3 in the AD hippocampus. The authors hypothesized that METTL3 is likely undergoing aberrant misfolding and/or aggregation similar to the typical aggregation of misfolded proteins in AD (Huang et al., 2020).

Amyloid-beta peptides are produced by successive cleavage of APP by beta-secretase and gamma-secretase at the plasma membrane. An involvement of m6A RNA methylation in amyloid-beta regulation was suggested when folic acid-induced elevation of the source molecule of m6A, SAM, was accompanied by reduced production of amyloid-beta (N. Li et al., 2021; Li et al., 2015). Through the control of *APP* mRNA translation caused by the binding of m6A reader FMRP, it appears that m6A methylation also altered the levels of the APP (Chang et al., 2017; Edens et al., 2019). Additionally, it was discovered that inhibition of the m6A reader hnRNPA2B1 resulted in abnormal splicing of the beta-secretase 1 transcript (Kolisnyk et al., 2017). The glioblastoma stem cells experienced an altered m6A pattern and changed expression of the disintegrin and

metalloproteinase domain-containing protein 19 (ADAM19) mRNAs as a result of METTL3 or METTL14 knockdown (Cui et al., 2017). Due to its inherent alpha-secretase activity, ADAM19 can take part in the non-amyloidogenic processing of the precursor protein APP (Tanabe et al., 2007). Interestingly, an amyloid-beta 1-40 peptide treatment of RPE cells resulted in increased levels of FTO, but FTO inhibition further aggravated the amyloid-beta 1-40-induced cell degeneration (Hu et al., 2022). In rat primary cortical neurons, amyloid-beta treatment was observed to decrease levels of METTL3 and alter the expression of synaptic scaffold proteins such as postsynaptic density protein 95. Conversely, overexpression of METTL3 was found to prevent the loss of this synaptic protein caused by beta-amyloid. In addition, overexpression of METTL3 in amyloid-beta-induced mice AD model reversed synaptic degeneration and cognitive impairment (Zhao et al., 2021).

Amyloid-beta aggregation causes alterations in kinase/phosphatase activity which results in tau protein hyperphosphorylation. Once hyperphosphorylated, tau dissociates from microtubules promoting destabilization of the cytoskeleton. Moreover, unbound tau molecules aggregate into massive fibril formations creating a toxic environment. The first evidence of a link between FTO and tau phosphorylation was provided by Pitman and colleagues using human neuroblastoma SH-SY5Y. With the use of FTO knockdown, they observed reduced levels of tau phosphorylation at Ser 396 residue (Pitman et al., 2013). AMPK was hypothesized to participate in this process for its phosphorylation state was affected by FTO knockdown in the former work of Pitman's group (Pitman et al., 2012). A direct connection between FTO, tau, and AD was provided by Li et al who manipulated levels of FTO neurons isolated from 3xTg AD mice. In their work, FTO knockdown reduced levels of tau phosphorylation (Ser 262) whereas FTO overexpression resulted in the opposite effect. Changes in the tau phosphorylation state appeared to be dependent on participation of the mammalian target of rapamycin (mTOR) (H. Li et al., 2018). The loss of m6A by reduction of METTL3, METTL14, or YTHDF levels exacerbated tau toxicity and led to more pronounced locomotive deficits in the fruit fly AD model, which expresses the human disease tau isoform (Shafik et al., 2021).

2.4.2 Mitochondrial impairment

The central nervous system requires about 20% of the body's total basal oxygen consumption to maintain neuronal energy demand. Mitochondria, which are responsible for the majority of energy production in cells, are also one of the main sites of reactive oxygen species (ROS) production and play a crucial role in apoptotic responses. Numerous studies have shown that mitochondrial abnormalities are important contributors to the pathogenesis of neurodegenerative diseases, such as AD, where they appear to be

both an early trait and a late-phase contributor. Even before neurofibrillary tangles and senile plaques appeared in the brains of AD patients, there was evidence of mitochondrial malfunction (Lim et al., 2020). Amyloid-beta can have an impact on the mitochondrial electron transport chain and ultimately cause oxidative stress due to increased ROS generation (Parks et al., 2001).

The mammalian mitochondrial genome encodes a set of 2 rRNAs, 22 tRNA, and 13 mRNA, all of which are essential for proper mitochondrial function. Similarly to RNAs of nuclear origin, mitochondrial RNAs (mtRNAs) have been described to undergo dynamic post-transcriptional modifications (reviewed e.g. in (Morena et al., 2018)). These modifications are often important for the normal function of mitochondrial gene expression machinery. The dysfunction of several enzymes responsible for epitranscriptome modifications was connected to oxidative phosphorylation impairment (Garone et al., 2017; Trixl et al., 2018).

Although m6A in mtRNA has been so far described solely in plants (Z. Wang et al., 2017), two adenosine dimethylations (m62A936 and m62A937) have been found in mitochondrial 12S rRNA in mammals. Loss of dimethyltransferase responsible for m62A - mitochondrial transcription factor B1, has been reported to affect mitoribosome assembly and consequently translation of mitochondrial genes (Metodiev et al., 2009).

Several lines of evidence point to a link between m6A modification and mitochondrial metabolism. Such results were almost exclusively gained by manipulating enzymes participating in the m6A pathway, which are mostly localized to the nucleus or cytoplasm. Myotubes overexpressing FTO exhibited mitochondrial dysfunction which manifested as reduced oxidative phosphorylation and enhanced oxidative stress (Bravard et al., 2011). FTO-deficient adipocytes underwent mitochondrial uncoupling induced by higher UCP1 levels (Tews et al., 2013). Cheng and co-authors saw an increased mitochondrial mass in hematopoietic stem cells from m6A methyltransferase Mettl3 conditional knockout mice (Cheng et al., 2019). The role of yeast m6A methyltransferase Ime4 in mitochondrial functions has also been reported (Yadav and Rajasekharan, 2018). Mammalian AlkB homolog 1 (ALKBH1) which possesses a wide range of enzymatic activities including m6A demethylase activity was shown to be primarily localized in mitochondria. Although its function is still poorly understood, ALKBH1-deficient HEK293 cells showed altered mitochondrial DNA (mtDNA) copy number and mitochondrial impairment (Müller et al., 2018).

Signaling pathways related to mTOR are participating in key cellular bioenergetics processes. Disruption of mTOR signaling cascades has been considered a major risk factor for AD and is indicated to play a considerable role in AD pathology (Yates et al., 2014). FTO and mTOR relationship was observed in various cell types. Mouse embryonic

fibroblasts (MEFs) and HEK293 lacking FTO displayed decreased activation of mTOR complex 1 (mTORC1) (Gulati et al., 2013). mTOR signaling induced nuclear FTO accumulation dependent on estrogen receptor alpha (Zhu et al., 2016). In mouse primary myoblasts, FTO down-regulation suppressed mitochondria biogenesis and energy production, likely by affecting the activity of the mTOR and peroxisome proliferator-activated receptor-gamma coactivator-1 alpha (PGC-1α) pathway (X. Wang et al., 2017). Altered FTO expression in clear cell renal cell carcinoma had an effect on mitochondrial activity and ROS production by regulating PGC-1α mRNA and consequently its protein levels (Zhuang et al., 2019).

The first demonstration of a connection between m6A and mitochondrial activity in neuronal cells was shown by Chen and colleagues. Human SH-SY5Y and rat PC-12 cells with overexpressed FTO developed elevated mitochondrial-generated oxidative stress and lower respiratory complex II activity (X. Chen et al., 2019). Shi proposed that nuclear receptor-interacting protein 1, a gene required for mitochondrial control, is less expressed because of the activity of METTL3, resulting in preserved mitochondrial function in Down syndrome-affected brain tissue (Shi et al., 2021).

An indirect proof of a relationship between RNA methylation and mitochondrial function has been observed through the usage of betaine and cycloleucine, a methyl donor and an inhibitor of methylation, respectively. Several research groups described the ability of both betaine and cycloleucine to regulate m6A RNA methylation levels (J. N. Chen et al., 2019; Kang et al., 2018; Xinxia Wang et al., 2015). Zhou and coworkers observed a connection between betaine and m6a methylation in adipose tissue. In their work, betaine treatment was followed by lowered FTO levels and a corresponding increase in m6a methylation. Furthermore, betaine affected levels of mitochondrial proteins PGC-1α and carnitine palmitoyltransferase (Zhou et al., 2015). Betaine supplementation was sighted to enhance mitochondrial respiration *in vivo* (Singhal et al., 2020) as well as *in vitro* (Lee, 2015; L. Zhang et al., 2019). However, it is important to keep in mind that betaine can act as a methyl donor in multiple metabolic pathways and therefore its effect on mitochondrial metabolism cannot be simply explained by RNA methylation.

2.4.3 Neuroinflammation and oxidative stress

Innate immune cells in the CNS, principally microglia and astrocytes, produce pro-inflammatory cytokines and reactive oxygen species during the inflammation process within the brain, known as neuroinflammation. Although neuroinflammation serves as a defense mechanism against pathogenic attack or cellular stress, it has been shown that it is chronically activated and exerts harmful consequences in various neurodegenerative

diseases. Synaptic dysfunctions, the suppression of neurogenesis, and cell death can result from the release of pro-inflammatory chemicals and an unbalanced ROS environment (Kwon and Koh, 2020).

The role of m6A has been observed both in inflammatory processes on the periphery and within the CNS. Several major inflammatory mediators (interleukin (IL)-6, TNF-α, toll-like receptor, NFκB) showed higher m6A levels (Chokkalla et al., 2019). It has been proposed that the m6A-binding protein YTHDF2 aggravates the inflammatory responses of macrophages (Yu et al., 2019). As a result of the loss of FTO, macrophages were observed to switch into pro-inflammatory M1-type macrophages (Gu et al., 2020). FTO was further associated with response to lipopolysaccharide (LPS) stimulation. LPS treatment was shown to result in changes in FTO levels (Luo et al., 2021; Zhang et al., 2013), and also lowered abundance of m6A decoration of specific transcripts and induced translation of alternative FTO variant (cFTO4) (Zhang et al., 2016). The expression of RNA demethylase METTL3 appears to be stimulated in macrophages following LPS treatment. Interestingly though, overexpression of METTL3 diminished the inflammatory response generated by LPS. The impact of METTL3 on LPS-induced inflammation in macrophages was mediated by NFκB (Jinghua Wang et al., 2019). Moreover, the levels of the m6A methyltransferase METTL3 in peripheral tissues were demonstrated to be enhanced by LPS, which was also accompanied by an increased amount of m6A (Feng et al., 2018). The METTL3 knockdown was reported to suppress the LPS-induced inflammatory response by controlling the alternative splicing of myeloid differentiation primary response 88 (*MYD88*) transcript in favor of *MYD88S*, a splice variant that reduces the production of inflammatory cytokines (Feng et al., 2018).

Within CNS, microRNA-421-3p targets YTHDF1 to impede the translation of p65 mRNA, preventing an inflammatory response in cerebral ischemia/reperfusion injury (Zheng et al., 2020). Additionally, inflammation and apoptosis brought on by ischemia and reperfusion injury were observed to be decreased following elevated expression of m6A binding protein, IGFBP3, which was induced by inhibition of miR-19a-3p (Chai et al., 2020). Silencing of METTL14 inhibited the m6A alteration of eukaryotic translation elongation factor 1 alpha 2 and stimulated the Akt/mTOR pathway, which in turn suppressed spinal cord neuron apoptotic death and secretion of inflammatory cytokines (Gao et al., 2022).

Microglia, the brain's initial line of defense against invasive infections, are activated by environmental risk stimuli to operate in a neuroprotective manner. However, continuous inflammation can result in irreparable CNS damage when microglia that have been activated for a long time emit inflammatory cytokines (IL-1β, IL-6, TNF-α, IL-18, etc.). Li et al. found that rat primary microglia that were differentiated into pro-inflammatory M1-like, anti-inflammatory M2-like, and unstimulated phenotypes had distinguishable m6A

methylation patterns, suggesting a potential regulatory mechanism during microglia's pro-inflammatory and anti-inflammatory response (Q. Li et al., 2021). A similar outcome was observed by Ding, who saw a distinct m6A methylome in LPS-stimulated microglia. These authors found that IGF2BP1, a protein that binds to m6A, was the most highly regulated m6A modifier in activated microglia. Further investigation by them revealed IGF2BP1 to be an important mediator of LPS-induced m6A alteration and microglial activation, most likely via promoting the stability of ceruloplasmin and guanylate-binding protein 11 mRNAs in an m6A-dependent manner (Ding et al., 2022). Interestingly, an m6A methyltransferase METTL3 expression was increased together with the expression of inflammatory markers (IL-1, IL-6, TNF-α, IL-18, NF-kB, and tumor necrosis factor receptor associated factor 6 (TRAF6)) in LPS-mediated microglial inflammation. METTL3 was identified to be the contributor to LPS-induced inflammation, as its overexpression in microglia increased pro-inflammatory cytokine production through activation of the TRAF6-NF-kB pathway (Wen et al., 2022).

Astrocytes are most certainly a significant contributor to AD pathogenesis and may even be substantially contributing to its initiation. Astrocyte function changes were observed in the brains of AD patients as well as in model systems (González-Reyes et al., 2017). Astrocytes can dispose of potentially neurotoxic waste products like amyloid-beta and tau through a glymphatic system (Iliff et al., 2014, 2012). In addition, astrocytes are not only the main producers of apolipoprotein E (APOE), they might even regulate APOE expression in neuronal cells (Harris et al., 2004). Genetic variations of APOE were identified as potent risk factors for sporadic AD, though their role in AD pathogenesis is still not clear as both aggregating and clearance effects on amyloid-beta were observed (González-Reyes et al., 2017).

In the hippocampus and cortex of AD patients, m6A methylation was shown to be reduced in neurons, but astrocytes and some microglia displayed higher methylation (Zhao et al., 2021). Contrarily, the m6A methylation in microglia, astrocytes, and neurons was found to be reduced in *Tyrobp*-/- mice, which exhibits similar traits to AD, including learning and memory problems as well as higher levels of phosphorylated tau and amyloid deposits in the hippocampus and cortex (Lv et al., 2022). However, more data on the function of m6A in astrocytes is virtually missing.

As a response to insults, astrocytes go through a process known as reactive gliosis, which is characterized by altered morphology, increased levels of GFAP, and the production of a variety of mediators, that affect the function of neurons and can in some scenarios lead to neuronal apoptosis. For example, gamma-aminobutyric acid and glutamate were discovered to be released by reactive astrocytes, which can cause synaptic and memory loss (Jo et al., 2014). Reactive astrocytes were found in the post-

mortem brains of AD patients (Beach and McGeer, 1988). Also, amyloid-beta treatment was shown to induce oxidative stress and ROS generation in astrocytes (Abramov et al., 2004).

Studies indicate there is a regulatory relationship between oxidative stress and m6A. Overall, the induction of oxidative stress was observed to increase m6A levels in various models (Anders et al., 2018; Arumugam et al., 2021; Zhao et al., 2019). Anders found out that the abundance of m6A modification within transcripts raised in response to oxidative stress and the YTHDF3 reader protein was recognized to selectively bind these stress-induced de novo methylation sites, indicating an important function for YTHDF3 in determining the selectivity of the stress response (Anders et al., 2018). Zhao suggested that the m6A increase in oxidative stress could be driven by elevated expression of WTAP and METTL3 (Zhao et al., 2019). But changes in other m6A machinery proteins were detected. An increase in methyltransferases (METTL3, METTL1) and readers (YTHDF1-3, YTHDC2), and a decrease in demethylases (FTO, ALKBH5) was observed following Fumonisin B1 induced ROS generation (Arumugam et al., 2021). It was also shown that modulation of m6A machinery proteins can affect the state of oxidative stress. While overexpression of METTL3 elicited inhibitory effects on apoptosis and oxidative stress induced by colistin (Jian Wang et al., 2019), oxidative stress was triggered in Von Hippel-Lindau-deficient cells with overexpressed FTO (Zhuang et al., 2019). A high level of FTO and consequently reduction of the m6A levels in dopaminergic neurons was followed by increased expression of the N-methyl-D-aspartate receptor (NMDAR) 1, oxidative stress, and Ca^{2+} influx, and ultimately resulted in neuronal loss and neuroinflammation (X. Chen et al., 2019). Knockdown of hnRNPA2/B1 caused apoptosis and production of ROS in glioma U251 and SHG44 cells. On a molecular level, hnRNPA2/B1 knockdown decreased the expression of matrix metalloproteinase-2 and phosphorylated STAT3 (Deng et al., 2016). ADAM19, a protein that is frequently elevated in human brain cancers including astrocytoma and glioblastoma and whose expression is also associated with inflammation, was affected by the knockdown of METTL3 or METTL14 (Cui et al., 2017).

2.4.4 Memory impairment

Among key clinical manifestations of AD are deficits in learning and memory. Learning and memory are believed to be based on synaptic plasticity, a capability to alter synaptic transmission strength or effectiveness in an activity-dependent manner. Several crucial mechanisms have been identified to promote synaptic plasticity, including long-term potentiation, a series of chemical reactions that lead to an increase in the strength of the synaptic connections.

Recent research shows that the buildup of m6A has a significant function in learning and memory. In response to behavioral experience, the amount of m6A rose in the medial prefrontal cortex of mice. Modified mRNAs included genes involved in neural plasticity. The observed rise in m6A levels following training was correlated with the altered abundance of FTO and the m6A methyltransferase METTL3 (Widagdo et al., 2016). It has been demonstrated that METTL3 directly affects the control of hippocampal-dependent memory formation. Long-term memory consolidation was found to be greatly improved by overexpressing METTL3 in the dorsal hippocampus of wildtype mice (Z. Zhang et al., 2018), whereas memory consolidation was found to be inhibited by METTL3 deletion in the forebrain (Z. Zhang et al., 2018; Zhao et al., 2021). Deletion of METTL14 was found to significantly impair striatal-mediated learning-related behavior and increase neuronal excitability (Koranda et al., 2018). Furthermore, cued fear memory consolidation was strengthened by targeted FTO knockdown in the medial prefrontal cortex (Widagdo et al., 2016). The levels of FTO in mouse dorsal hippocampal CA1 neurons were reduced by contextual fear conditioning (Walters et al., 2017).

Numerous m6A-modified neuronal transcripts encode proteins that affect synaptic plasticity (Chang et al., 2017). Modulation of the m6A pathway can affect the expression status of such proteins. Activity-regulated cytoskeleton-associated protein (ARC) is one such example. The activation of ARC, which is crucial for the synaptic plasticity of memory consolidation, occurs in response to learning or when long-term potentiation is induced (Korb and Finkbeiner, 2011). According to earlier research, Alzheimer's disease patients' brains exhibit aberrant ARC expression, which disrupts synaptic plasticity (Wu et al., 2011). The amyloid-beta treatment causes a drop in ARC protein levels (Wang et al., 2006). Recently, it was established that the *ARC* mRNA is the target of METTL3. While METTL3 knockdown leads to lower *ARC* mRNA m6A modification and decreased ARC protein expression, METTL3 overexpression can restore *ARC* expression that had been suppressed by amyloid-beta treatment. Similarly to METTL3, YTHDF1 was found to alter the abundance ARC (C. Xu et al., 2022). Furthermore, YTHDF1 was found to encourage the translation of target transcripts in response to neural stimulation. Mice lacking YTHDF1 exhibit deficiency in learning and memory, impaired synaptic transmission, and reduced long-term potentiation. Interestingly, similar traits were observed in mice with METTL3 depletion (Shi et al., 2018).

Kumar demonstrated a correlation between global translation inhibition and an increase in the m6A signal brought on by NMDAR stimulation. The rise in m6A levels, possibly caused by the decrease in FTO levels, was accompanied by a redistribution of m6A-marked RNAs from currently translating to inactive ribosomes. Furthermore, the

authors demonstrated that FTO inhibition suppresses NMDAR-mediated alterations in m6A levels (Kumar et al., 2022).

In Fragile-X Syndrome, the lack of FMRP results in excessive protein synthesis in dendrites, resulting in an increase in the number of dendritic spines and impaired synaptic function (Bassell and Warren, 2008; Richter et al., 2015). Hippocampal neurons that had YTHDF3 knocked down showed abundant dendritic filopodia in place of mature dendritic spines, and impaired synaptic transmission (Merkurjev et al., 2018). The dendritic loss was observed after reduced expression of hnRNPA2B1 in the entorhinal cortex (Berson et al., 2012). It is noteworthy that FTO is abundant in the nucleus, dendrites, and vicinity of dendritic spines of mouse dorsal hippocampal CA1 neurons (McTaggart et al., 2011). FTO controls the demethylation of particular mRNAs in the dopaminergic signaling pathway, shifting their expression levels and leading to modified dopaminergic transmission (Hess et al., 2013).

2.5 Streptozotocin model of Alzheimer's disease-like changes

Streptozotocin (STZ) is a glucosamine-nitrosourea molecule particularly toxic to insulin-producing beta cells. Peripherally given STZ is employed in studies to generate experimental diabetes mellitus type 1 and 2 (Akinlade et al., 2021). Nevertheless, ICV administration of STZ is regarded as an *in vivo* experimental model of sporadic AD. ICV injection of STZ was demonstrated to cause memory impairment, altered cholinergic neurotransmission, astrogliosis, oxidative stress, abnormalities in cerebral oxidative energy metabolism, and mitochondrial disruption, which are all symptoms that accompany AD (Grieb, 2016).

Several investigations on cultured brain cells attempted to demonstrate at a cellular level the changes symptomatic of AD pathology that are regularly found in animal models, despite the fact that the *in vitro* STZ model is not as widely utilized as its *in vivo* counterpart. STZ treatment of mouse neuronal N2A cells resulted in decreased cholinergic signaling, beta-amyloid accumulation, tau hyperphosphorylation, reduced glucose uptake, raised mitochondrial stress, increased apoptosis, and DNA damage, according to Biswas (Biswas et al., 2016). The same group compared STZ-mediated alterations in neuronal N2A and astrocytic C6 cell lines in a subsequent investigation. Their findings revealed that apoptosis and the cellular stress response to STZ occur in a reasonably consistent manner on a biochemical level, regardless of cell type (Biswas et al., 2017). Similarly, hallmarks of AD such as neuronal apoptosis, synaptic loss, and tau hyper-phosphorylation, as well as mitochondrial fragmentation were seen in STZ-challenged hippocampal HT-22 cells (Park et al., 2020).

3 Aims of the thesis

Brain development and energy homeostasis have been closely linked to RNA demethylase FTO. *FTO* expression alterations are related to changes in energy balance, and these modifications may be harmful to one's health. Recent theories suggest that bioenergetic state disruption may contribute to the development of neurodegenerative diseases, such as the etiopathogenesis of Alzheimer's disease. This study focused on the function of FTO in model glial and neuronal cells. The goal was to analyze how FTO inhibition affects cell differentiation, oxidative metabolism, and the expression profile of selected proteins essential for neuroenergetics, and to see whether modulation of FTO function has an impact on the resilience of cells towards streptozotocin, an *in vitro* model of AD pathogenesis.

AIM 1 – *In vitro* model of neurons, SH-SY5Y cell line

- 1.1 The effect of FTO inhibition on differentiation of SH-SY5Y cells.
- 1.2 The impact of FTO inhibition on protein profiling of undifferentiated and differentiated SH-SY5Y cells.
- 1.3 The role of FTO inhibition on mitochondrial oxygen consumption and glycolysis of differentiated SH-SY5Y cells.
- 1.4 The role of FTO inhibition in the resilience of differentiated SH-SY5Y cells towards streptozotocin.

AIM 2 – *In vitro* model of astrocytes, CCF-STTG1 cell line

- 2.1 The effect of FTO suppression on mitochondria and energy metabolism of CCF-STTG1 cells.
- 2.2 FTO suppression-induced alterations of proteome of CCF-STTG1 cells.
- 2.3 The role of FTO inhibition in sensitivity of CCF-STTG1 to streptozotocin.

4 Methods

4.1 Reagents and chemicals

Fetal bovine serum, Dulbecco's modified Eagle's medium and Ham's F-12 nutrient medium were from Gibco (purchased from Thermo Fisher Scientific, Waltham, MA, USA). Laemmli sample buffer was from Bio-Rad (Hercules, CA, USA). Sucrose, Tris, HEPES, acrylamide and bisacrylamide were purchased from SERVA (Heidelberg, Germany). Pyruvate, ADP and cytochrome c were obtained from Boehringer Ingelheim (Ingelheim, Germany). SuperSignal West Dura chemiluminescent substrate was from Pierce Biotechnology (Rockford, IL, USA). Annexin V Dyomics 647 and Annexin V binding buffer were from Exbio (Vestec, Czech Republic). The lipofectamine RNAiMAX reagent, SilencerTM Select Negative Control No. 2 siRNA (4390846), FTO siRNAs (s35510 and s35512), Hoechst 33342, Hoechst 33258, MitoTracker Green FM, MitoTracker Red CMXRos were all from Invitrogen (Carlsbad, CA, USA). An inhibitor of FTO, MO-I-500, was kindly provided by Mark Olsen (Glendale, AZ, USA). Unless otherwise noted, all other compounds were obtained from Sigma Aldritch (St. Louis, MO, USA).

Anti-mouse and anti-rabbit secondary antibodies were purchased from GE Healthcare (Chicago, IL, USA). Primary antibodies against BCL-2, PARP1, NRF2, CASP3, AMPKa1/2, phospho-AMPKa1/2 (T172), GFAP, YTHDF3, TH, MAP2, TUBB3, nestin, tau, GAP43, ENO1, alpha-tubulin, GRP75, PRX2, PRX6, mTOR, phospho-mTOR (S2448), p70S6K, phospho-p70S6K (T389), actin and GAPDH were obtained from Santa Cruz Biotechnology. Anti-ERK1/2, anti-phospho-ERK1/2 (T202/Y204), anti-Akt, anti-phopsho-Akt (S473), anti-IRβ, anti-IRS-1, anti-IRS-2, anti-SIRT1, anti-YTHDF1 and YTHDF2 antibodies were purchased from Cell Signaling Technology. Antibodies towards BAX, FTO, ALKBH5, METTL3, YTHDC1, YTHDC2, PGC-1α and OXPHOS coctail were obtained from Abcam. Antibodies for SDHA, SYP and NSE were from Thermo Fisher Scientific.

4.2 *In vitro* models

The human astrocytoma cell line CCF-STTG1 and the human neuroblastoma SH-SY5Y cell line were obtained from the European Collection of Authenticated Cell Cultures (ECACC). Another origin of the SH-SY5Y neuroblastoma cell line that was used in this study was from the American Tissue Culture Collection (ATCC). CCF-STTG1 cells were cultured in high glucose (4500 mg/L) Dulbecco's modified Eagle's medium with 10% fetal bovine serum (FBS) and 1% antibiotic antimycotic solution. SH-SY5Y cells were

maintained in a 1:1 mixture of high glucose (4500 mg/L) Dulbecco's modified Eagle's medium and Ham's F-12 nutrient medium, supplemented with 10% FBS and 1% antibiotic antimycotic solution. Both cell lines were kept at 37°C in a 5% CO_2 and saturated humidity environment. The cells employed in the tests ranged from the 5th to the 17th passage. The cells were grown in a low-serum medium (0.5-1% FBS) for an hour before and during times of experimental treatments to remove growth factors.

4.3 Neuronal differentiation

At 50% confluence, 10 μM all-trans retinoic acid (RA) dissolved in dimethyl sulfoxide (DMSO) was used to promote differentiation of ATCC-purchased SH-SY5Y cells. Differentiation lasted 6 days, with the reduced FBS (1%) cultivation medium containing RA being replenished every other day. All retinoid studies were carried out in the dark. Differentiation of SH-SY5Y obtained from ECACC continued after 5 days of RA treatment with additional 3-day incubation of cells with 0% FBS cultivation medium supplemented with brain-derived neurotrophic factor (BDNF) (50 ng/mL).

4.4 Neurite outgrowth

In the absence or presence of RA, SH-SY5Y cells were sown in six-well plates and cultured for six days. The cellular morphology was captured using a CCD digital camera (Tucsen TCC-5.0ICE) and an inverted microscope (Arsenal AIF 5013i-T). The five longest neurites from at least 10 random fields in each well were assessed using ImageJ tracing plug-in NeuronGrowth (Fanti et al., 2008) to determine neurite outgrowth. The neurite length was calculated by measuring the distance between the cell soma's center and the neurite tip. Neurites that were not entirely caught in the field of view and lacked either the cell body origin or the terminal point were not included in the analysis. The average neurite length was calculated using data from at least three separate differentiation experiments.

4.5 Experimental treatment

Cell transfection. The lipofectamine RNAiMAX reagent was used to transiently transfect cells according to the manufacturer's instructions. For 48 hours, cells were transfected with FTO siRNA or a negative control siRNA. The cells were cultured in fresh media for 24 hours after transfection before being subjected to further tests. The Silencer Select Negative Control No. 2 siRNA (4390846) was employed as a negative control since it does not target any gene product. FTO was silenced using a 1:1 combination of two FTO siRNAs (s35510 and s35512).

Inhibitor treatment. Stock solutions of 10 mM rhein dissolved in 0.1 M NaOH and 10 mM MO-I-500 in DMSO were prepared and kept in small aliquots at –20°C for up to a month. To inhibit FTO, cells were treated either with 10 μM rhein for 24 hours or 1 μM (SH-SY5Y) and 10 μM (CCF-STTG1) MO-I-500 for 72 hours. The control groups were always given the appropriate vehicle treatment.

Streptozotocin treatment. Streptozotocin (STZ) was dissolved in dH_2O immediately before its administration to the culture medium. Except for the viability screening experiments, which employed a wide range of doses (0.1-18 mM), all subsequent tests were conducted with cells exposed to 1.5 mM (SH-SY5Y) or 15 mM (CCF-STTG1) STZ for 48 hours. For combined experiments with the inhibitor, MO-I-500 was added to the cells 24 hours before STZ was added, and the cells were subsequently cultured in the presence of both drugs for the following 48 hours. Experimental groups without MO-I-500 and/or STZ received the proper vehicles (0.1% DMSO and/or 5% (v/v) dH_2O).

4.6 Cell viability tests

MTT. Mosmann's described technique (Mosmann, 1983) was used to determine cell viability. Cells were seeded at a density of 2 x 10^4 cells/well in 96-well plates 24 hours before experimental treatments. After treatment, the cells were incubated for 3 hours at 37°C in the presence of 3-(4,5-dimethyl-2-thiazolyl)-2,5-diphenyl-2H-tetrazolium bromide (MTT) at a concentration of 0.2 mg/mL in fresh DMEM supplemented with 0.5% FBS. After the time had passed, all except 15 uL of media was carefully discarded from each well without disrupting the cell layer, and the formed purple formazan crystals were dissolved with 60 uL of DMSO. The absorbance of the resulting colored solution, which reflects cell viability, was measured at 540 nm with a BioTek Synergy HT microplate reader.

LDH. A Cytotoxicity Detection Kit (Roche Applied Science, Basel, Switzerland) was used to measure the activity of released cytoplasmic lactate dehydrogenase (LDH) into the culture medium, according to the manufacturer's instructions. The input material was a culture medium from 2 x 10^4 cells growing in 96-well microplates. A shift in absorbance at 490 nm due to the LDH-driven reduction of tetrazolium salt to formazan was measured using a microplate reader (BioTek Synergy HT).

4.7 Determination of alpha-enolase activity

An ENO1 Human Activity Assay (Abcam, Cambridge, UK) was used to measure the activity of alpha-enolase. The assay procedure and sample preparation were carried out along with the manufacturer's instructions. Briefly, SH-SY5Y cells were collected by

scraping them off the flask and centrifugation (500 x g, 10 min, 4°C) followed by two-times rinse with cold PBS. The cell pellets were lysed in an extraction buffer and the protein content was determined using the bicinchoninic acid (BCA) assay. To capture the enzyme, samples (5 µg) were transferred to an assay microplate pre-coated with an alpha-enolase antibody. Following the addition of substrate solution containing 2-phospho-D-glycerate absorbance at 340 nm was measured with a plate reader (BioTek Synergy HT) using a kinetic read mode. The activity of enolase is assessed as a decrease in absorbance at 340 nm as a result of a linked reaction to the consumption of NADH.

4.8 Flow cytometry

Detection of Apoptosis. Annexin V/Hoechst 33258 staining and flow cytometric analysis were used to evaluate the rate of apoptosis or necrosis. Before the experimental treatments, cells were seeded at a density of 10^5 cells per well in 24-well plates for 24 hours. Cells were collected by trypsinization after drug treatment, washed twice with phosphate-buffered saline (PBS), and resuspended in an Annexin binding buffer. After that, samples were incubated in the dark on ice and with 5 uL of Dyomics 647-labeled Annexin V for 30 minutes. Cells were then washed once in Annexin binding buffer and stained with Hoechst 33258 (1 mg/mL). Finally, the fluorescence was measured using a flow cytometer (BD LSR II) and the data were analyzed using Kaluza 2.1 software.

Measurement of Mitochondrial Membrane Potential and Mitochondrial Mass. MitoTracker Red CMXRos and MitoTracker Green fluorescent dyes were used to assess the mitochondrial membrane potential (MMP) and mitochondrial mass, respectively. While the MitoTracker Red probe's fluorescence intensity is reliant on MMP, MitoTracker Green dye accumulates in mitochondria independent of MMP, making it an useful approach for measuring mitochondrial mass. Approximately 10^5 experimentally treated cells were incubated in the dark for 30 minutes at 37°C with both MitoTracker probes (40 nM) in wells of a 24-well size microplate. The cells were then harvested using trypsin, washed with PBS, and the fluorescence was quantified using a flow cytometer (BD LSR II). The results were assessed using the Kaluza 2.1 program.

4.9 Detection of intracellular reactive oxygen species

The dihydroethidium (DHE) fluorescent probe, which primarily detects superoxide and hydrogen peroxide, was used to measure the generation of reactive oxygen species (ROS). On 24-well plates, CCF-STTG1 cells were seeded and given pharmacological treatments in accordance with the information in the *Cell treatments* section. Following a

rinse in fresh growth media, cells were live-stained at 37°C for 30 min in the dark with DHE (10 µM) and Hoechst 33342 (1 µg/mL). Due to its capacity to block complex III of the mitochondrial electron transport chain, antimycin A (3 µM) was utilized as a positive control for ROS production. Cells were then rinsed three times with 37°C PBS and examined using a fluorescence microscope (Arsenal AIF 5013i-T, 10 x eyepieces and 20 x objective lens). Average cellular DHE fluorescence intensity and percentage of DHE-positive cells were quantified from the assessment of fluorescence microscopy images using ImageJ software. Individual cells were segmented using the signal from Hoechst 33342 positive cells.

4.10 RNA isolation and m6A quantification

Isolation of total RNA and purification of mRNA. RNAzol RT reagent (Molecular Research Center, Cincinnati, OH, USA) was used to separate total RNA from cells. The Dynabeads mRNA DIRECT Purification Kit (Invitrogen, Carlsbad, CA, USA) was then used to extract mRNA from total RNA. Both isolation processes were carried out according to the manufacturer's guidelines. NanoDrop One (Thermo Fisher Scientific, Waltham, MA, USA) was used to determine the concentration and purity of RNA.

Quantification of m6A in mRNA. The EpiQuik m6A RNA Methylation Quantification Kit (Epigentek, Farmingdale, NY, USA) was used to assess global m6A levels in isolated mRNA, following the manufacturer's recommendations and utilizing 200-300 ng input.

4.11 Cell lysis and protein extraction

Seeded cells were rinsed twice with ice-cold PBS and extracted by scraping. After centrifugation (1000 x g, 10 min, 4°C), the cell pellet was resuspended in protease and phosphatase inhibitor-containing RIPA buffer (50 mM Tris, 150 mM NaCl, 1 mM ethylenediaminetetraacetic acid, 0.5% sodium deoxycholic acid, 0.1% sodium dodecylsulfate, and 1% NP-40; pH 7.4) and homogenized by passing the lysate through a 22-gauge needle 20 times). Cell homogenates were subjected twice to sonication for 30 seconds at 50% power with an ultrasonic homogeniser (Bandelin SONOPULS HD 2070.2) and held on ice for 15 minutes with vortexing every 3 minutes. To separate cell debris, homogenates were centrifuged (14000 x g, 15 min, 4°C) and the supernatant was collected.

4.12 Protein determination

The bicinchoninic acid (BCA) test was used to assess the protein content. Cell lysates were incubated at 37°C for 30 min in the presence of cupric ions, BCA, and an alkaline environment before the absorbance at 562 nm was measured using a microplate reader (BioTek Synergy HT).

4.13 Gel electrophoresis and Western blot analysis

For use in sodium dodecyl sulfate polyacrylamide gel electrophoresis (SDS-PAGE), cell lysate was solubilized with a Laemmli sample buffer. Samples (10-20 µg of protein) were electrophoretically separated on 7–10% polyacrylamide gels before being transferred to nitrocellulose membranes. The blocking of membranes was done as a 1 hour incubation in either 1% bovine serum albumin (for phospho-antibodies) or 5% non-fat milk, both of which were dissolved in TBS-T buffer (10 mM Tris, 150 mM NaCl, 1% (v/v) Tween 20; pH 8.0). After blocking, membranes were incubated with primary antibodies on an orbital shaker (overnight at 4°C). The secondary horseradish peroxidase-labeled antibody was applied for 1 hour at room temperature after a brief wash of membranes in TBS-T. Both primary and secondary antibody incubations were done in 1% non-fat milk TBS-T. Following a subsequent brief wash of membranes in TBS-T, the protein bands were visualized by chemiluminescence detection with SuperSignal West Dura chemiluminescent substrate in accordance with the manufacturer's instructions and captured on a film in the dark.

4.14 Protein extraction for isoelectric focusing

Cells were washed twice with cold PBS, harvested by scraping them off the flask, collected by centrifugation (1000 x g, 10 min), and kept at -80°C until further sample processing. The cell pellets were resuspended in TE buffer (10 mM TRIS, 1 mM EGTA; pH 7.5) containing protease inhibitors and sonicated 10 times with 5 second burst at 60% amplitude using an ultrasonic homogeniser (Bandelin SONOPULS HD 2070.2). The cell lysates were centrifuged at 3000 x g for 5 min (4°C) in order to remove cell debris. The BCA test was used to determine the total protein content of supernatant collected from cell lysates. Samples (1 mg of protein) were precipitated in ice-cold acetone and then processed in accordance with the previously detailed methodology (Ujcikova et al., 2016) (Ujcikova 2016). The samples were then placed into the reswelling tray.

4.15 Two-dimensional electrophoresis

In an Immobiline DryStrip reswelling tray (GE Healthcare), the pH 3-11 NL immobilized pH gradient gel strips were rehydrated overnight in the sample-containing rehydration solution. Isoelectric focusing was performed at 14°C using a Multiphor II device (GE Healthcare). Step-by-step, the voltage was raised from 150 V (2 hours) to 500 V (1 hour), then to 3500 V (12 hours), and then to 500 V (3 h). Before being subjected to SDS-PAGE, the strips were washed with ultrapure water, quickly dried on filter paper, and adjusted in an equilibration buffer containing 1% dithiothreitol. The strips were then equilibrated for 10 min in an equilibration buffer containing 2.5% iodoacetamide (IAA) and covered with 0.5% agarose. SDS-PAGE was run vertically at a constant current of 90 mA. The equipment was maintained at 15°C using the Hoefer SE 600 Unit (GE Healthcare).

The freshly prepared 2D gels were immediately fixed by soaking for 1 hour in a fixing solution (50% methanol and 7% glacial acetic acid) and then incubated overnight with a gentle agitation in colloidal Coomassie Brilliant Blue G-250 (CBB) staining solution (17% ammonium sulphate, 34% methanol, 3% orthophosphoric acid, and 0.1% Coomassie G-250) as described by Fountoulakis (Fountoulakis et al., 1999). Ultrapure sterile water was used for the destaning process. Gels stained with CBB were kept at 4°C in 1% acetic acid.

Gels were scanned using an Epson Perfection 4990 photo desktop scanner, and PDQuest software (Bio-Rad, version 7.3.1) was used to quantify spot densities as described previously (Ujcikova et al., 2016). Only proteins whose level changed by at least a two-fold (Student's t-test, $p \leq 0.05$) were chosen for MS.

4.16 Protein identification by MALDI-TOF/MS-MS

Sample preparation and MALDI-TOF/MS-MS analysis were carried out in accordance with previously established techniques (Ujcikova et al., 2016, 2014). Selected CBB-stained spots were removed from the gels, fragmented, and then combined with buffer A (50 mM ammonium bicarbonate and 50 mM DTT in 50% acetonitrile) in microcentrifuge tubes. After 5 minutes of sonication, the supernatant was removed and the gel pieces were combined with buffer A containing 50 mM IAA and then sonicated once more. The supernatant was removed and the samples were resuspended in buffer A containing 50 mM DTT and sonicated for the third time to eliminate any excess IAA. The supernatant was then discarded and samples were sonicated for 5 minutes in ultrapure water. Following the removal of the water, samples were sonicated additionally for five minutes in acetonitrile. Acetonitrile was discarded before the addition of trypsin (5 ng in

10 µL of 50 mM buffer A) for overnight incubation of the gel fragments at 37°C. Trifluoroacetic acid and acetonitrile were then added, at final concentrations of 1% and 30%, respectively, to stop the proteolysis. After 10 minutes of sonication, an 0.5 mL aliquot of the trypsin digest was placed onto the MALDI target and left to dry. A small drop of an alpha-cyano-hydroxycinnamic acid solution (2 mg/mL in 80% acetonitrile) was then placed on the area with the dried trypsin digest and allowed to dry. A 4800 Plus MALDI TOF/TOF analyzer (Applied Biosystems/MDS Sciex) equipped with a Nd:YAG laser (355 nm, 200 Hz) was used for MALDI-TOF/MS-MS measurements.

In-house Mascot server 2.2.07 was used to analyze the data, and it was matched against the comprehensive Uni_human_reviewed database (20273 sequences; 11324606 residues). The following database search criteria were used: enzyme = trypsin; taxonomy = Homo sapiens (Human). Cysteine carbamidomethylation, methionine oxidation and deamidation were specified as fixed or variable modifications, respectively. A maximum of two missed cleavages was allowed. Only hits that were classified as significant (MASCOT score ≥ 56, $p \leq 0.05$) were considered. Ions scores as a non-probabilistic basis for ranking protein hits were used to determine protein scores.

4.17 Protein quantification by label-free LC-MS/MS

Seeded cells were rinsed twice with ice-cold PBS and extracted by scraping. After centrifugation (1000 x g, 10 min, 4°C), the cell pellet was resuspended in protease and phosphatase inhibitor-containing TMES buffer (20 mM Tris, 3 mM $MgCl_2$, 1 mM EDTA, 250 mM sucrose; pH 7.4) and homogenized with a 22-gauge needle (20 strokes). The homogenate was mixed 1:1 with 100 mM triethylammonium bicarbonate buffer containing 2% sodium deoxycholate and sonicated using three 10 seconds bursts of a Bandelin UW 2070 sonicator (at 50% amplitude). Sonicated lysates were pelleted by centrifugation (14000 x g, 10 min, 4°C) and the supernatant was collected, adjusted to 1 mg/mL protein concentration, and stored at −80°C in small aliquots.

Mass spectrometry analysis was carried out by the Proteomic Core Facility in BIOCEV using the following protocol. Mass spectrometry samples were prepared using 20 µg input of protein. Tris(2-carboxyethyl)phosphine (10 mM) and chloroacetamide (40 mM) incubation for 30 minutes at 60°C were used for the reduction and blocking of cysteines, respectively. Trypsin was used to digest the samples overnight at 37°C (1:30 trypsin:protein ratio). After digestion, samples were acidified with trifluoroacetic acid to a final concentration of 1%. Sodium deoxycholate was eliminated using ethyl acetate extraction, and peptides were desalted using house-made stage tips packed with C18 disks (Empore) according to Rappsilber et al. (Rappsilber 2007). The LC separation of

peptides was performed using nano reversed phase columns (EASY-Spray column, 50 cm x 75 µm ID, PepMap C18, 2 µm particles, 100 Å pore size). Buffer A for the mobile phase was composed of water and formic acid at 0.1%. Acetonitrile and 0.1% formic acid comprised mobile phase buffer B. Samples were loaded onto the C18 PepMap100 trap column (5 µm particle size, 300 µm x 5 mm, Thermo Scientific) for 4 min at 18 µL/min flow rate. The loading buffer was made up of water, 2% acetonitrile, and 0.1% trifluoroacetic acid. A gradient from 4% to 35% of buffer B was used for the elution of peptides within 2 hours. By electrospray ionization, eluting peptide cations were transformed into gas-phase ions and then analyzed on a Thermo Orbitrap Fusion (Q-OT- qIT, Thermo Scientific). Using the orbitrap at 120K resolution (at 200 m/z), survey scans of peptide precursors from 350 to 1400 m/z were carried out. Tandem MS was performed using isolation at 1.5 Th with the quadrupole, HCD fragmentation with a normalized collision energy of 30, and rapid scan MS analysis in the ion trap. The maximum injection time was 35 ms, and the MS2 ion count objective was set to 104. The MaxQuant software (version 1.6.3.4) was used to analyze and quantify data. For both proteins and peptides, the false discovery rate (FDR) of 1% was used, and a minimum peptide length was set to seven amino acids. The MS/MS spectra search against the Homo Sapiens database was conducted using the Andromeda search engine. Enzyme specificity was set as C-terminal to Arg and Lys, with cleavage of proline bonds and a maximum of two missed cleavages permitted. Protein N-terminal acetylation and oxidation of methionines were specified as variable modifications for the peptide search and carbamidomethylation of cysteines was set as a fixed modification. The “match between runs” feature of MaxQuant was used to transfer identifications to other LC-MS/MS runs based on their masses and retention time (maximum deviation 0.7 min) and this was also used in quantification experiments. The label-free algorithm in MaxQuant was used to perform quantifications. The difference between the control and treatment groups was then calculated using binary logarithms of intensity ratios. Only differences of at least 1.5 fold determined for at least 2 observed values out of 3 replicates were considered.

4.18 Functional annotation and protein interaction analysis

A list of differentially regulated proteins acquired from label-free MS/MS was submitted to the DAVID bioinformatics database tool against the whole genome background of Homo sapiens. Gene ontology (GO) terms for biological function, cellular compartment, and molecular function annotated directly by the annotation source were used. Functional annotations passing the thresholds (modified Fisher Exact p-value (EASE score) ≤ 0.05, count ≥ 3) were reported.

Functional and physical protein associations within the provided list of differentially regulated proteins were researched using STRING software (version 11.5) with the minimum interaction confidence score set to 0.3 and considering the following active interaction sources: experiments, databases, co-expression. Detection of clusters of associated proteins within the STRING network was done with the MCL clustering algorithm and the inflation parameter set to 2.

4.19 Real-time determination of glycolysis

Glycolytic parameters were quantified as the extracellular acidification rate (ECAR) using the XF24 Seahorse Extracellular Flux analyser (Agilent Technologies, Inc., Santa Clara, CA, USA). In the Agilent Seahorse XF24 cell culture microplate (Agilent Technologies, Inc.), cells were plated at a density of 3 x 10^4 per well and cultured for an overnight period at 37°C with 5% CO_2. Cells were then handled in accordance with the instructions in the sections on *Neuronal differentiation* and *Experimental treatment*. On the day of the experiment, 500 µL of pre-warmed, unbuffered DMEM (#D5030, pH 7.4) with 2 mM L-glutamine was substituted for the old media. Following this, cells were incubated for 45 minutes at 37°C in a non-CO_2 incubator to culture the cells, and glycolysis was measured using the XF24 Seahorse Extracellular Flux Analyzer using optimized Glyco Stress Test design injections: 15 mM glucose, 1 µM oligomycin, and 50 mM 2-deoxyglucose (2-DG). The nuclei were stained with Hoechst 33342 (5 µg/mL) during the final injection for data normalization using cell count. The cells were counted using the Gen 5.3 software and BioTek Cytation 3 plate reader in fluorescence mode. By subtracting non-glycolytic acidification (ECAR following 2-DG), rates of glycolysis, maximal, and reserve glycolytic capacity were calculated (Fig. 5).

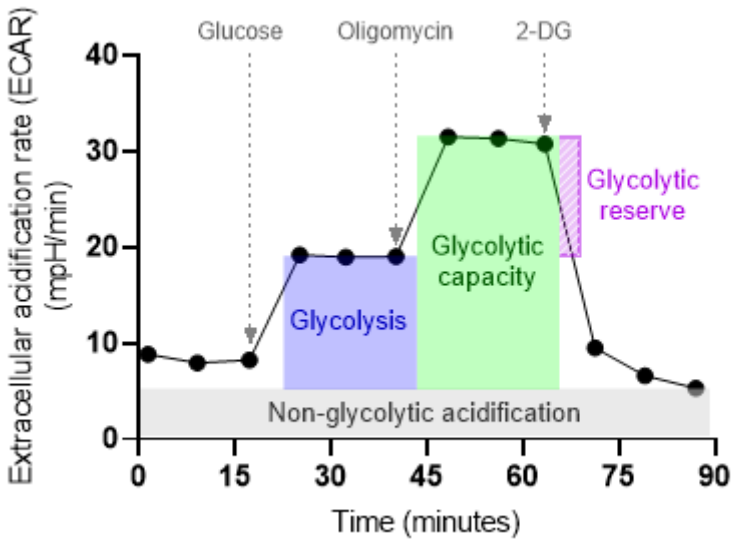

Fig. 5. Schematic plot of Glyco Stress Test experiment for assessment of fundamental parameters of glycolytic activity: glycolysis, maximal glycolytic capacity, and glycolytic reserve.

4.20 Real-time determination of mitochondrial respiration

Mitochondrial respiration was measured as extracellular oxygen consumption rate (OCR) using the XF24 Seahorse Extracellular Flux analyser (Agilent Technologies, Inc., Santa Clara, CA, USA), the Oxygraph 2-k respirometer (Oroboros Instruments Corporation, Innsbruck, Austria), and the MitoXpress Xtra Oxygen Consumption Assay (Agilent).

Seahorse Extracellular Flux analyser. Cells were plated at a density of 3 × 10^4/well in the Agilent Seahorse XF24 cell culture microplate (Agilent Technologies, Inc.) and incubated overnight at 37°C in 5% CO_2. Subsequently, cells were treated as described in *Neuronal differentiation* and *Experimental treatment* sections. On the day of the experiment, the media was replaced with 500 µL of respiration medium (unbuffered DMEM (#D5030) supplemented with 15 mM glucose, 2 mM L-glutamine, and 1 mM pyruvate; pH 7.4). After that, cells were cultured for 45 minutes at 37°C in a non-CO_2 incubator, and mitochondrial function was assessed using the XF24 Seahorse Extracellular Flux analyser with Mito Stress Test design injections optimized for different cells types: 1 µM oligomycin, 1/3 µM FCCP (SH-SY5Y/CCF-STTG1), 1 µM rotenone/antimycin A. Hoechst 33342 (5 µg/mL) was used during the final injection to stain nuclei for cell count-based data normalization. The fluorescence mode plate reader (BioTek Cytation 3) and Gen 5.3 software were used to count the cells. By removing the OCR values following rotenone/antimycin A injection, data on proton leak, basal respiration, ATP-linked respiration, and maximum respiration rates were obtained (Fig. 6).

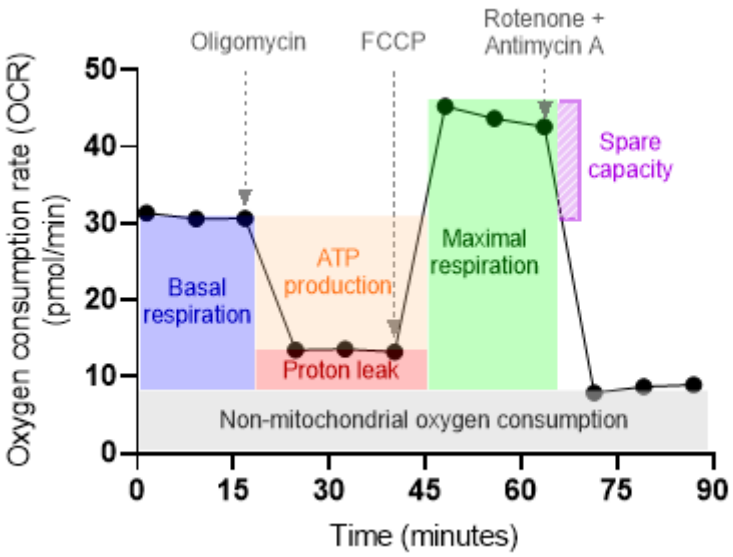

Fig. 6. Schematic plot of Mito Stress Test experiment for assessment of fundamental parameters of mitochondrial function: basal respiration, ATP-linked respiration, proton leak, maximal respiration, and spare respiratory capacity.

Oxygraph 2-k respirometer. Cells were harvested by trypsinization, washed with PBS, and resuspended in MIR05 medium (110 mM sucrose, 0.5 mM EGTA, 3 mM $MgCl_2$, 80 mM KCl, 60 mM K-lactobionate, 10 mM KH_2PO_4, 20 mM taurine, 20 mM HEPES, 1 g/L bovine serum albumin; pH 7.1). Oxygraph was used to evaluate the ADP-stimulated respiration of permeabilized cells using 2 x 10^6 cells and the following treatments: 8 µM digitonin, 10 mM glutamate, 5 mM malate, 2.5 mM ADP, 0.2 µM rotenone, 10 mM succinate, 2.5 µM antimycin A, 0.25 mM N,N,N′,N′-tetramethyl-p-phenylenediamine (TMPD), 1 mM ascorbate, 5 mM sodium azide. The efficient concentration of digitonin for cell membrane permeabilization was determined by titration protocol (data not shown). Respiration rates driven by activation of complex I, complex II, or complex IV were evaluated by deducting the oxygen consumption rate before and after the addition of specific inhibitors (Fig. 7). Note: Activity of complex II is not inhibited during the assessment of complex I, but is considered negligible without saturating concentration of succinate.

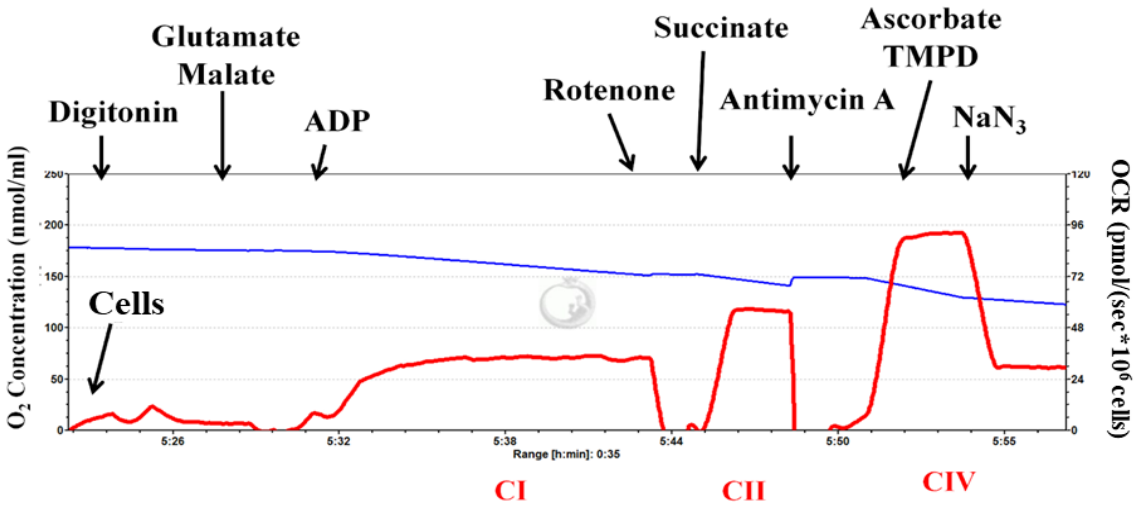

Fig. 7. Example Oxygraph-2K measurement of maximal ADP-stimulated respiration of permeabilized cells. Mitochondrial respiratory rates are measured after the addition of substrates: glutamate and malate (complex I), succinate (complex II), ascorbate/TMPD (complex IV), and inhibitors: rotenone (complex I), antimycin A (complex III) and sodium azide (complex IV). CI: complex I, CII: complex II, CIV: complex IV, OCR: oxygen consumption rate. Adapted from Djafarzadeh 2017.

MitoXpress Xtra Oxygen Consumption Assay. Using the MitoXpress Xtra Oxygen Consumption Assay (Agilent), real-time measurements of extracellular oxygen consumption in whole cells were used to evaluate cellular respiration. Cells in the density of 8 x 10^4 cells/well were seeded in 96-well black-wall clear-bottom TC+ plates 24 h before drug treatments. The assay was carried out in accordance with the manufacturer's instructions. Briefly, cells were given fresh, pre-warmed, FBS-free growth medium containing reconstituted oxygen-sensing fluorophore. Afterward, wells were immediately coated with mineral oil to prevent oxygen from the air from reaching the cells. The plate was then read kinetically using a BioTek Synergy HT microplate reader in time-resolved fluorescence mode for more than 180 min at a constant temperature of 37°C. Oxygen consumption rates were calculated using the differences in the fluorescence signal over time and corrected for protein content. Prior to the addition of oil, cells were treated with 1.5 µM FCCP to assess the maximum respiration rates.

4.21 Intracellular ATP Measurement

The intracellular ATP concentration was carried out in line with the ATP test kit's instructions (ATP Bioluminescence Assay Kit CLS II) with a few minor adjustments. Trypsinization was used to harvest the cells, which were then washed twice with ice-cold PBS. Samples containing 10^5 cells were centrifuged at 800 x g for 10 min, and the pelleted cells were reconstituted in TE solution (100 mM Tris, 4 mM EDTA; pH 7.75) and heated at

95°C for 7 min to lyse them. The BioTek Synergy HT microplate reader was then used to read each sample in luminescence mode after it had been combined with a luciferase reagent in a white 96-well plate.

4.22 Statistical Analysis

At least three replicates of each condition were used in every experiment. GraphPad Prism 8 software was used to perform the statistical analysis and construct graphs. Data are presented as means ± S.E.M. The statistical significance of comparing exactly two groups was evaluated using the unpaired Student's t-test. For more than two groups of one factor, standard one-way analysis of variance (ANOVA) was employed. Two-way ANOVA was performed to determine statistically significant differences between groups in a two-factor design experiment. A p-value less than 0.05 was considered to be statistically significant. If ANOVA revealed a statistically significant difference, it was followed by the Newman-Keuls or Dunnett's post hoc test for multiple comparisons between groups.

5 Results

5.1 AIM 1 – *In vitro* model of neurons, SH-SY5Y cell line

5.1.1 The effect of FTO inhibition on differentiation of SH-SY5Y cells

5.1.1.1 Retinoic acid induced neuronal differentiation of SH-SY5Y cells

We have used a combination of retinoic acid (RA) and low serum media to promote the differentiation of SH-SY5Y cells into a neuronal phenotype according to a previously described methodology (Ammer and Schulz, 1994). The morphology of SH-SY5Y cells was examined using phase-contrast microscopy to confirm the differentiation process. While undifferentiated SH-SY5Y cells often grew in clusters and had few truncated processes on their non-polarized cell bodies. Long-term exposure to RA caused the majority of the cells to take on a more characteristic neuronal shape. After receiving RA treatment, cells were more dispersed and exhibited a decrease in the cell body mass, and extension of neurites by about twofold (Fig. 8). Neurite outgrowth was tracked using ImageJ software and the NeuronGrowth plugin to assess the degree of neuronal differentiation.

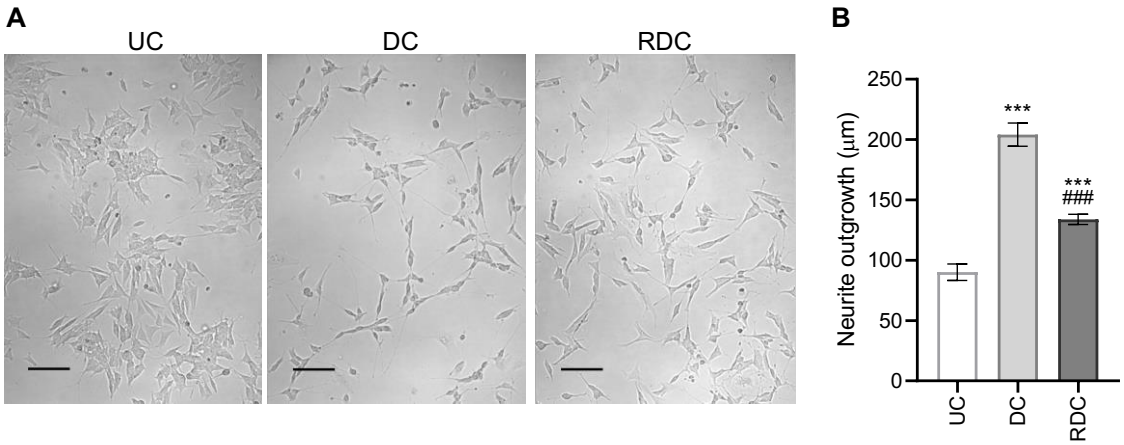

Fig. 8. Effects of rhein and retinoic acid (RA) on cellular morphology of SH-SY5Y cells. Cell morphology was assessed using optical microscopy. (A) Microphotographs of untreated undifferentiated cells (UC), RA-differentiated cells (DC), and RA-differentiated cells in the presence of rhein (RDC). Scale bar: 100 µm. (B) Comparison of neurite outgrowth in UC, DC, and RDC. Data are presented as mean ± S.E.M. ANOVA followed by Newman-Keuls post hoc test was used to assess statistical significance (*** $p \leq 0.001$ vs UC; ### $p \leq 0.001$ vs DC).

We further evaluated the differentiation process by monitoring the changes in the levels of specific markers by Western blotting. While the level of the neural progenitor cell

marker nestin was decreased about 2-fold in differentiated cells, there was a significant increase in the content of the neuronal markers microtubule-associated protein 2 (MAP2), neuron-specific enolase (NSE), beta-3 tubulin (TUBB3), and synaptophysin (SYP), as well as the dopaminergic neuron-specific marker tyrosine hydroxylase (TH) by 1.5-, 1.3-, 3-, and 20-fold, respectively (Fig. 9).

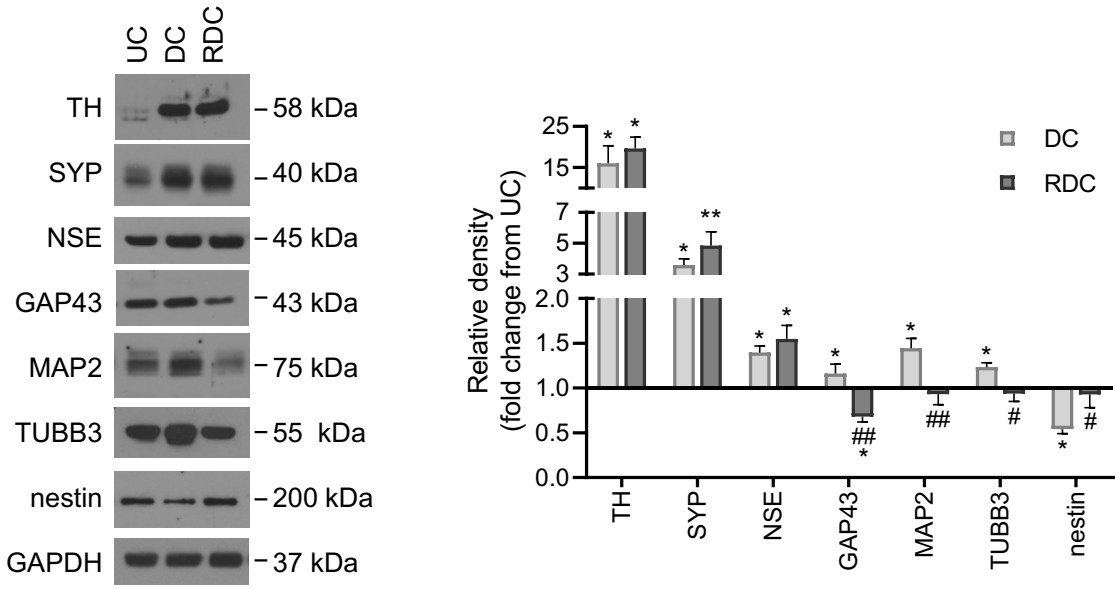

Fig. 9. Effects of rhein and retinoic acid (RA) on relative levels of neuronal differentiation markers in SH-SY5Y cells. Left: Representative Western blots showing levels of tyrosine hydroxylase (TH), synaptophysin (SYP), nestin, microtubule-associated protein 2 (MAP2), neuron-specific enolase (NSE), growth associated protein 43 (GAP43) and beta-3 tubulin (TUBB3) in untreated undifferentiated cells (UC), RA-differentiated cells (DC) and RA-differentiated cells in the presence of rhein (RDC). Right: Quantification of immunoblots by densitometry with normalization to GAPDH levels and expressed as fold change from UC. Data are presented as mean ± S.E.M. ANOVA followed by Newman-Keuls post hoc test was used to assess statistical significance (* $p \leq 0.05$, ** $p \leq 0.01$ vs UC; # $p \leq 0.05$, ## $p \leq 0.01$ vs DC).

Moreover, the proteome of SH-SY5Y cells exposed to 10 µM RA for 6 days was examined using two-dimensional gel electrophoresis and mass spectrometry (MS). MS analysis led to the identification of 15 differentially expressed proteins between samples from control and RA-treated cells. One protein was up-regulated by 3.3-fold following neuronal differentiation and the levels of 14 additional proteins (including alpha-enolase) were reduced by 2- to 3.7-fold. A list of identified proteins and their functional annotations is provided in the table below (Tab. 1). Differentially expressed proteins were implicated in the regulation of the cytoskeleton, RNA processing, protein folding, apoptosis, metabolism, and cell signaling.

Tab. 1. List of differently expressed proteins of DC vs UC identified by MALDI-TOF MS/MS analysis of CBB-stained gel spots and associated biological processes.

Spot	Gene ID	Protein name	FC	Molecular functions and biological processes
1	C1QBP	Complement component 1 Q subcomponent-binding protein, mitochondrial	↑ 3.3	adaptive immunity, apoptosis, transcription
2	ACTB	Actin, cytoplasmic 1	↓ 2.9	ATP binding, membrane organization
3,4	ENO1	Alpha-enolase	↓ 2.1, ↓ 3.7	glycolysis, gluconeogenesis
5	CBX1	Chromobox protein homolog 1	↓ 3.2	chromatin binding, enzyme binding
6	1433Z	14-3-3 protein zeta/delta	↓ 2.1	adapter protein, signal transduction
7	NPM	Nucleophosmin	↓ 2.0	chaperone, cell aging, signal transduction
8	HNRPC	Heterogeneous nuclear ribonucleoproteins C1/C2	↓ 3.2	ribonucleoprotein, mRNA processing
9	NDKA	Nucleoside diphosphate kinase A	↓ 2.3	cell proliferation, signal transduction, nucleotide metabolism
10	RLA0	60S acidic ribosomal protein P0	↓ 2.3	ribonucleoprotein, translation
11,12	TCPG	T-complex protein 1 subunit gamma	↓ 2.3, ↓ 2.3	chaperone, ATP binding
13	STIP1	Stress-induced-phosphoprotein 1	↓ 2.2	co-chaperone, response to stress, RNA binding
14	HNRPL	Heterogeneous nuclear ribonucleoprotein L	↓ 3.0	ribonucleoprotein, RNA processing
15	PGAM1	Phosphoglycerate mutase 1	↓ 2.6	glycolysis
16	PCBP1	Poly(rC)-binding protein 1	↓ 2.3	ribonucleoprotein, mRNA splicing
17	PRDX1	Peroxiredoxin-1	↓ 2.1	antioxidant, cell proliferation

FC: fold change

5.1.1.2 FTO inhibitor rhein treatment impedes the differentiation of SH-SY5Y cells

To examine the effect of rhein on SH-SY5Y cell differentiation, the cells were treated for 24 hours in the presence of 10 μM rhein before administering RA and then examined after 6 days of rhein and RA coincubation. In cells affected by rhein, there was no discernible clustering typically seen in undifferentiated cells. The rhein-treated cells had a look that was partially reminiscent of that seen after RA-induced differentiation, although there was less prominent cell stretching and decreased neurite outgrowth. Mean neurite length was still significantly higher than in undifferentiated cells (by about 40%), but potently reduced in contrast to that seen in the RA-treated cells lacking rhein treatment (Fig. 8).

In addition, we have observed that the expression patterns of TH, SYP, and NSE in rhein-treated cells resembled those seen in cells that had undergone RA differentiation.

Strikingly, however, levels of markers MAP2, TUBB3, and nestin remained unchanged with respect to undifferentiated cells. In contrast to both undifferentiated and RA-differentiated cells, the cytoskeletal protein GAP43 had an interesting opposite trend and was down-regulated compared to controls (Fig. 9).

Next, we examined how rhein affected both the levels and enzymatic activity of alpha-enolase. Alpha-enolase (ENO1) activity was considerably reduced (by 25 %) in differentiated cells compared to undifferentiated cells, corroborating the findings from MS studies. Surprisingly, compared to differentiated cells, rhein-treated cells displayed increased ENO1 activity (by 18 %), almost reaching the baseline activity of undifferentiated cells (Fig. 10A). A consistent pattern was discovered when protein levels of ENO1 were assessed (Fig. 10B).

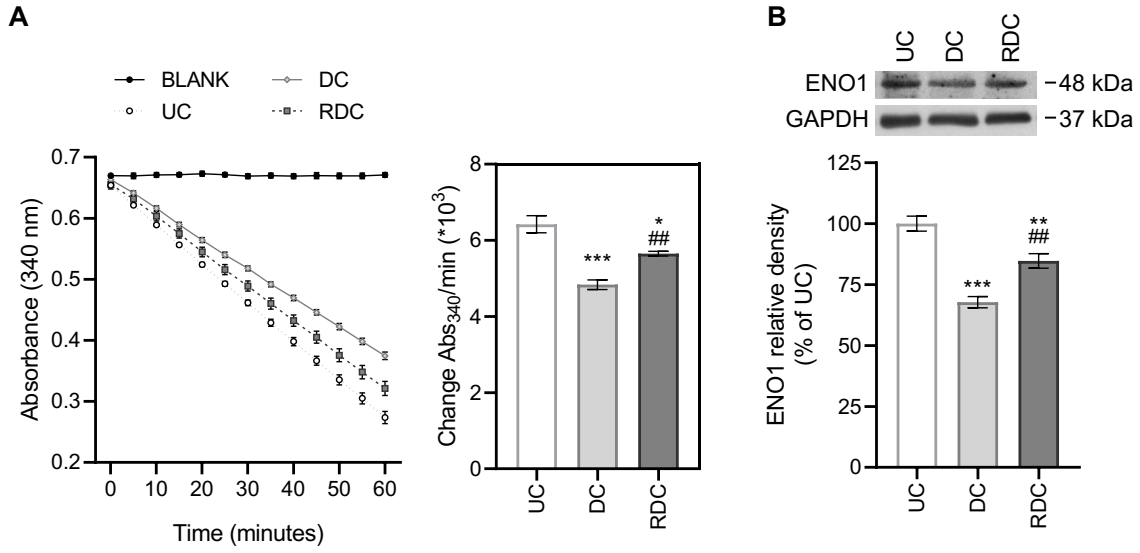

Fig. 10. Effects of rhein and retinoic acid (RA) on alpha-enolase (ENO1) activity in SH-SY5Y cells. (A) Detection and quantification of ENO1 enzymatic activity from untreated undifferentiated cells (UC), RA-differentiated cells (DC), and RA-differentiated cells in the presence of rhein (RDC). (B) Representative immunoblot and changes in the relative protein levels of ENO1 in UC, DC, and RDC. Quantification of immunoblots was done by densitometry with normalization to GAPDH levels and expressed as fold change from UC. Data are presented as mean ± S.E.M. ANOVA followed by the Newman-Keuls test was used to assess statistical significance (* $p \leq 0.05$, ** $p \leq 0.01$ *** $p \leq 0.001$ vs UC; # $p \leq 0.05$ vs DC).

5.1.2 The impact of FTO inhibition on protein profiling of undifferentiated and differentiated SH-SY5Y cells

We investigated how the proteome of both undifferentiated and RA-differentiated SH-SY5Y cells was affected by a 24-hour treatment with 10 μM rhein. The differential 2D proteomic analysis detected 8, and 12 spots with changed density in samples from

undifferentiated, and differentiated SH-SY5Y cells treated with rhein, respectively (Fig. 11). Mass spectrometry was used to identify the proteins that were differentially expressed. In undifferentiated and differentiated SH-SY5Y cells exposed to rhein, expression levels of 7, and 10 proteins, respectively, were found to be altered at least twofold. All the identified proteins were down-regulated in rhein-treated cells (Tab. 2). These proteins participate in the regulation of transcription and translation, cytoskeleton structure, cellular metabolism, and antioxidant defense (Tab. 2).

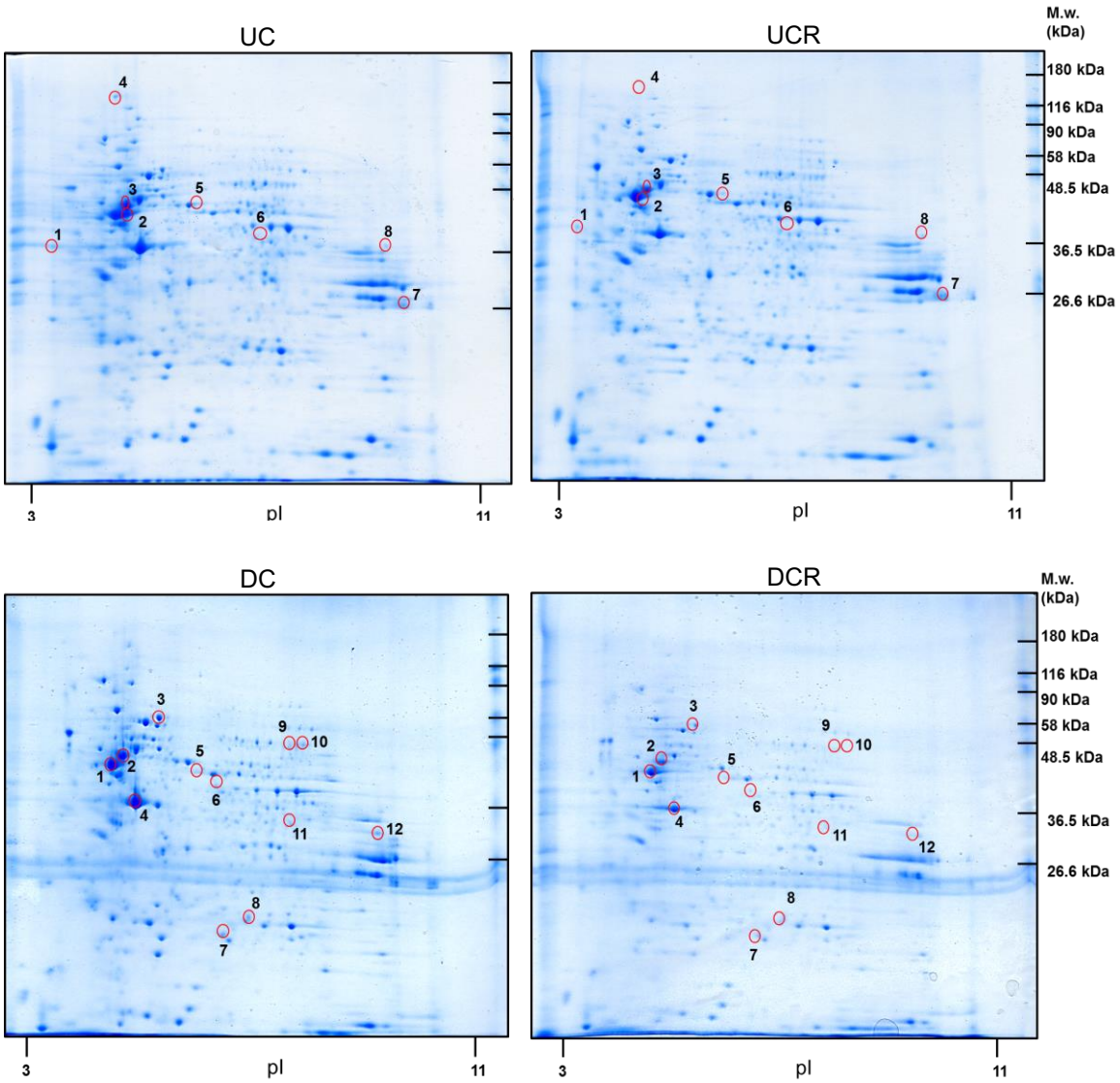

Fig. 11. Effect of rhein on protein expression in SH-SY5Y cells. Representative CBB-stained 2-DE gel images of proteins expressed in undifferentiated and differentiated cells either untreated (UC, DC, respectively) or treated with 10 μM rhein for 24 h (UCR, DCR, respectively). Spots that underwent statistically significant changes in protein abundance as a result of treatment with rhein are highlighted with red circles. These spots were excised from gels for MS analysis.

Tab. 2. List of differently expressed proteins of UCR vs UC (group U) or DCR vs DC (group D) identified by MALDI-TOF MS/MS analysis of CBB-stained gel spots and associated biological processes.

Group	Spot	Gene ID	Protein name	FC	Molecular functions and biological processes
U	1	ACTB	Actin, cytoplasmic 1	↓ 2.5	ATP binding, membrane organization
U	2,4	TBB5	Tubulin beta chain	↓ 6.2, ↓ 5.2	GTP binding, microtubule-based process, cell division
U	3	TBA1A	Tubulin alpha-1A chain	↓ 2.1	GTP binding, microtubule-based process, cell division
U	5	PDIA3	Protein disulfide-isomerase A3	↓ 2.7	formation and breakage of disulfide bonds, protein folding
U	6	ACTZ	Alpha-centractin	↓ 2.8	ATP-binding, vesicle-mediated transport
U	7	ROA1	Heterogeneous nuclear ribonucleoprotein A1	↓ 3.9	ribonucleoprotein, mRNA splicing
U	8	THIM	3-ketoacyl-CoA thiolase, mitochondrial	↓ 3.6	fatty acid metabolism, transit peptide
D	1	TBB5	Tubulin beta chain	↓ 2.5	GTP binding, microtubule-based process, cell division
D	2	TBA1B	Tubulin alpha-1B chain	↓ 2.5	GTP binding, microtubule-based process, cell division
D	3	GRP75	Stress-70 protein, mitochondrial (mortalin)	↓ 2.3	chaperone, erythropoiesis process
D	4	ACTB	Actin, cytoplasmic 1	↓ 3.3	ATP binding, membrane organization
D	5,6	HNRH1	Heterogeneous nuclear ribonucleoprotein H	↓ 4.4, ↓ 2.7	ribonucleoprotein, mRNA splicing
D	7	PRDX3	Thioredoxin-dependent peroxide reductase, mitochondrial	↓ 2.6	antioxidant, detoxification of reactive oxygen species
D	8	PRDX6	Peroxiredoxin-6	↓ 2.7	antioxidant, detoxification of reactive oxygen species
D	9,10	HNRPL	Heterogeneous nuclear ribonucleoprotein L	↓ 2.5, ↓ 2.8	ribonucleoprotein, mRNA splicing

FC: fold change

Furthermore, we used the Western blotting technique to determine the relative abundance of a few proteins associated with the cytoskeleton (tubulin alpha (TUBA)), metabolism (mortalin (GRP75)), or antioxidant processes (thioredoxin-dependent peroxide reductase (PRX3), peroxiredoxin 6 (PRX6)) in order to validate the findings from 2-DE and MS analyses. An identical trend (down-regulation) in levels of these selected proteins in rhein-affected cells was observed (Fig. 12). Levels of TUBA were significantly (by about 70%) decreased in both undifferentiated and differentiated SH-SY5Y cells treated with rhein. Rhein treatment caused the GRP75, PRX3, and PRX6 levels in RA-differentiated cells to decrease by around 15-45%.

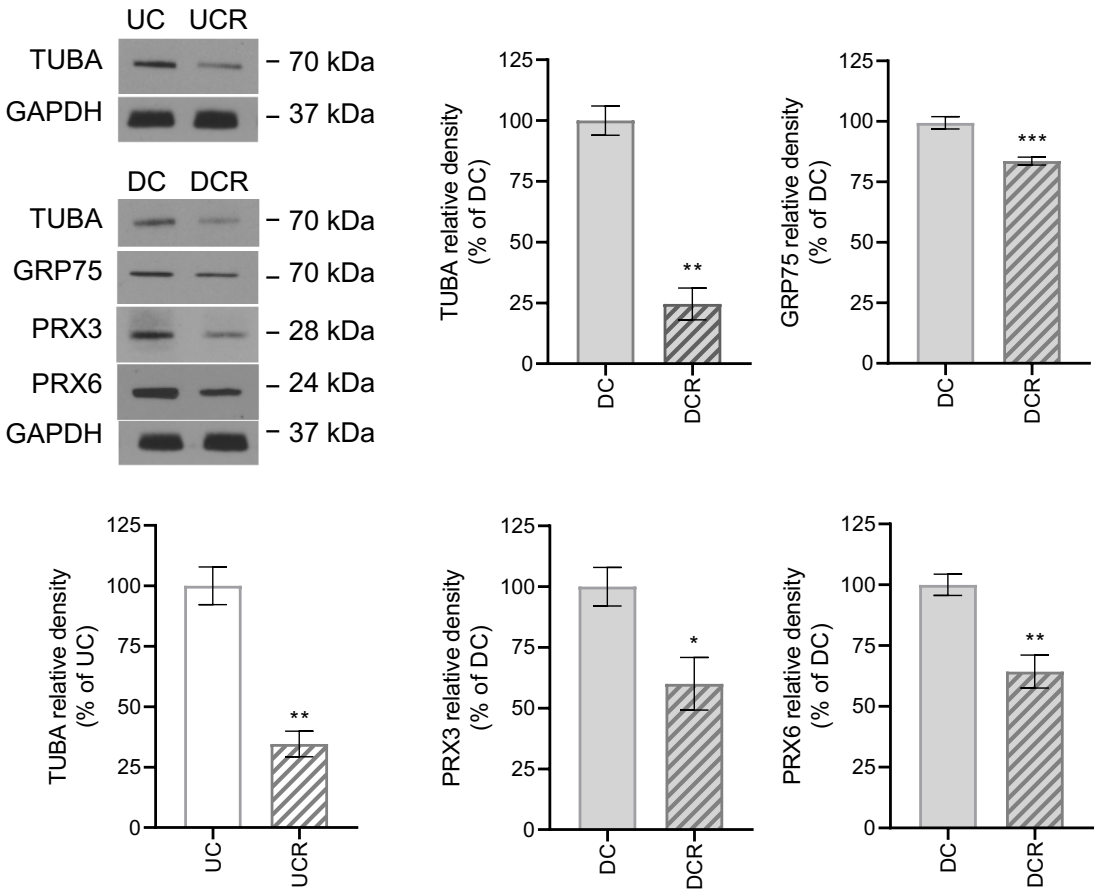

Fig. 12. Validation of 2D gel electrophoresis and mass spectrometry data by Western blot analysis. The relative expression levels of selected proteins were determined in samples from undifferentiated and differentiated SH-SY5Y cells either not treated (UC, DC, respectively) or treated by rhein for 24h (UCR, DCR, respectively). Representative Western blot bands show levels of alpha-tubulin (TUBA), mortalin (GRP75), and peroxiredoxins 3 and 6 (PRX3, PRX6). Immunoblot bands were quantified by densitometry with normalization to GAPDH levels. The bar graphs show the percent changes in the normalized values for each protein relative to the matched control group. Data are presented as mean ± S.E.M. Student's t-test was used to assess statistical significance (* $p \leq 0.05$, ** $p \leq 0.01$, *** $p \leq 0.001$).

5.1.3 The role of FTO inhibition on mitochondrial oxygen consumption and glycolysis of differentiated SH-SY5Y cells

5.1.3.1 Differentiation of SH-SY5Y cells by RA and BDNF

Due to the nature of the intended research, which needed cells to remain adherent throughout the whole procedure, we changed the model cell line for the SH-SY5Y purchased from ECACC. Previously used SH-SY5Y cells of ATCC origin were inclined to easily detach from the well plate surface during simple washing or media exchange. Unfortunately, we were unable to promote the adhesion of these cells even after applying

various plate surface coatings. For reasons not fully understood, SH-SY5Y cells from ECACC did not display this detachment tendency. However, ECACC SH-SY5Y cells required an extra differentiation step in the form of BDNF supplementation since RA was not enough to promote neuronal phenotype. SH-SY5Y cells of ECACC origin were cultivated with 10 µM RA for 5 days and 50 ng/mL BDNF for additional 3 days. Phase-contrast microscopy was used to assess the morphology of SH-SY5Y cells in order to validate the differentiation procedure (Fig. 13A). Levels of the neuronal markers MAP2, NSE, GAP43, SYP, and TUBB3 were significantly higher in the RA-BDNF treated cells (by about 3-, 1.3-, 1.2, 6-, and 1.2-fold, respectively) compared to the control cells, according to the analysis of protein content by Western blotting (Fig. 13B).

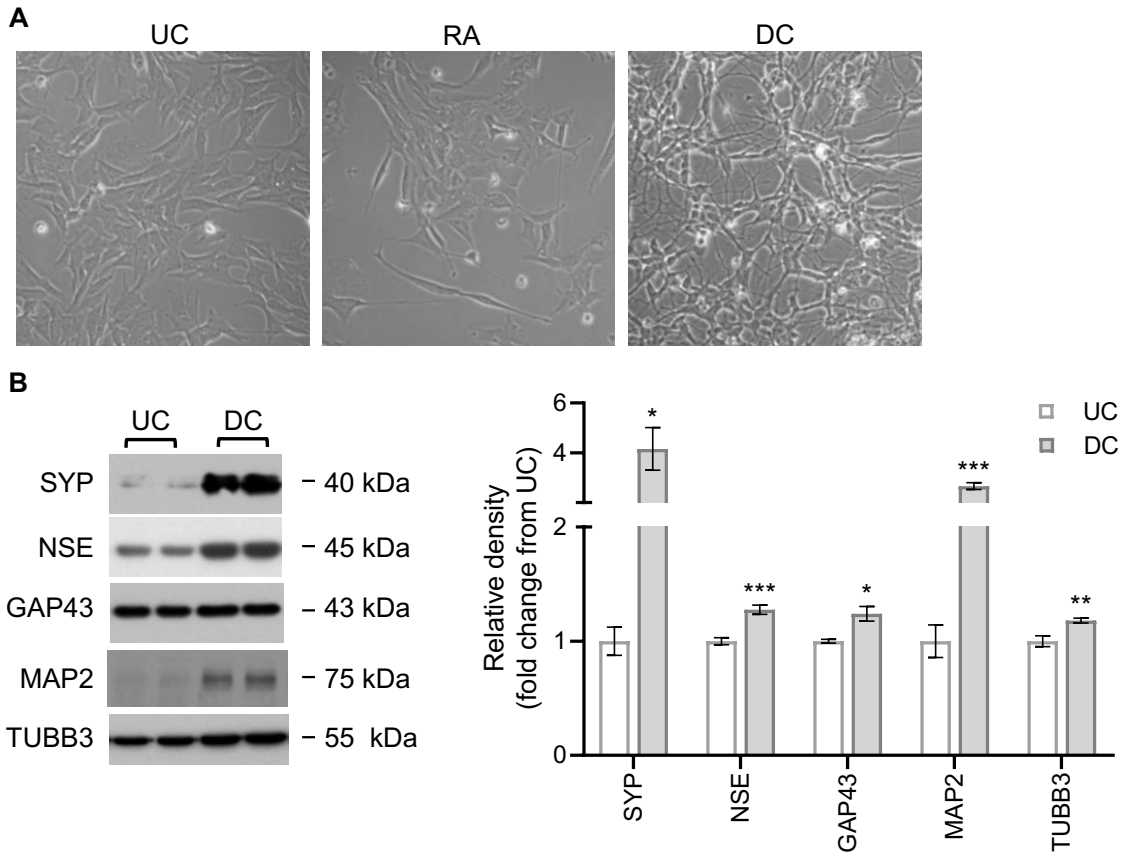

Fig. 13. Differentiation of SH-SY5Y cells by RA and BDNF. (A) Microphotographs of untreated undifferentiated cells (UC), RA-differentiated cells (RA), and BDNF-RA-differentiated cells (DC). (B) Left: Representative Western blots showing levels of synaptophysin (SYP), microtubule-associated protein 2 (MAP2), neuron-specific enolase (NSE), growth associated protein 43 (GAP43), and tubulin beta-3 (TUBB3). Right: Quantification of immunoblots by densitometry with normalization to total protein (Ponceau S staining), expressed as fold change from UC. Data are presented as mean ± S.E.M. Student's t-test was used to assess statistical significance between groups (* $p \leq 0.05$, ** $p \leq 0.01$, *** $p \leq 0.001$). RA: retinoic acid, BDNF: brain-derived neurotrophic factor.

5.1.3.2 The effect of FTO inhibition on glycolytic parameters

The extracellular acidification rates (ECAR) of live differentiated SH-SY5Y cells treated with FTO inhibitor MO-I-500 were assessed by Seahorse Extracellular Flux Analyzer. Glucose, oligomycin, and 2-deoxyglucose (2-DG) injections were used to measure ECAR representative of glycolysis, maximum glycolytic capacity, and non-glycolytic acidification, respectively. No significant changes were observed in any of the measured parameters following FTO inhibition by MO-I-500 (Fig. 14B).

We proceeded to verify the findings from extracellular acidification by using silencing of FTO instead of pharmacological inhibition. The effectiveness of silencing was validated by immunoblot detection of FTO protein levels. The treatment of cells with FTO siRNA resulted in about 80% decrease in FTO signal (Fig. 14A). Correspondingly to FTO inhibition, FTO siRNA did not result in significant changes in glycolytic parameters in differentiated SH-SY5Y cells (Fig. 14C).

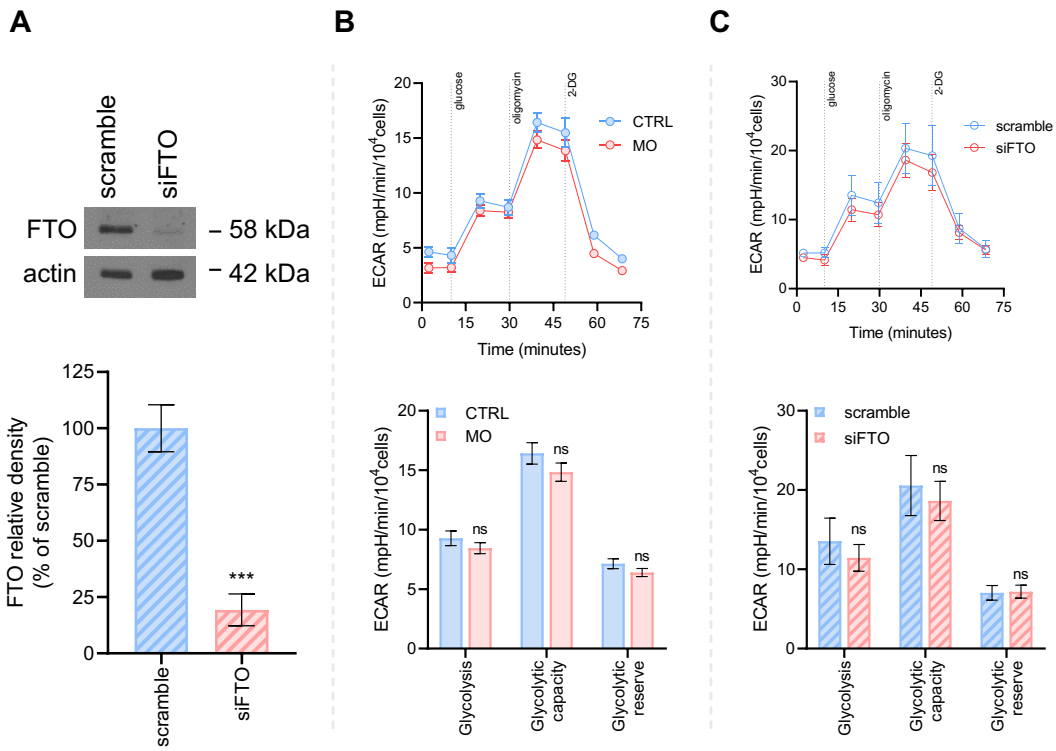

Fig. 14. Effect of FTO inhibitor MO-I-500 and FTO silencing on glycolytic parameters of SH-SY5Y cells. Cells were treated with 1 μM MO-I-500 for 72 h (MO) or FTO siRNA for 48 h (siFTO). Control groups were treated with the vehicle (0.1% DMSO for 72 h in the CTRL group, negative control siRNA for 48h in the scramble group). (A) Representative Western blot of FTO and quantification of relative changes of its protein levels by densitometry with normalization to actin. FTO relative density is expressed as percent change from scramble. (B,C) Extracellular acidification rate (ECAR) measurement by Seahorse XF24 and analysis of glycolytic rate, capacity, and reserve parameters. Data are presented as mean ± S.E.M. Student's t-test was used to assess statistical significance between groups (ns $p > 0.05$,*** $p \leq 0.001$).

5.1.3.3 The effect of FTO inhibition on mitochondrial respiration rates

We have previously observed that treatment of undifferentiated SH-SY5Y cells by FTO inhibitor rhein is followed by reduced capacity of the mitochondrial electron transport chain (Cockova, 2017). Now, we used an FTO inhibitor MO-I-500 and FTO siRNA treatment to investigate the role of FTO in the mitochondrial respiration of differentiated SH-SY5Y cells. First, we focused on the analysis of mitochondrial respiration in live adherent cells with Seahorse high-resolution respirometry (Fig. 15A). Differentiated SH-SY5Y cells treated with FTO inhibitor suffered from reduced basal, ATP-linked, and FCCP-induced uncoupled (maximal) respiration (all by about 25%) without displaying affected spare respiratory capacity. The amount of proton leak measured after oligomycin injection was also unchanged between the treated group and the control.

Analysis of the extracellular oxygen consumption rate showed that silencing of FTO is accompanied by lower respiration under basal (by 32%), ATP-linked (by about 30%), and uncoupled conditions (by almost 40%). Thus, a similar outcome as in cells treated with FTO inhibitor was observed in these parameters. In contrast, siFTO treatment induced a significant decrease in both, proton leak (by 30%) and reserve capacity (by about 60%) (Fig. 15B). However, irrespective of cell treatment, we detected very similar respiration rates in the uncoupled state and under basal conditions. As a result, we observed almost non-existent spare respiratory capacity of differentiated SH-SY5Y cells.

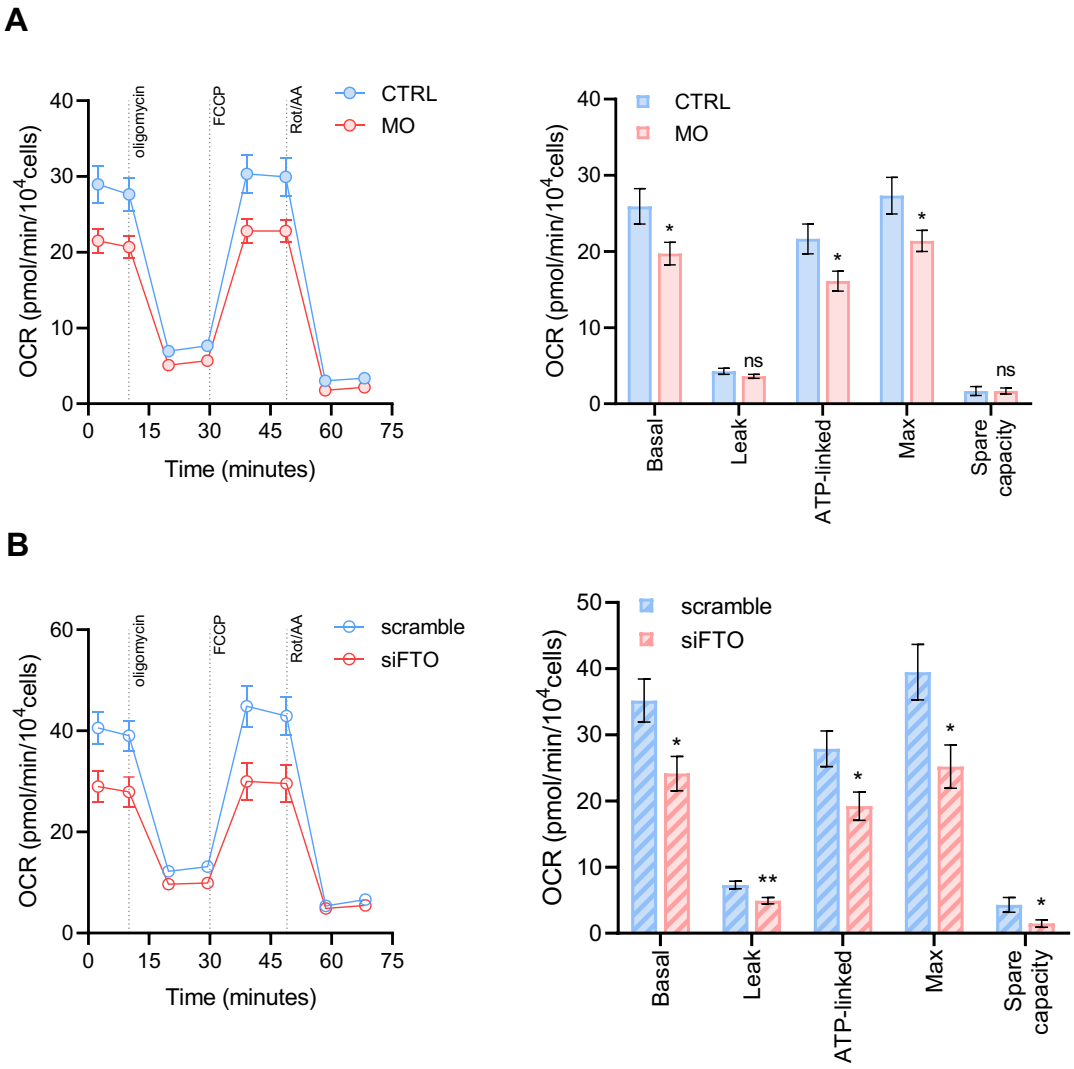

Fig. 15. Effect of FTO inhibitor MO-I-500 and FTO silencing on respiration of SH-SY5Y cells. Cells were treated with 1 μM MO-I-500 for 72 h (MO) or FTO siRNA for 48 h (siFTO). Control groups were treated with the vehicle (0.1% DMSO for 72 h in the CTRL group, negative control siRNA for 48h in the scramble group). (A,B) Oxygen consumption rate (OCR) measurement by Seahorse XF24 and analysis of individual parameters for basal respiration, ATP-linked respiration, proton leak, maximal respiration, and spare respiratory capacity. Data are presented as mean ± S.E.M. Student's t-test was used to assess statistical significance between groups (ns $p > 0.05$, * $p \leq 0.05$, ** $p \leq 0.01$).

5.1.4 The role of FTO inhibition in the resilience of differentiated SH-SY5Y cells towards streptozotocin

Using a range of streptozotocin (STZ) doses (0.1-3 mM) throughout a 48 hour incubation period, we conducted the MTT test to determine the impact on the viability of cells. The concentration-dependent detrimental effect of STZ dose on neurons was observed (Fig. 16). Cell viability began to decline at a dose of 1 mM STZ (by about 25%), and reached a death rate of approximately 50% at 1.5 mM STZ.

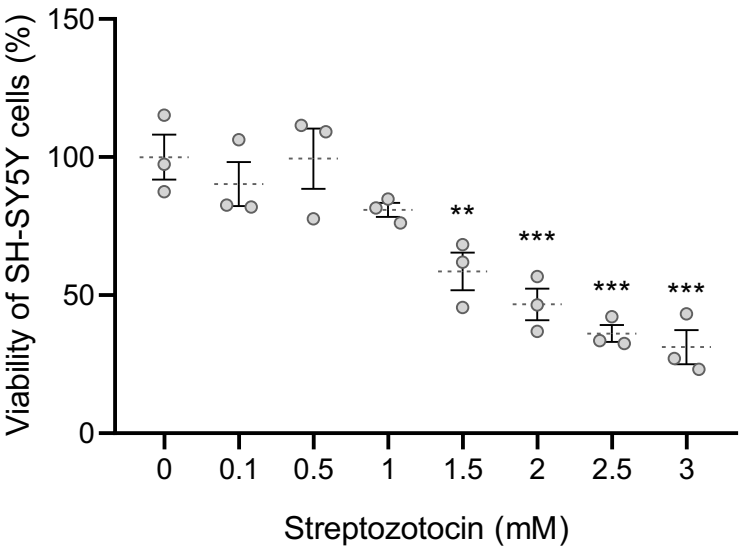

Fig. 16. Effects of streptozotocin dose on SH-SY5Y viability. The viability of SH-SY5Y cells treated with different concentrations of streptozotocin for 48 h is expressed as a percentage change from the untreated control group (0 mM). Values are presented as mean ± S.E.M. ANOVA followed by Dunnett's post hoc test was used to assess statistical significance when comparing means of treated groups with the control group (** $p \leq 0.01$ and *** $p \leq 0.001$).

Next, we explored how the pretreatment of cells with the FTO inhibitor MO-I-500 may impact the responsiveness of cells to the STZ. We employed 1.5 mM STZ to induce a 50% death rate of differentiated SH-SY5Y. Our findings imply that FTO inhibition has no discernible impact on SH-SY5Y cell death brought on by STZ as no significant difference was observed in the survival rate of STZ-affected cells with or without inhibited FTO (Fig. 17).

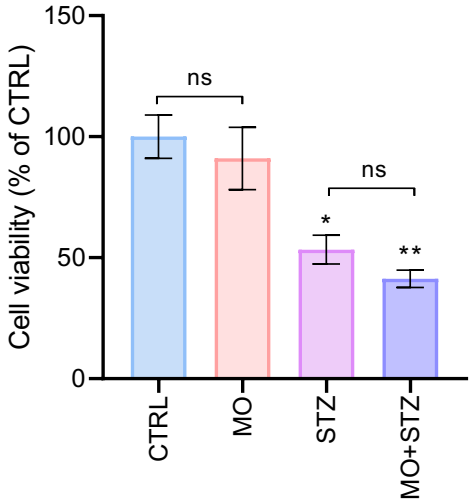

Fig. 17. Effects of streptozotocin and FTO inhibitor MO-I-500 on SH-SY5Y viability. Viability of SH-SY5Y cells treated with vehicle (CTRL), 1.5 mM streptozotocin (STZ), 1 μM MO-I-500 (MO) or co-treated with 1 μM MO-I-500 and 1.5 mM streptozotocin (MO+STZ) is expressed as percentage change from control group (CTRL). Values are presented as mean ± S.E.M. ANOVA followed by Newman-Keuls test was used to assess statistical significance (ns $p > 0.05$,* $p \leq 0.05$ and ** $p \leq 0.01$ vs CTRL). Only selected statistical comparisons are reported in graphs: CTRL vs STZ, CTRL vs MO, CTRL vs MO+STZ, STZ vs MO+STZ.

5.2 AIM 2 – *In vitro* model of astrocytes, CCF-STTG1 cell line

5.2.1 The effect of FTO suppression on mitochondria and energy metabolism of CCF-STTG1 cells

5.2.1.1 FTO inhibitor MO-I-500 affects mitochondria and cellular bioenergetics

Using the Seahorse instrument, the extracellular acidification rates (ECAR) of live CCF-STTG1 cells treated with the FTO inhibitor were measured. To determine the ECAR indicative of glycolysis, maximum glycolytic capacity, and non-glycolytic acidification, glucose, oligomycin, and 2-deoxyglucose (2-DG) injections were utilized. After FTO suppression by MO-I-500, no discernible alterations were seen in any of the assessed parameters (Fig. 18).

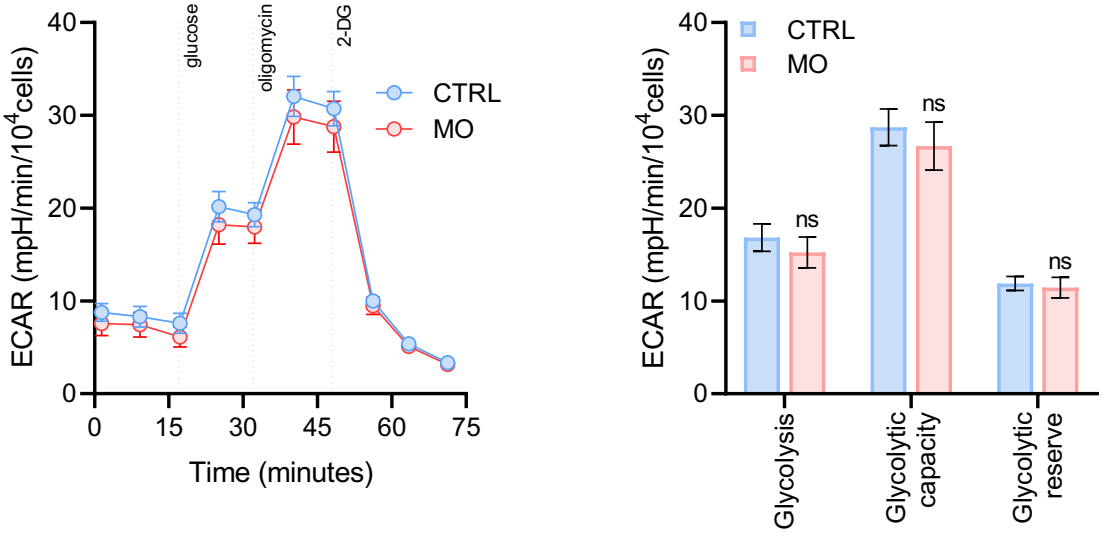

Fig. 18. Effect of FTO inhibitor MO-I-500 on glycolytic parameters of CCF-STTG1 cells. Extracellular acidification rate (ECAR) measurement by Seahorse XF24 and analysis of glycolytic rate, capacity, and reserve parameters was performed in control (CTRL) and MO-I-500 treated (MO) cells. Data are presented as mean ± S.E.M. Student's t-test was used to assess statistical significance between groups (ns $p > 0.05$).

Next, we investigated the effect of FTO inhibitor MO-I-500 on mitochondrial respiration. A Seahorse real-time measurement of the extracellular oxygen consumption of whole adherent cells was used to assess the respiration rates of astrocytes. Following MO-I-500 treatment, basal, ATP-linked, and FCCP-driven maximal respiration rates were significantly increased (all by about 25%), but oligomycin-induced mitochondrial leak did not change (Fig. 19A). Permeabilized cells were further utilized for assessment of the function of respiratory chain complexes with Oxygraph respirometer. A potent increase by approximately 120% in oxygen consumption driven by complex IV activity was observed in cells affected by the FTO inhibitor. Oxygen consumption due to complex I and complex II was slightly, yet not significantly elevated in MO-I-500 treated cells (Fig. 19B).

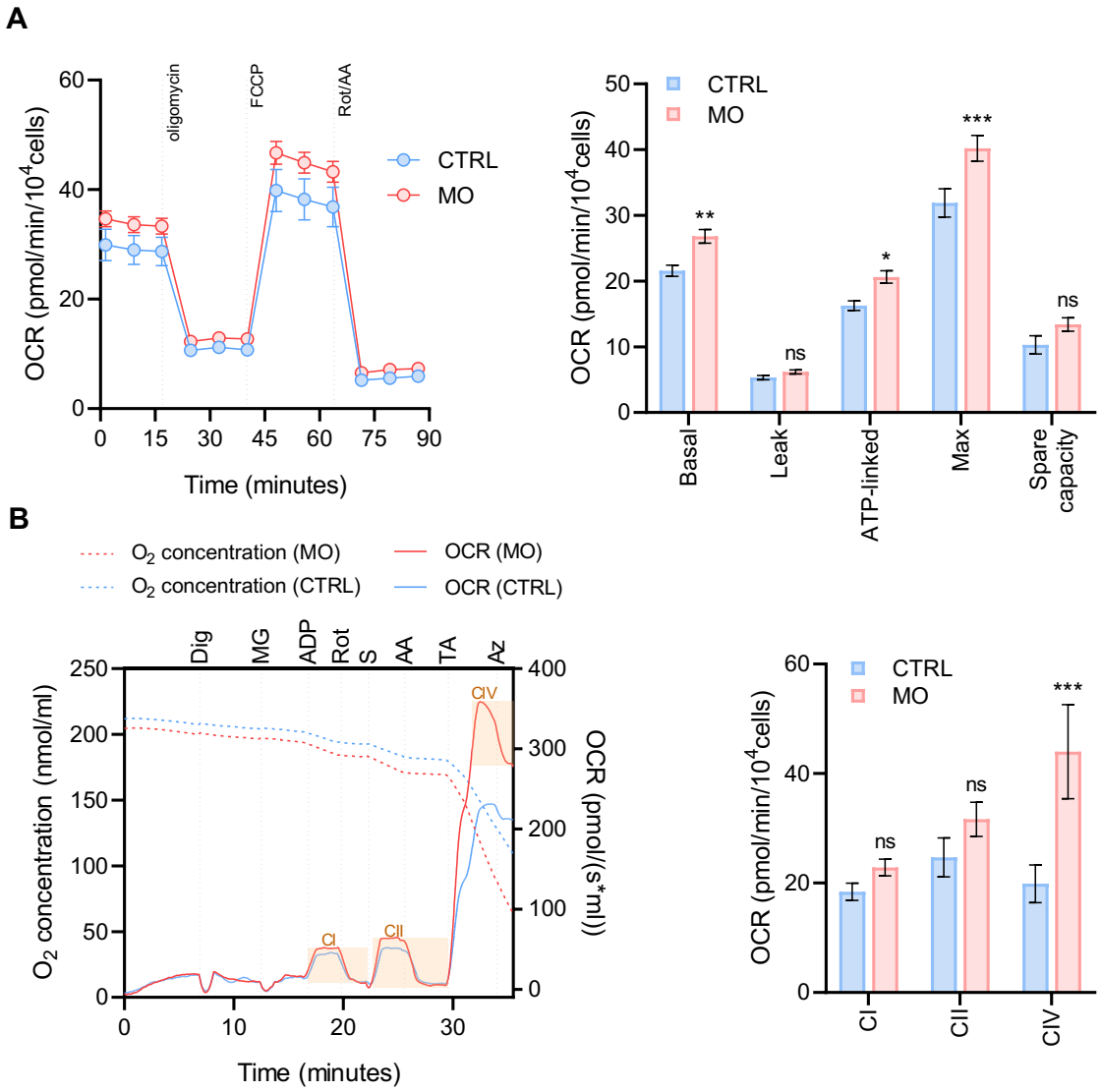

Fig. 19. Effect of FTO inhibitor MO-I-500 on respiration of CCF-STTG1 cells. (A) Seahorse XF24 measurement of oxygen consumption rate (OCR) and evaluation of individual parameters for basal respiration, proton leak, ATP-linked respiration, maximal respiration, and spare capacity in control (CTRL) and MO-I-500 treated (MO) cells. (B) Representative Oxygraph O2k assessment of OCR under specific treatments and analysis of respiration driven by complex I (CI), complex II (CII), and complex IV (CIV) in CTRL and MO groups. Treatments were digitonin (Dig), malate + glutamate (MG), adenosine diphosphate (ADP), rotenone (Rot), succinate (S), antimycin A (AA), TMPD + ascorbate (TA), and sodium azide (Az). Data are presented as mean ± S.E.M. Student's t-test was used to assess statistical significance between groups (ns $p > 0.05$, * $p \leq 0.05$, *** $p \leq 0.001$).

By using Western blot analysis, the relative protein levels of selected OXPHOS subunits were determined. Subunits succinate dehydrogenase subunit A (SDHA), ATP synthase F1 subunit alpha (ATP5A), and ubiquinol-cytochrome C reductase core protein 2 (UQCRC2) did not vary in relative levels between controls and cells treated with inhibitor. Interestingly, however, complex I (NADH dehydrogenase 1 beta subcomplex subunit 8,

(NDUFB8)) and complex IV (cytochrome c oxidase subunit 1 (MT-CO1)) subunits were increased by around 1.6 and 1.7 fold, respectively, in inhibitor-treated cells compared to controls (Fig. 20).

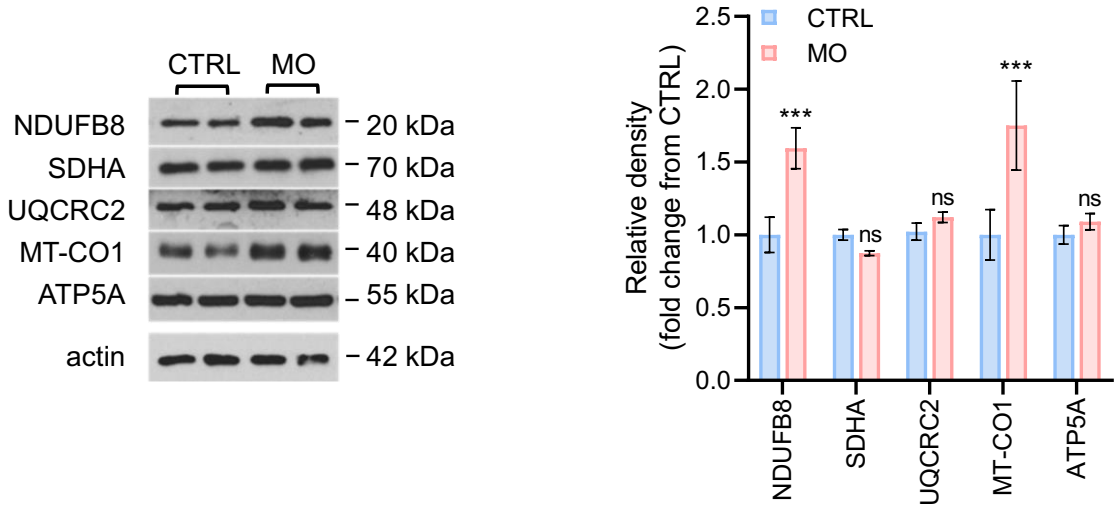

Fig. 20. Effect of FTO inhibitor MO-I-500 on relative levels of OXPHOS complexes subunits in CCF-STTG1 cells. Left: Representative Western blot images of subunits of complex I (NDUFB8), complex II (SDHA), complex III (UQCRC2), complex IV (MT-CO1), and complex V (ATP5A) in control (CTRL) and MO-I-500 treated (MO) cells. Right: Quantification of immunoblots by densitometry with normalization to actin, expressed as fold change from CTRL. Data are presented as mean ± S.E.M. Student's t-test was used to assess statistical significance between groups (ns $p > 0.05$, *** $p \leq 0.001$).

Quantification of the intracellular amount of ATP using bioluminescence assay showed elevated ATP levels by nearly 2.5 fold in CCF-STTG1 cells treated by MO-I-500 (Fig. 21).

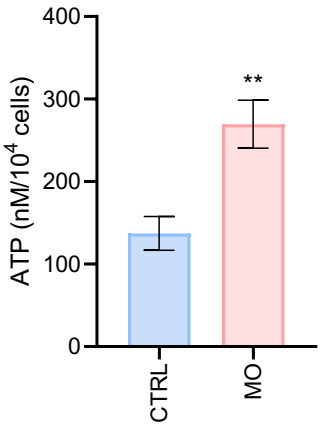

Fig. 21. Effect of FTO inhibitor MO-I-500 on intracellular ATP pool in CCF-STTG1 cells. Control cells (CTRL), MO-I-500 treated cells (MO). Data are presented as mean ± S.E.M. Student's t-test was used to assess statistical significance between groups (** $p \leq 0.01$).

The membrane potential and mass of the mitochondria were measured by flow cytometry analysis of MitoTracker Red and MitoTracker Green, respectively, labeled CCF-STTG1 cells. The median fluorescence intensity of MitoTracker Red did not differ between the control and the inhibitor-treated group (Fig. 22A). But surprisingly, suppression of FTO caused a 2-fold rise in the MitoTracker Green probe median fluorescence intensity (Fig. 22B).

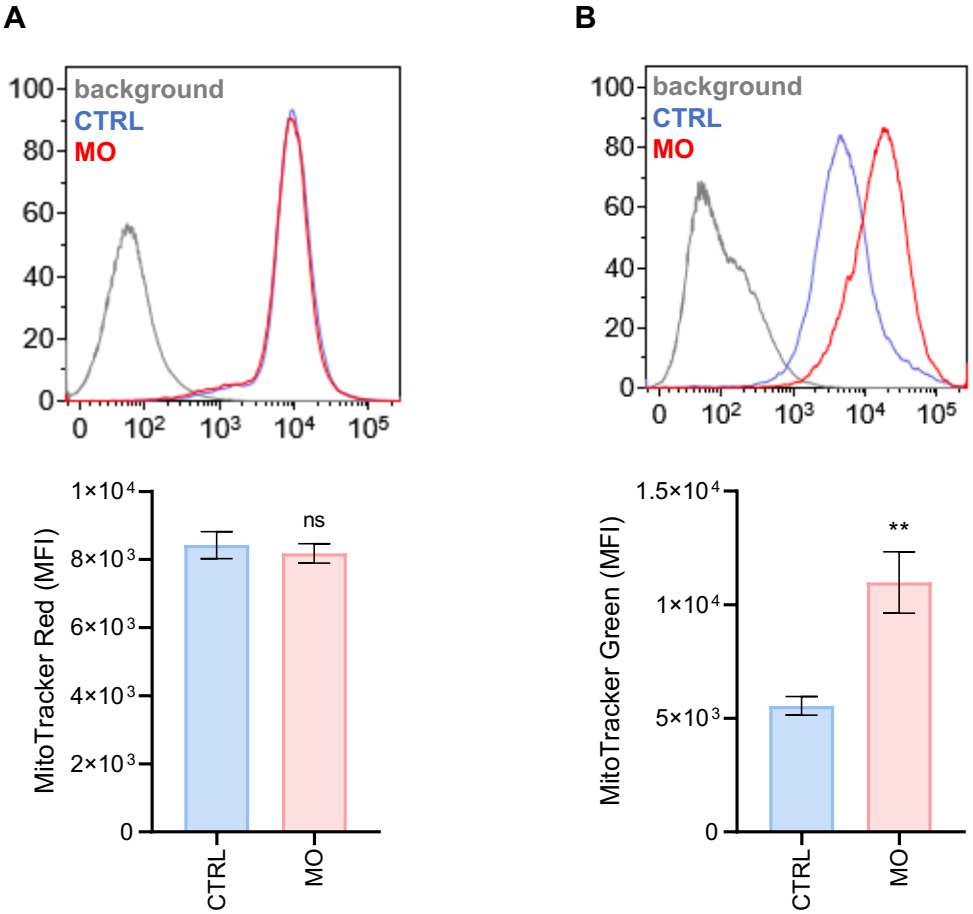

Fig. 22. Effect of FTO inhibitor MO-I-500 on mitochondrial parameters in CCF-STTG1 cells. Mitochondrial mass and mitochondrial membrane potential in controls (CTRL) and MO-I-500 treated (MO) cells were evaluated by flow cytometric analysis using MitoTracker Green (A) and MitoTracker Red CMXRos (B) probes, respectively. (A, B) Top: Representative distribution of cell fluorescence signal. Bottom: Graph showing relative median fluorescence intensity (MFI). Data are presented as mean ± S.E.M. Student's t-test was used to assess statistical significance between groups (ns $p > 0.05$, ** $p \leq 0.01$).

Finally, we investigated relative levels of a few key proteins with regard to mitochondrial bioenergetics by Western blot. The analysis did not reveal significant differences in levels of mammalian target of rapamycin (mTOR), p-mTOR, sirtuin-1 (SIRT1), AMP-activated protein kinase (AMPK), p-AMPK, ribosomal protein S6 kinase beta-1 (p70S6K), p-p70S6K and protein kinase B (Akt). The relative levels of

phosphorylated Akt (p-Akt), however, increased two times in FTO inhibitor-treated cells when compared to controls. PGC-1α was another protein that showed a change; its levels increased approximately 1.5-fold following FTO inhibitor administration (Fig. 23).

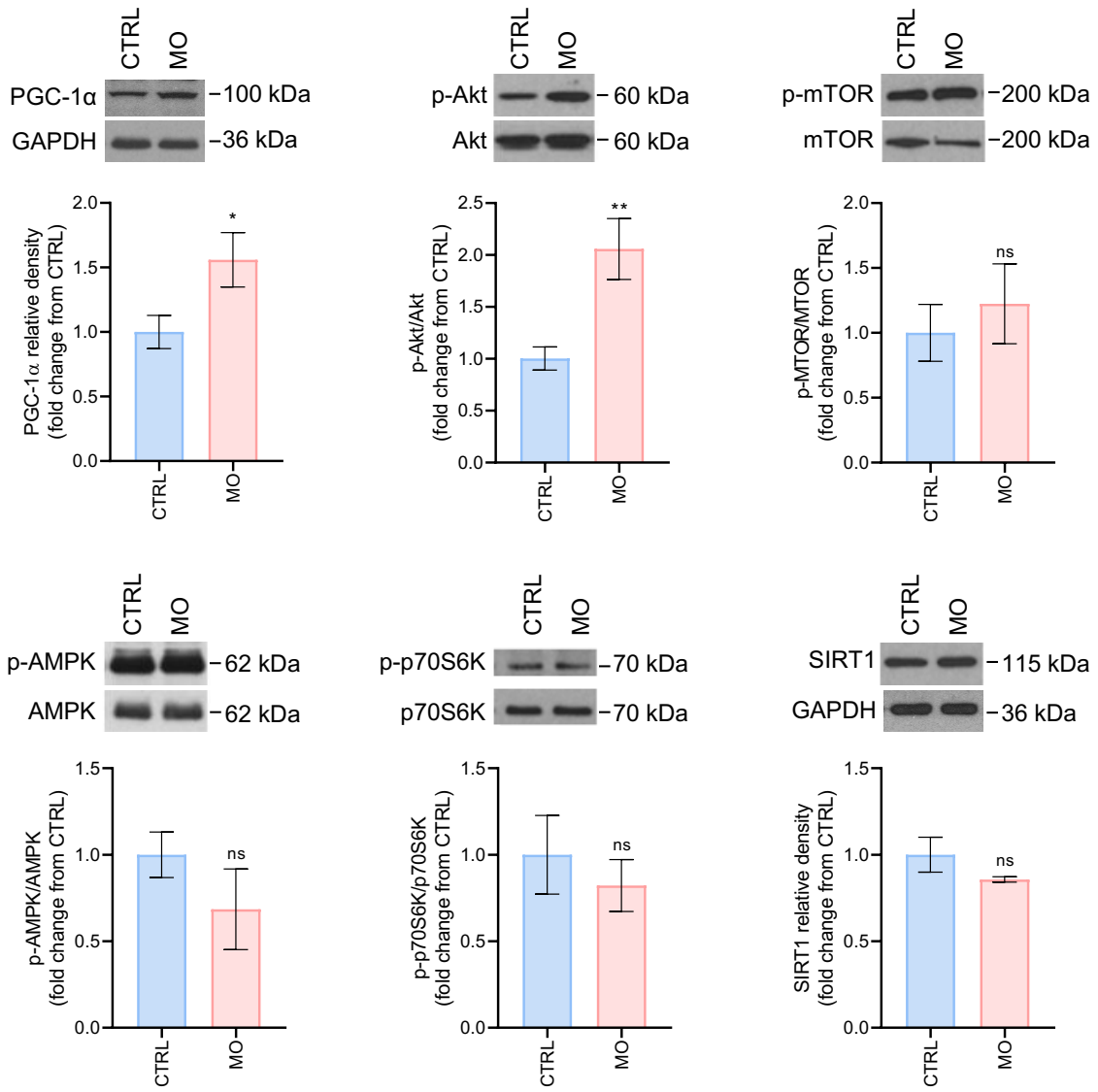

Fig. 23. Effect of FTO inhibitor MO-I-500 on relative levels of selected mitochondrial biogenesis pathway proteins in CCF-STTG1 cells. Representative immunoblots and densitometric quantification of PGC-1α, Akt, mTOR, AMPKα1/2, p70S6K, and SIRT1 in control (CTRL) and MO-I-500 treated (MO) cells. Quantification was done with normalization to GAPDH, expressed as fold change from CTRL. Single protein levels or ratios of phosphorylated (p-) protein to total protein were evaluated. Data are presented as mean ± S.E.M. Student's t-test was used to assess statistical significance between groups (ns $p > 0.05$, * $p \leq 0.05$, ** $p \leq 0.01$).

5.2.1.2 Verification of findings from FTO inhibition by FTO silencing

The effect of FTO silencing was confirmed by examining the levels of FTO protein using a Western blot. FTO signal was reduced by roughly 70% in CCF-STTG1 cells after treatment with FTO siRNA (Fig. 24).

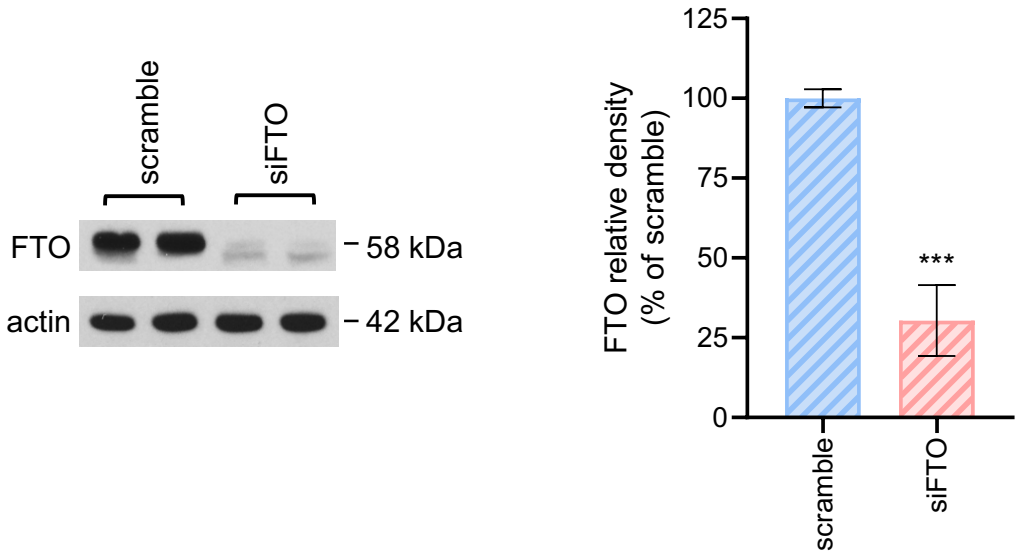

Fig. 24. Validation of FTO silencing efficiency in CCF-STTG1 cells. Left: Representative FTO immunoblot in control (scramble) and FTO siRNA treated (siFTO) group. Right: Quantification of FTO immunoblots by densitometry with normalization to actin, expressed as percentage change from the scramble. Data are presented as mean ± S.E.M. Student's t-test was used to assess statistical significance between groups (*** $p \leq 0.001$).

Similarly to MO-I-500 treatment, FTO siRNA treatment of CCF-STTG1 cells did not lead to significant changes in ECAR values assessed by Seahorse (Fig. 25A).

We found a comparable increase in maximum respiration rate after FTO silencing compared to controls as was shown after MO-I-500 treatment using Seahorse oxygen consumption measurements. But comparing controls and cells with silenced FTO, basal respiration, ATP-linked respiration, and mitochondrial leak did not change (Fig. 25C). Oxygraph respirometer assessment of oxygen consumption rate (OCR) in permeabilized cells did not reveal any substantial differences in complex I, and complex II driven OCR. Similar to inhibitor treatment, FTO silencing was followed by an increase in oxygen consumption mediated by complex IV activity by more than 100% (Fig. 25B). Comparable to inhibitor treatment, levels of both NDUFB8 and MT-CO1 OXPHOS subunits were discovered to be changed following FTO silencing. While the levels of SDHA, ATP5A, UQCRC2, and MT-CO1 did not significantly differ between control and treated cells,

protein levels of NDUFB8 and MT-CO1 increased by about 50 and 25%, respectively, in cells affected by FTO silencing (Fig. 25E).

Analysis of intracellular ATP concentration and mitochondrial mass showed similar only less pronounced changes (by about 60% and 20%, respectively) after FTO silencing, in contrast to MO-I-500 treatment (Fig. 25D,F). Just as with inhibitor treatment, Mitotracker Red CMXRos determination of MMP did not reveal significant changes due to FTO silencing (Fig. 25G).

Western blot detection of mTOR, p-mTOR, SIRT1, AMPK, p-AMPK, p70S6K, p-p70S6K, and Akt protein levels also did not reveal any discernible differences between control and treated cells. Consistent with the outcomes of FTO inhibition, PGC-1α protein levels were markedly higher (by around 30%) in FTO silenced cells, and, surprisingly, p-Akt increased by nearly 4-fold after FTO silencing (Fig. 25H).

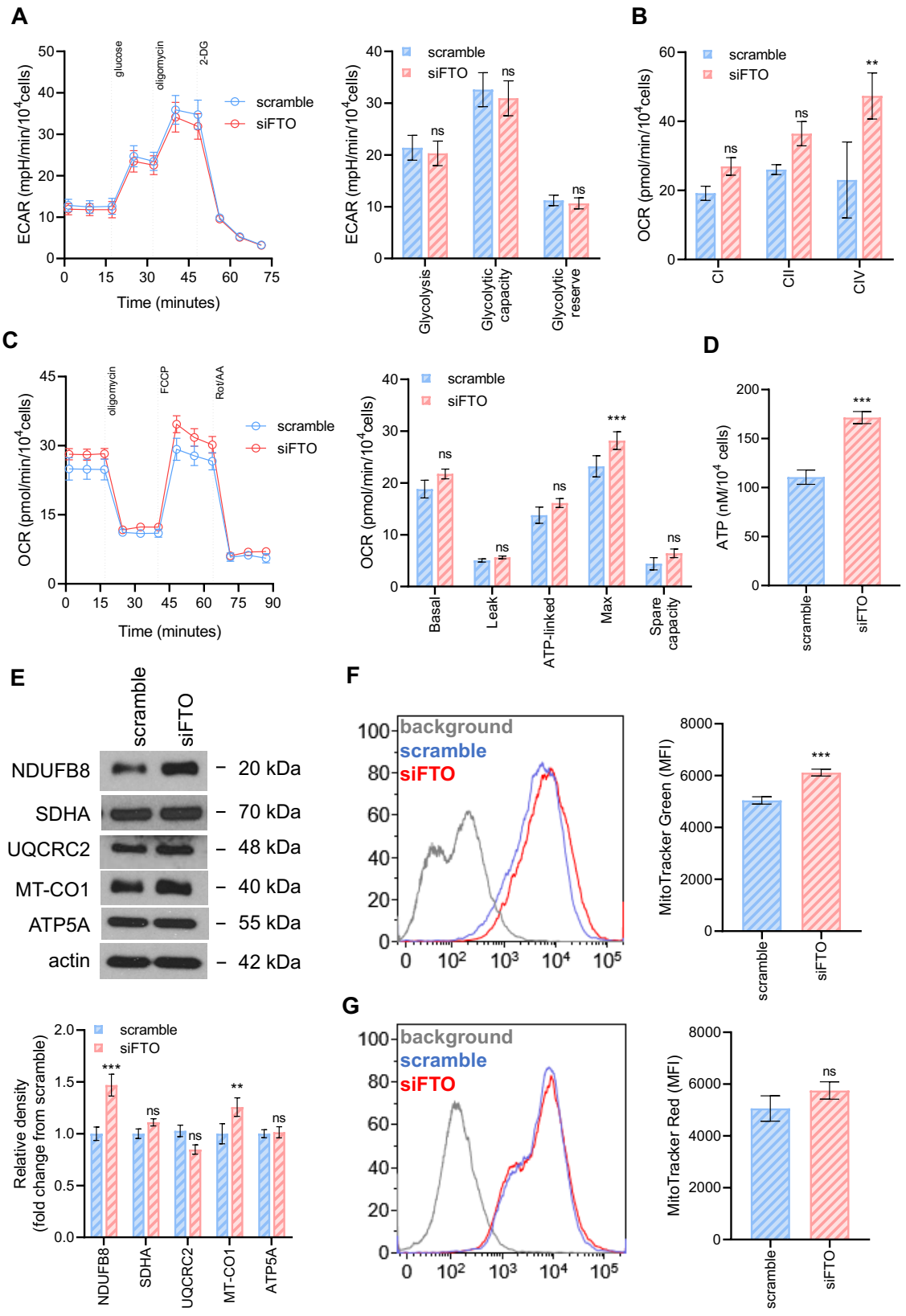
A
ECAR (mpH/min/10^4cells)
glucose
oligomycin
2-DG
scramble
siFTO
Time (minutes)
Glycolysis
Glycolytic capacity
Glycolytic reserve
ns
B
OCR (pmol/min/10^4cells)
CI
CII
CIV
**
C
FCCP
Rot/AA
Basal
Leak
ATP-linked
Max
Spare capacity
***
D
ATP (nM/10^4 cells)
E
NDUFB8
SDHA
UQCRC2
MT-CO1
ATP5A
actin
20 kDa
70 kDa
48 kDa
40 kDa
55 kDa
42 kDa
Relative density (fold change from scramble)
F
background
MitoTracker Green (MFI)
G
MitoTracker Red (MFI)

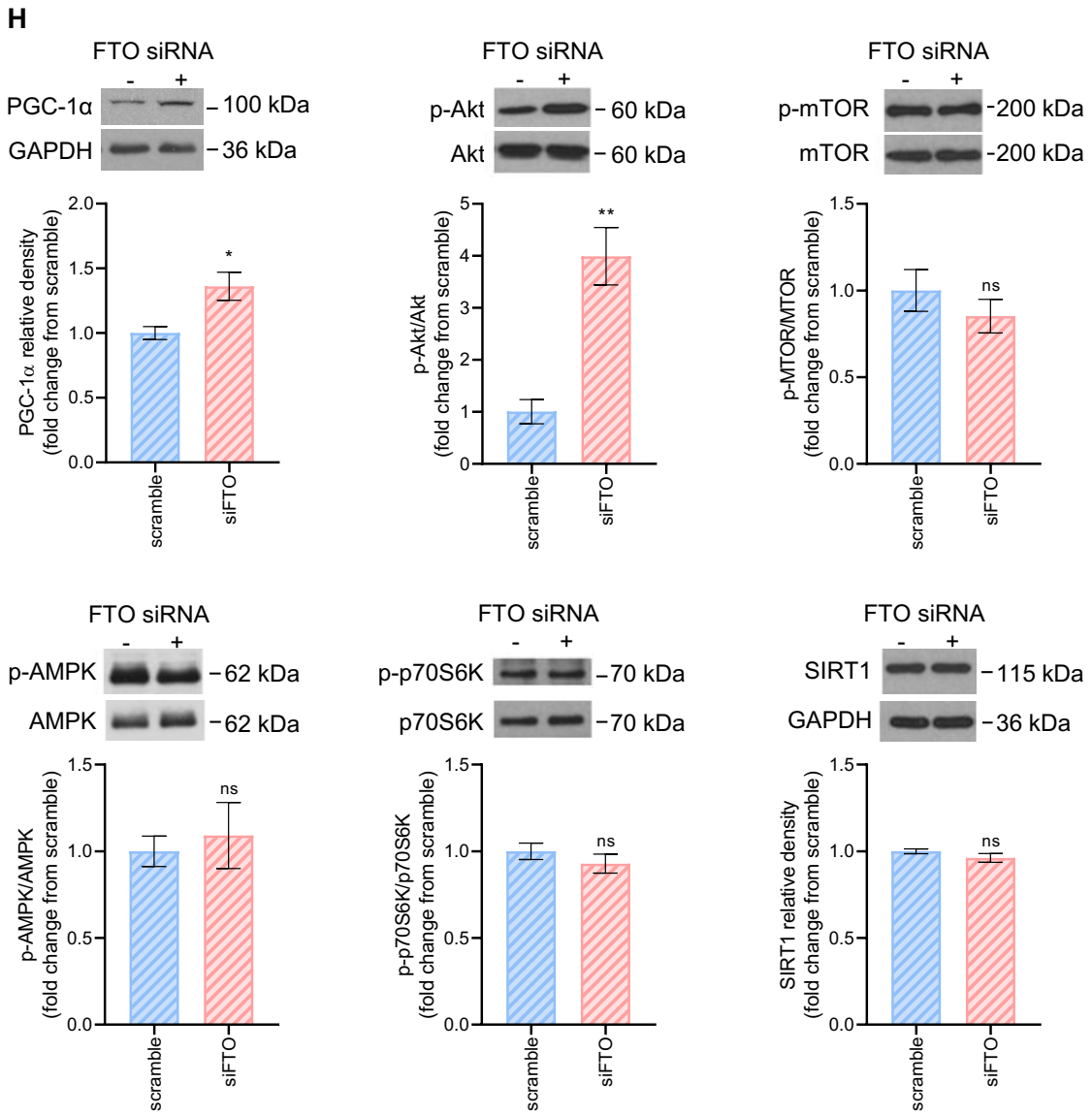

Fig. 25. The effect of FTO silencing on mitochondria and energy metabolism of CCF-STTG1 cells. Cells were treated with negative control siRNA (scramble) or FTO siRNA (siFTO). (A) Extracellular acidification rate (ECAR) measurement by Seahorse XF24 and analysis of glycolytic rate, capacity, and reserve parameters. (B) Oxygen consumption rate (OCR) driven by complex I (CI), complex II (CII), and complex IV (CIV). (C) Seahorse XF24 measurement of OCR and evaluation of individual parameters for basal respiration, ATP-linked respiration, proton leak, maximal respiration, and reserve capacity. (D) Intracellular ATP levels. (E) Representative immunoblots and densitometric quantification of subunits of complex I (NDUFB8), complex II (SDHA), complex III (UQCRC2), complex IV (MT-CO1), and complex V (ATP5A). (F) MitoTracker Green and (G) MitoTracker Red CMXRos assessment of mitochondrial mass and mitochondrial membrane potential, respectively. (F, G) Left: Representative distribution of cell fluorescence signal. Right: Graph showing relative median fluorescence intensity (MFI). (H) Representative immunoblots and densitometric quantification of PGC-1α, Akt, mTOR, AMPKα1/2, p70S6K, and SIRT1. Immunoblots were normalized to GAPDH and expressed as fold change from the scramble. Single protein levels or ratios of phosphorylated (p-) protein to total protein were evaluated. Data are presented as mean ± S.E.M. Student's t-test was used to assess statistical significance between groups (ns $p > 0.05$, * $p \leq 0.05$, ** $p \leq 0.01$, ** $p \leq 0.001$).

5.2.2 FTO suppression-induced alterations of the proteome of CCF-STTG1 cells

We used label-free MS/MS analysis to find differences in proteomes of CCF-STTG1 cells following treatment with FTO inhibitor MO-I-500 or after FTO silencing. Relative to the control, 116 proteins were identified to be differentially expressed more than 1.5-fold in the MO-I-500 treated group and 170 proteins in the siFTO group (supplementary table ST1). FTO was detected among the differentially regulated proteins after FTO silencing. Being down-regulated by approximately 5-fold in the siFTO group relative to the scramble group, it further serves as validation of silencing efficiency.

The differentially regulated proteins were further analyzed with the DAVID software for gene ontology (GO) term annotation enrichment and with the STRING software tool for functional and physical protein associations. Significant GO annotations for MO and siFTO groups are specified in the figure (Fig. 26). Interestingly, the cellular component GO term for mitochondrion was detected among significantly enriched annotations in both the inhibitor-treated group and FTO-silenced group. In addition, several functional clusters of 6 or more associated proteins were detected within the STRING interaction network (Tab. 3), including clusters of proteins relevant to mitochondrial functioning (Fig. 27).

Tab. 3. Functional protein clusters among differentially expressed proteins identified with label-free MS/MS in CCF-STTG1 cells treated with MO-I-500 (MO) or FTO siRNA (siFTO).

Cluster ID	Proteins	Main functional association
MO_1	AAMP, EMG1, FAU, HLTF, INTS7, LAGE3, LSM7, NAA10, NOP10, PDCD5, POLR1B, RPL29, RPP30, RPS7, SCD, SNRPF, SUMO1	gene expression regulation
MO_2	APOBEC3B, ATP5G1, COA3, COX7A2L, MPC1, MT-CO1, NDUFA7, SDHC	mitochondria function
MO_3	ATAD2, HIST2H3A, HIST2H3D, KDM5C, RRM1, RRM2, UHRF1	chromatin organization
siFTO_1	H1F0, H3F3A, H3F3B, HIST1H3A, HIST1H3J, HIST2H3A, HIST2H3D	gene expression regulation
siFTO_2	ATP5G1, COA3, MT-CO1, NDUFB8, UQCRH, USMG5	mitochondria function
siFTO_3	AP3B1, AP3S1, AP5B1, CPD, SYNJ1, TGOLN2	vesicle transport

Please refer to supplementary table ST1 for full protein names.

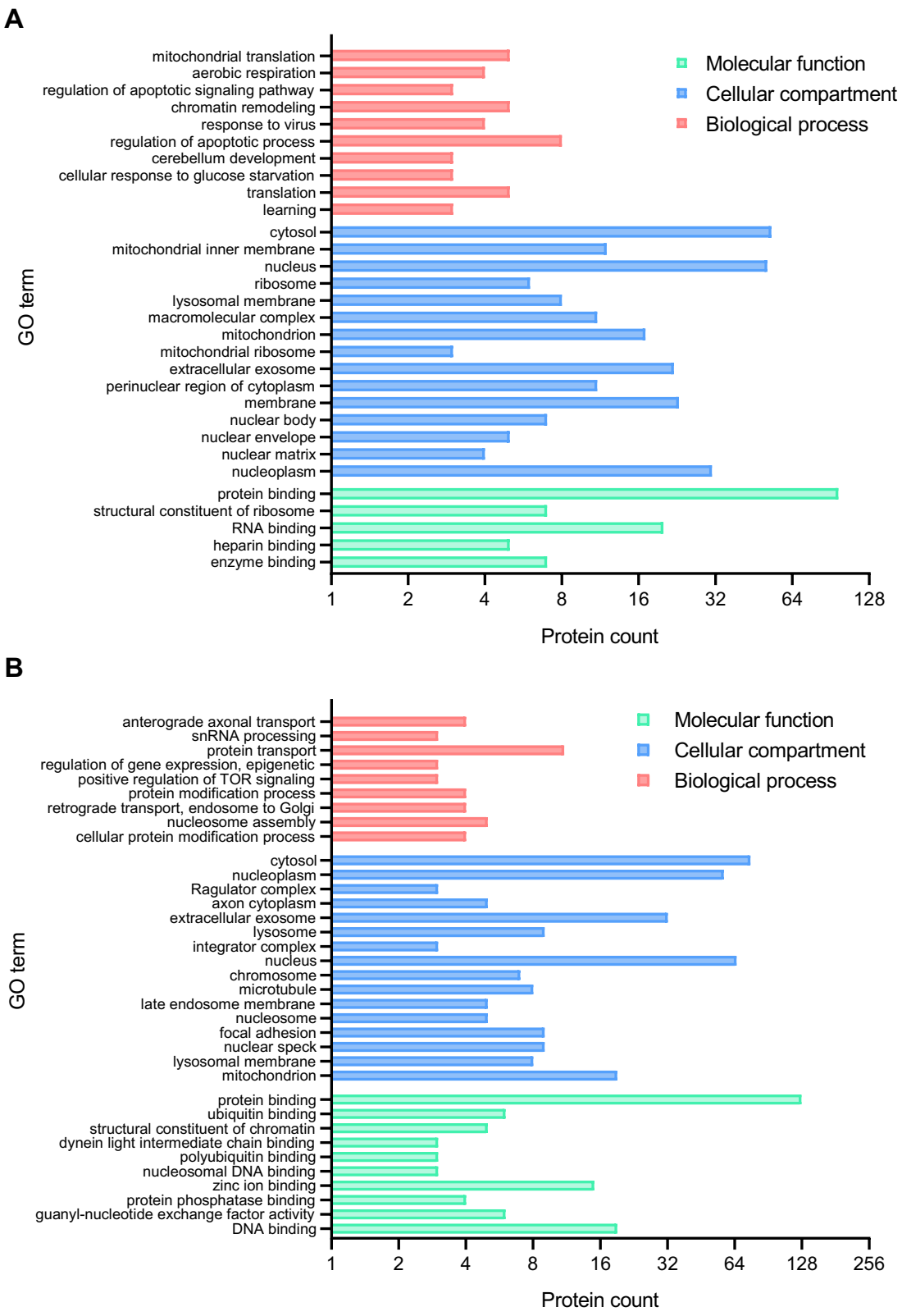

Fig. 26. Gene Ontology (GO) enrichment analysis of differentially expressed proteins in CCF-STTG1 cells. Statistically significantly (adjusted $p \leq 0.05$) enriched GO terms within the molecular function, cellular component, and biological process categories are reported. (A) Enriched GO terms of differentially expressed proteins after MO-I-500 treatment relative to controls. (B) Enriched GO terms of differentially expressed proteins after FTO silencing treatment relative to negative control silencing.

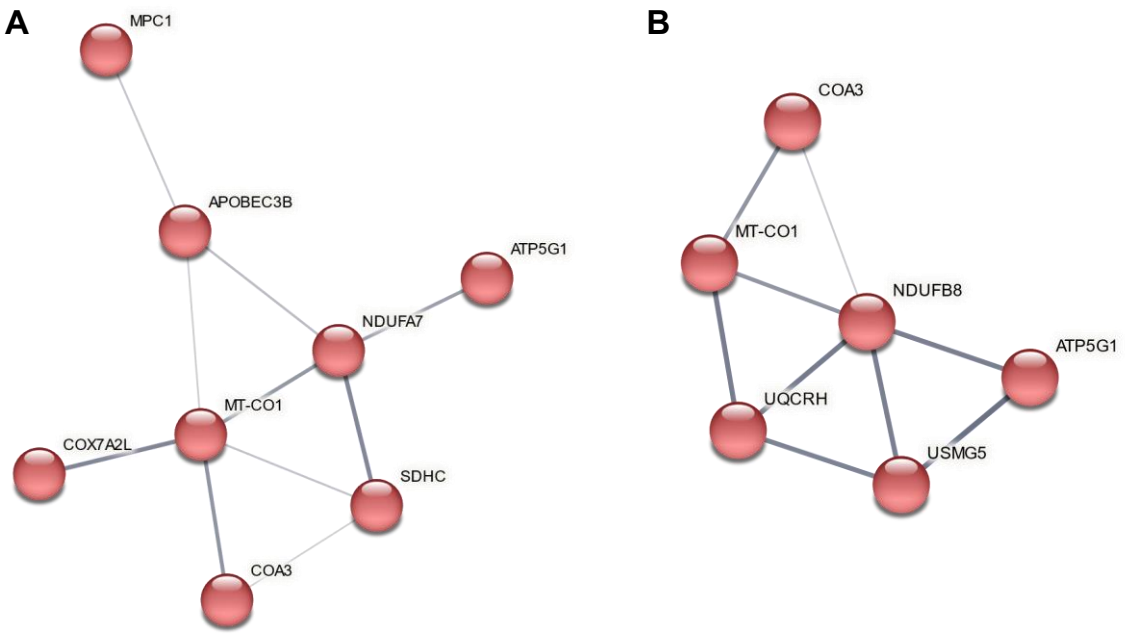

Fig. 27. STRING protein interaction networks of the functional cluster of mitochondrial proteins identified among differentially expressed proteins in CCF-STTG1 cells. (A) The cluster of differentially expressed mitochondrial proteins after MO-I-500 treatment relative to controls. (B) The cluster of differentially expressed mitochondrial proteins after FTO silencing treatment relative to negative control silencing. Refer to Tab. 4 for full protein names.

We have investigated fold changes of these mitochondrion-linked proteins from both groups, MO and siFTO. Among the 11 proteins, 4 were differentially regulated by more than 1.5-fold in a similar manner in the MO and the siFTO group, and 7 in an opposite direction or only in one group (Tab. 4). Most of the proteins were associated with the functioning of the respiratory chain.

Tab. 4. List of mitochondrial metabolism-relevant proteins identified with label-free MS/MS in CCF-STTG1 cells treated with MO-I-500 (MO) or FTO siRNA (siFTO). Reported is fold change (FC) against respective control.

Gene ID	Protein name	FC MO	FC siFTO	Mitochondrial function
MT-CO1	Cytochrome c oxidase subunit 1	1.68	1.56	OXPHOS
COA3	Cytochrome c oxidase assembly factor 3 homolog	1.50	1.54	OXPHOS
ATP5G1	ATP synthase F(0) complex subunit C1	3.98	1.64	OXPHOS
NDUFA7	NADH dehydrogenase 1 alpha subcomplex subunit 7	-1.50	1.13	OXPHOS
NDUFB8	NADH dehydrogenase 1 beta subcomplex subunit 8	-1.26	1.75	OXPHOS
UQCRH	Cytochrome b-c1 complex subunit 6	1.16	-1.54	OXPHOS
SDHC	Succinate dehydrogenase cytochrome b560 subunit	-1.66	1.17	OXPHOS
COX7A2L	Cytochrome c oxidase subunit 7A-related protein	4.51	-1.03	OXPHOS
USMG5	ATP synthase membrane subunit DAPIT	-1.24	-1.65	OXPHOS
APOBEC3B	DNA dC->dU-editing enzyme APOBEC-3B	1.87	1.27	mtDNA editing
MPC1	Mitochondrial pyruvate carrier 1	1.50	1.95	pyruvate transport

Green text: FC ≥ 1.5, red text: FC ≤ -1.5.

5.2.3 The role of FTO inhibition in the sensitivity of CCF-STTG1 to streptozotocin

5.2.3.1 Streptozotocin reduces astrocyte viability in a concentration-dependent manner

In the initial investigations, we used the MTT test to assess the effect on the viability of CCF-STTG1 cells by using a wide range of STZ concentrations (0.5-18 mM) throughout a 48-hour incubation period (Fig. 28). At a STZ dosage of 3 mM, astrocyte viability began to significantly diminish (by roughly 15%), and as the dose increased, the viability of the cells continued to decline. We employed 15 mM STZ, which resulted in a roughly 50% drop in viability when compared to control cells in all following studies.

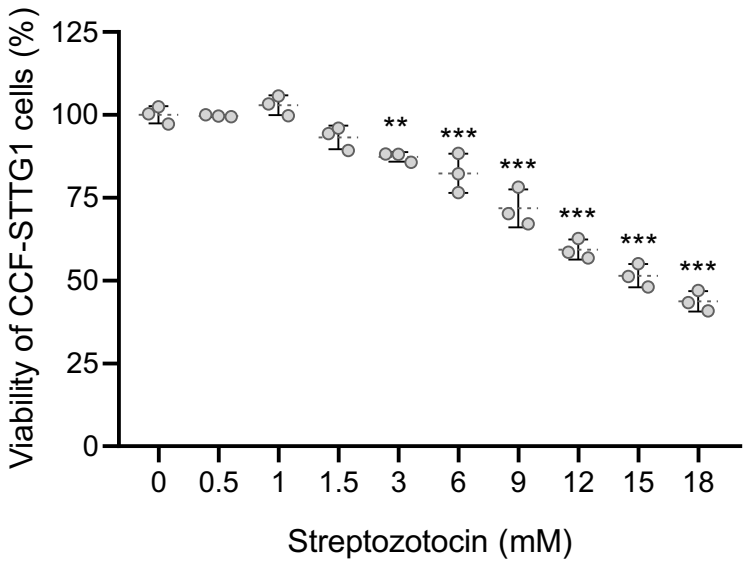

Fig. 28. Effects of streptozotocin dose on the viability of CCF-STTG1 cells. The viability of cells treated with different concentrations of streptozotocin for 48 h is expressed as a percentage change from the untreated control group (0 mM). Data are presented as mean ± S.E.M. ANOVA followed by Dunnett's post hoc test was used to assess statistical significance when comparing means of treated groups with the control group (** $p \leq 0.01$ and *** $p \leq 0.001$).

5.2.3.2 Streptozotocin induces changes in m6A machinery proteins

Firstly, we used Western blotting to determine how 48-hour treatment with 15 mM STZ on CCF-STTG1 cells affected the expression of proteins involved in N6-methyladenosine (m6A) regulation. STZ administration resulted in a significant overexpression (by more than 100%) of m6A demethylase FTO. Additionally, the level of m6A reader protein YTH domain-containing family protein 1 (YTHDF1) showed a statistically significant, albeit modest, rise (by around 20%). The expression of the reader proteins YTHDF2, YTHDF3, YTH domain-containing protein 1 (YTHDC1), and YTHDC2, as well as RNA demethylase AlkB homolog 5 (ALKBH5) and N6-adenosine-methyltransferase 70 kDa subunit (METTL3), did not significantly change, according to our findings (Fig. 29).

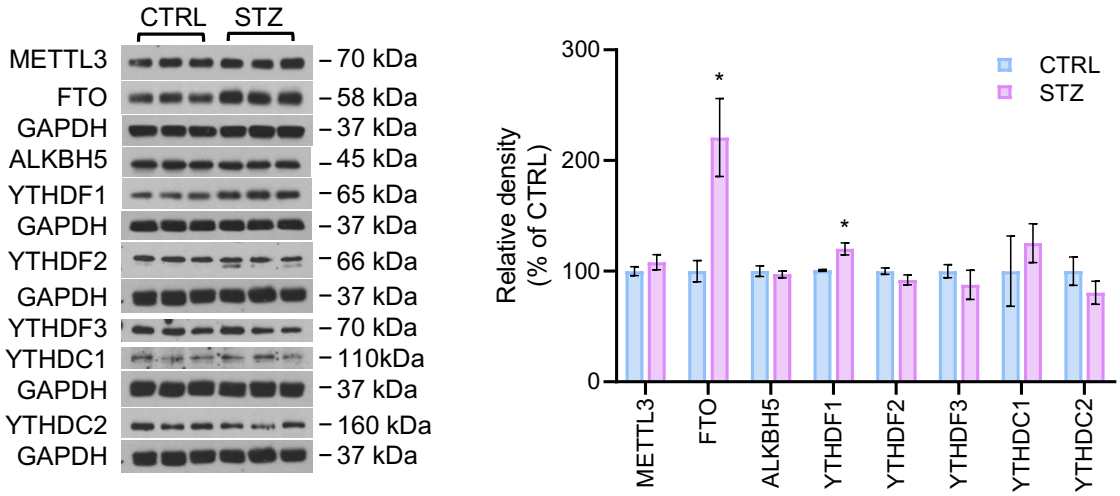

Fig. 29. Effect of streptozotocin on the relative expression of the m6A machinery enzymes in CCF-STTG1 cells. Cells were treated with vehicle (CTRL) or incubated in the presence of 15 mM streptozotocin (STZ) for 48 h. Left: Representative images of Western blots of m6A demethylases FTO and ALKBH5, methyltransferase METTL3, and reader proteins YTHDF1-3, YTHDC1-2. Right: Quantification of immunoblots by densitometry with normalization to GAPDH, expressed as a percentage change from CTRL. Values are presented as mean ± S.E.M. Student's t-test was used to assess statistical significance between groups (* $p \leq 0.05$ vs CTRL).

An antibody-based quantification kit was used to quantify the global m6A levels in mRNA (Fig. 30). When FTO was inhibited by 10 μM dose of MO-I-500 for 72 h, m6A levels significantly increased by approximately 90%. We observed a drop in m6A level by about 70% when STZ was added to CCF-STTG1 cells. The decrease in m6A in cells treated with STZ was consistent with previously observed elevated levels of FTO, although the impact was not statistically significant. Similarly, although the FTO inhibitor resulted in elevated m6A levels of STZ-stressed cells, the difference between STZ and MO+STZ was not statistically significant.

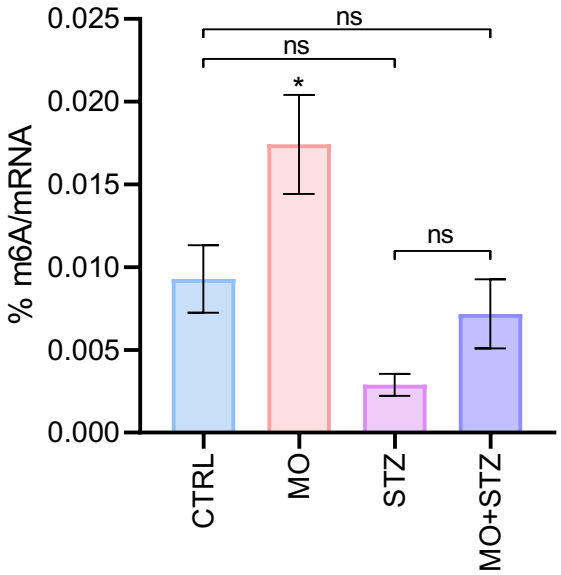

Fig. 30. Effect of streptozotocin and FTO inhibitor MO-I-500 on m6A content in CCF-STTG1 cells. The percentage of m6A methylation levels in mRNA was determined in cells treated with vehicle (CTRL), 15 mM streptozotocin (STZ), 10 μM MO-I-500 (MO), or co-treated with 10 μM MO-I-500 and 15 mM streptozotocin (MO+STZ). Values are presented as mean ± S.E.M. ANOVA followed by the Newman-Keuls test was used to assess statistical significance (ns $p > 0.05$,* $p \leq 0.05$). Only selected statistical comparisons are reported in graphs: CTRL vs STZ, CTRL vs MO, CTRL vs MO+STZ, STZ vs MO+STZ.

5.2.3.3 The survival of astrocytes damaged by streptozotocin is enhanced by FTO inhibition

The MTT and LDH leakage tests were then used to examine the impact of MO-I-500 on cell viability and cytotoxicity, respectively. The 24 h pretreatment of astrocytes with MO-I-500 did not have a detrimental effect on cell survival, but it did partially increase the resilience of these cells to the toxic effects of streptozotocin (Fig. 31). Inhibitor treatment increased survival of STZ-stressed cells by about 20% and reduced LDH release by 15% in comparison to rates of STZ group.

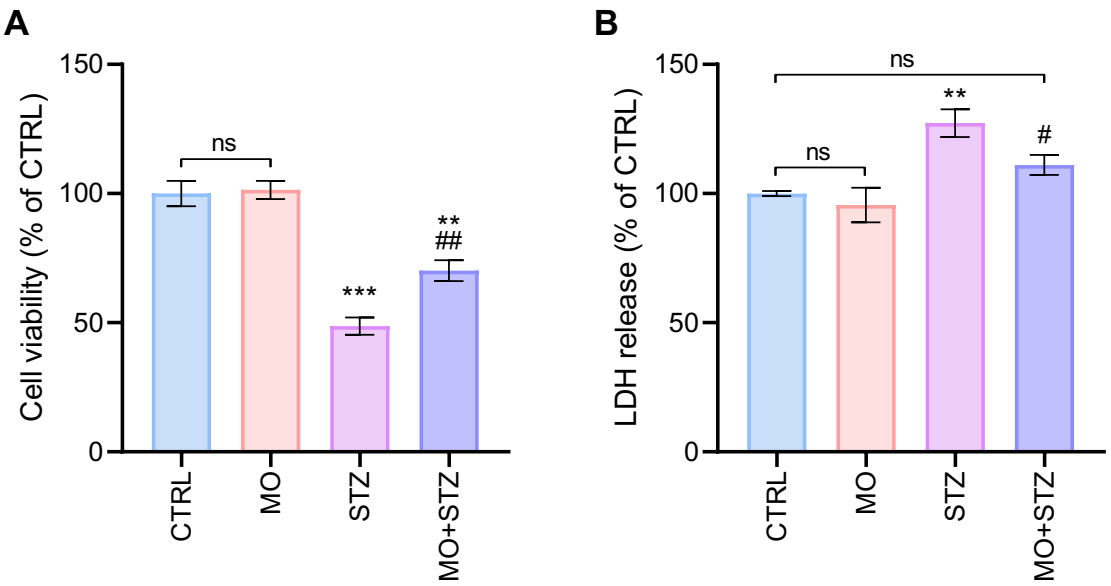

Fig. 31. Effect of streptozotocin and FTO inhibitor MO-I-500 on CCF-STTG1 cell survival. (A) Cell viability and (B) lactate dehydrogenase (LDH) release was evaluated in cells treated with vehicle (CTRL), 15 mM streptozotocin (STZ), 10 μM MO-I-500 (MO) or co-treated with 10 μM MO-I-500 and 15 mM streptozotocin (MO+STZ). Data are expressed as a percentage change from CTRL. Values are presented as mean ± S.E.M. ANOVA followed by Newman-Keuls test was used to assess statistical significance (ns $p > 0.05$, ** $p \leq 0.01$ and *** $p \leq 0.001$ vs CTRL; # $p \leq 0.05$ and ## $p \leq 0.01$ vs STZ). Only selected statistical comparisons are reported in graphs: CTRL vs STZ, CTRL vs MO, CTRL vs MO+STZ, STZ vs MO+STZ.

Flow cytometry examination of apoptosis and necrosis by using Annexin V/Hoechst 33258 dual staining provided additional evidence for the cytoprotective impact of FTO inhibition. Treatment with STZ significantly decreased cell survival and correspondingly increased both apoptosis and necrosis. When challenged with STZ, the presence of the FTO inhibitor moderately improved astrocyte survival (by about 10%), mostly because of a reduced necrosis rate (Fig. 32).

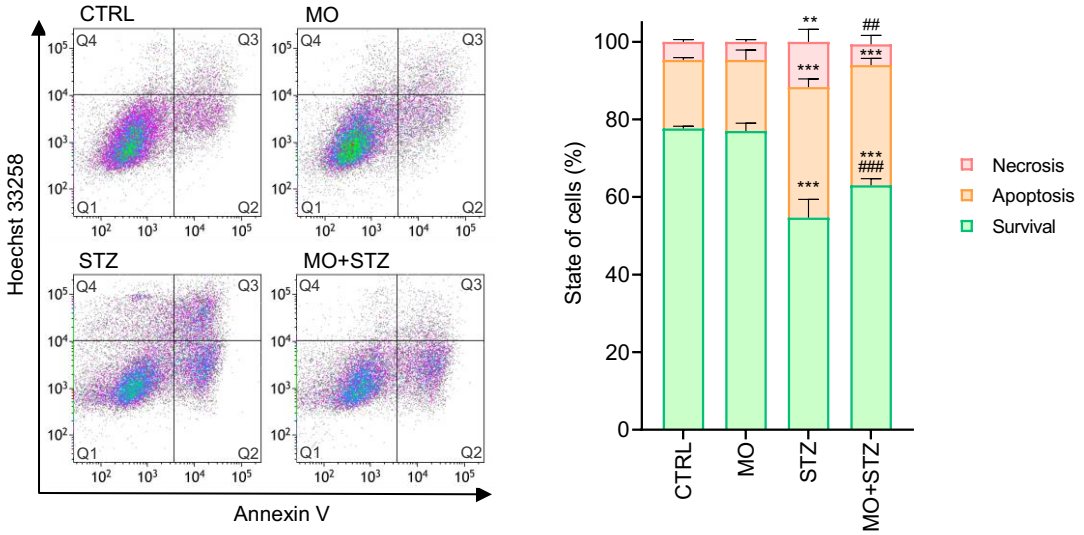

Fig. 32. Effect of streptozotocin and FTO inhibitor MO-I-500 on CCF-STTG1 cell apoptosis. Cells were treated with vehicle (CTRL), 15 mM streptozotocin (STZ), 10 µM MO-I-500 (MO), or co-treated with 10 µM MO-I-500 and 15 mM streptozotocin (MO+STZ). The cellular survival rate, apoptosis, and necrosis were determined by flow cytometry using Annexin V/Hoechst 33258 staining. Left: Representative scatter plots of Annexin V/Hoechst 33258 staining in cells under different experimental conditions. Rectangular gates indicate healthy (unstained, Q1), apoptotic (Annexin stained, Q2+Q3), or necrotic (exclusively Hoechst stained, Q4) populations of cells. Right: Quantification of the percentage of cells in the healthy, apoptotic, or necrotic state. Data are presented as mean ± S.E.M. ANOVA followed by the Newman-Keuls test was used to assess statistical significance (** $p \leq 0.01$ and *** $p \leq 0.001$ vs CTRL; ## $p \leq 0.01$ and ### $p \leq 0.001$ vs STZ). Only selected statistical comparisons are reported in graphs: CTRL vs STZ, CTRL vs MO, CTRL vs MO+STZ, STZ vs MO+STZ.

5.2.3.4 Streptozotocin-induced activation of apoptotic signaling is diminished by inhibition of FTO

Levels of proteins or their post-translationally modified variations exhibiting anti-apoptotic (nuclear factor erythroid 2–related factor 2 (NRF2), poly [ADP-ribose] polymerase 1 (PARP1), apoptosis regulator BCL-2, mitogen-activated protein kinase 3 and 1 (ERK1/2)) or pro-apoptotic (ubiquitinylated NRF2, cleaved PARP1, apoptosis regulator BAX, phosphorylated ERK1/2) behavior were assessed by Western blotting to further define the impact of FTO and STZ inhibition on the susceptibility of astrocytes to apoptosis. The ratios of pertinent pro- and anti-apoptotic mediators were computed in order to assess the level of apoptotic pathway activation (Fig. 33). As evidenced by increased ratios of ubiquitinylated NRF2/NRF2 (2.1-fold), cleaved PARP1/PARP1 (4.8-fold), BAX/BCL-2 (6.5-fold), and phosphorylated ERK/ERK (2.8-fold), treatment with STZ strongly activated apoptotic signaling pathways. When comparing STZ treatment to controls, analysis of the expression levels of caspase 3 (CASP3) revealed a 1.3-fold

increase in 32 kDa protein. Caspase 3 cleaved variants, however, were not detected, therefore we are unable to say if the observed effect is pro-apoptotic. Compared to the STZ group, pretreatment of cells with FTO inhibitor MO-I-500 led to a notable decline in all the measured ratios and CASP3 protein levels.

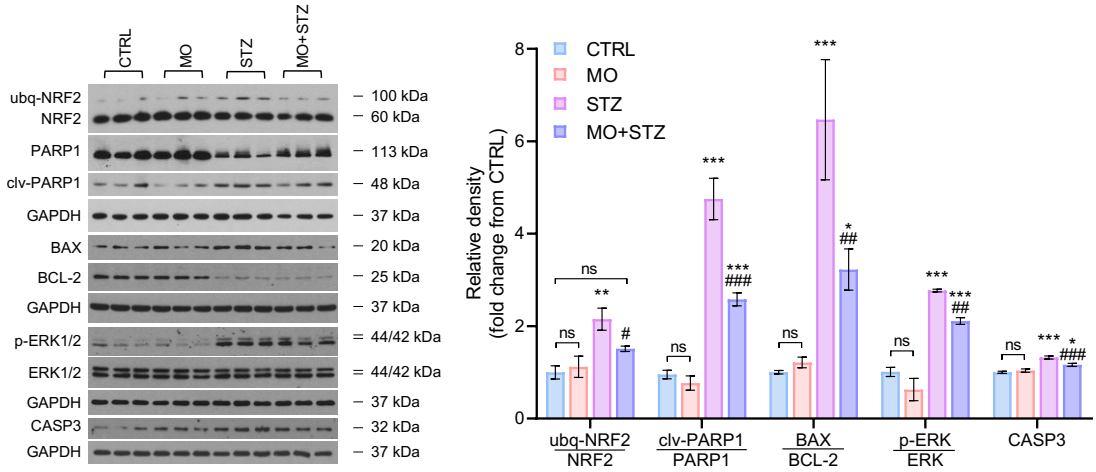

Fig. 33. Effect of streptozotocin and FTO inhibitor MO-I-500 on the expression of selected apoptotic signaling pathway proteins in CCF-STTG1 cells. Left: Representative immunoblots of BAX, BCL-2, PARP1, NRF2, ERK1/2, CASP3 or their modifications (polyubiquitinated (ubq-), cleaved (clv-), phosphorylated (p-)) from samples treated with vehicle (CTRL), 15 mM streptozotocin (STZ), 10 μM MO-I-500 (MO) or co-treated with 10 μM MO-I-500 and 15 mM streptozotocin (MO+STZ). Right: Quantification of immunoblots by densitometry with normalization to GAPDH, expressed as a fold change from CTRL. Single protein levels or ratios of pro- to anti-apoptotic markers were evaluated. Data are presented as mean ± S.E.M. ANOVA followed by Newman-Keuls test was used to assess statistical significance (ns $p > 0.05$, * $p \leq 0.05$, ** $p \leq 0.01$ and *** $p \leq 0.001$ vs CTRL; # $p \leq 0.05$, ## $p \leq 0.01$ and ### $p \leq 0.001$ vs STZ). Only selected statistical comparisons are reported in graphs: CTRL vs STZ, CTRL vs MO, CTRL vs MO+STZ, STZ vs MO+STZ.

5.2.3.5 FTO inhibition elicits a protective effect against GFAP elevation and streptozotocin-induced oxidative stress

We have investigated expression levels of glial fibrillary acidic protein (GFAP) and observed an increase after STZ administration, indicating that CCF-STTG1 cells were more reactive. While STZ raised GFAP levels by around 85%, relative levels of GFAP in the presence of the FTO inhibitor MO-I-500 were nearly identical to those seen in the control group (Fig. 34A). Because astrocyte activation into reactive astrocytes might happen under oxidative stress, we next assessed the production of intracellular reactive oxygen species (ROS) using dihydroethidium (DHE) probe and fluorescence microscopy image analysis. After STZ treatment, the average cellular DHE signal was significantly raised (by nearly 60%), indicating increased ROS generation. Interestingly,

streptozotocin's stimulatory effect was entirely eliminated in the presence of MO-I-500 (Fig. 34B-C). In addition, evaluation of the percentage of DHE-negative cells defined by intensity threshold showed that only about 6% of STZ-treated cells lacked DHE signal in contrast to 24% observed in controls (Fig. 34D).

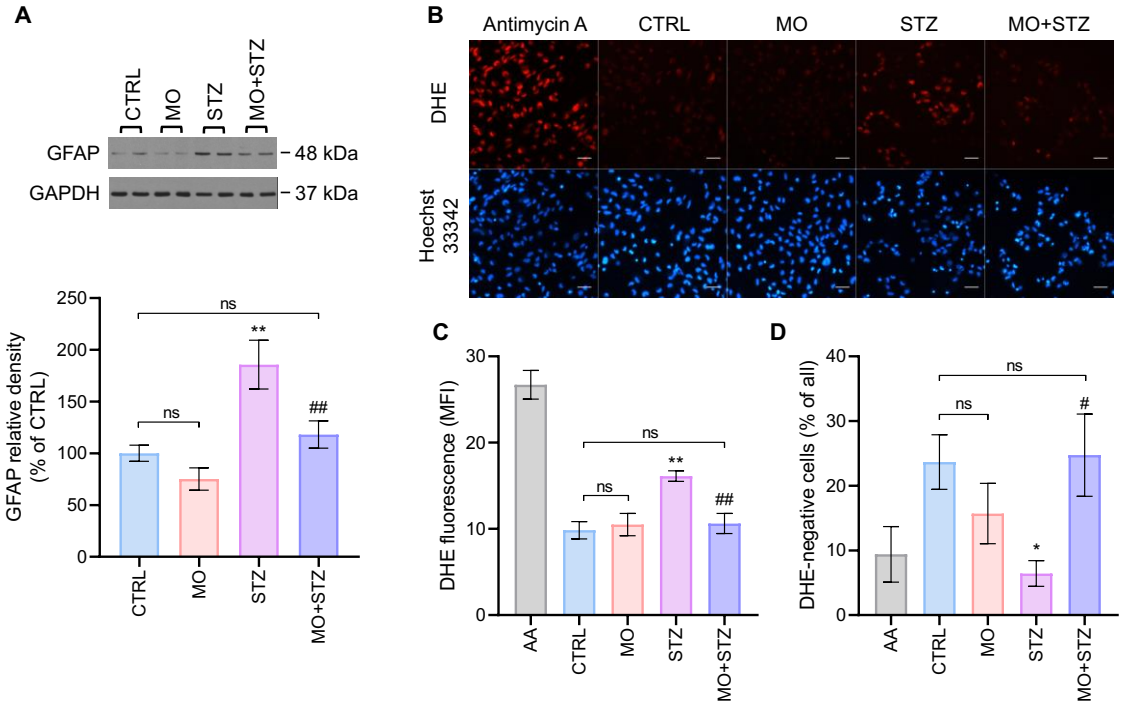

Fig. 34. Effect of streptozotocin and FTO inhibitor MO-I-500 on ROS generation and astrocyte activation. CCF-STTG1 cells were treated with vehicle (CTRL), 15 mM streptozotocin (STZ), 10 μM MO-I-500 (MO), or co-treated with 10 μM MO-I-500 and 15 mM streptozotocin (MO+STZ). (A) Representative immunoblot and densitometric quantification of GFAP as a marker indicative of astrocyte reactivity. Immunoblots were normalized to GAPDH and expressed as percentage change from CTRL. (B-D) Intracellular levels of ROS were determined by DHE fluorescence. Antimycin A (AA) treated cells were used as a positive control. (B) Representative fluorescence microscopy images of DHE signal in cells. (C) Quantification of mean cellular DHE fluorescence intensity (MFI). (D) Quantification of the percentage of cells lacking DHE signal. Scale bar: 10 μm. Nuclei were detected with Hoechst 33342. Data are presented as mean ± S.E.M. ANOVA followed by Newman-Keuls test was used to assess statistical significance (ns $p > 0.05$, * $p \leq 0.05$ and ** $p \leq 0.01$ vs CTRL; # $p \leq 0.05$ and ## $p \leq 0.01$ vs STZ). Only selected statistical comparisons are reported in graphs: CTRL vs STZ, CTRL vs MO, CTRL vs MO+STZ, STZ vs MO+STZ.

5.2.3.6 STZ and FTO inhibition affect mitochondria and cellular bioenergetics

The membrane potential and mass of the mitochondria were measured by flow cytometry analysis of MitoTracker Red and MitoTracker Green, respectively, labeled CCF-STTG1 cells. While STZ treatment caused MitoTracker Red fluorescence intensity in cells to decline significantly (by roughly 45%), suggesting damaged mitochondria with lower mitochondrial potential, this negative impact was lessened by the FTO inhibitor MO-I-500.

Only around 25% of the mitochondrial membrane potential was lost when cells were pretreated with the inhibitor (Fig. 35A). When compared to control cells, STZ-treated cells did not show any differences in the mitochondrial mass when stained with MitoTracker Green (Fig. 35B).

Next, we investigated the effects of STZ and the FTO inhibitor on mitochondrial respiration and intracellular ATP levels. Real-time measurement of the extracellular oxygen consumption of whole cells was used to assess the respiration rates in astrocytes. In STZ-treated cells, the baseline oxygen consumption rate was lowered to about half of the control level. The maximum respiration rate brought on by a strong protonophore uncoupler of mitochondrial oxidative phosphorylation (FCCP) too was suppressed in STZ-treated cells. The nearly nonexistent ability of these cells to promote respiration suggested a reduction in electron transport chain (ETC) capability. When compared to the STZ group, pretreatment of cells with MO-I-500 almost entirely restored basal mitochondrial respiration and moderately increased maximal oxygen consumption rate, indicating partial preservation of ETC capability (Fig. 35C).

In line with earlier findings, STZ-affected CCF-STTG1 cells had decreased intracellular ATP concentrations, as revealed by a bioluminescence assay used to measure ATP quantity. When FTO was blocked by MO-I-500, this impact was somewhat mitigated (Fig. 35D).

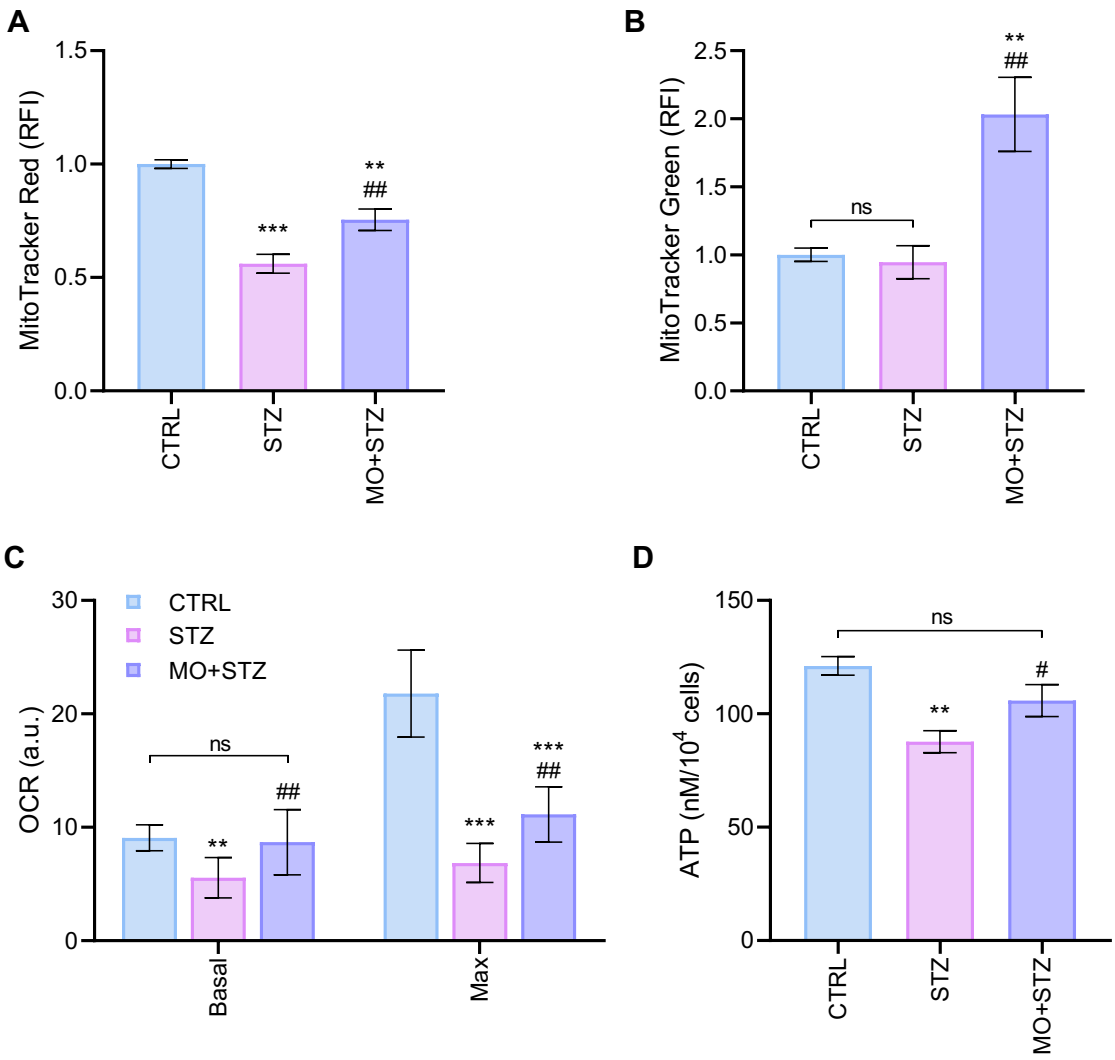

Fig. 35. Effect of streptozotocin and FTO inhibitor MO-I-500 on mitochondrial function and bioenergetics of CCF-STTG1 cells. Cells were treated with vehicle (CTRL), 15 mM streptozotocin (STZ), or co-treated with 10 µM MO-I-500 and 15 mM streptozotocin (MO+STZ). (A) Quantification of MitoTracker Red CMXRos fluorescence in cells as a measure of mitochondrial membrane potential, expressed as relative median fluorescence intensity (RFI). (B) Quantification of MitoTracker Green fluorescence in cells as a measure of mitochondrial mass, expressed as RFI. (C) Basal and FCCP-induced maximal oxygen consumption rates (OCR). (D) Intracellular ATP content. Data are presented as mean ± S.E.M. ANOVA followed by Newman-Keuls test was used to assess statistical significance (ns $p > 0.05$, ** $p \leq 0.01$ and *** $p \leq 0.001$ vs CTRL; # $p \leq 0.05$ and ### $p \leq 0.001$ vs STZ). Measured values for the MO group are not reported here due to data redundancy, the comparison of CTRL vs MO was reported previously in this work in section 5.2.1.1.

Analysis of the phosphorylation of the protein kinase 5' adenosine monophosphate-activated protein kinase (AMPK) by Western blotting supported the apparent change in energy status in cells impacted by STZ (Fig. 36). In reaction to energy stress, AMPK is considered as the master regulator of metabolism. In this study, we found that pretreatment of cells with the FTO inhibitor MO-I-500 did not result in an increase in

AMPK phosphorylation (p-AMPK), as it did in the STZ group. While STZ caused almost a 2-fold rise in the p-AMPK/AMPK ratio, astrocytes pretreated with MO-I-500 showed this ratio to be comparable to the control group.

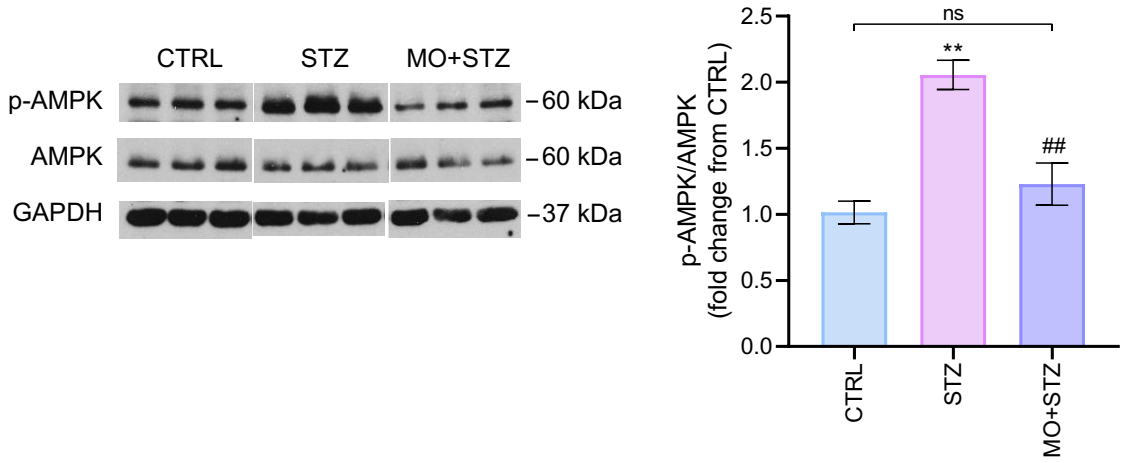

Fig. 36. Effect of streptozotocin and FTO inhibitor MO-I-500 on relative AMPK expression in CCF-STTG1 cells. Left: Representative immunoblot of phosphorylated (p-AMPKa1/2) and total AMPKα1/2 from samples treated with vehicle (CTRL), 15 mM streptozotocin (STZ), or co-treated with 10 μM MO-I-500 and 15 mM streptozotocin (MO+STZ). Right: Quantification of immunoblots by densitometry with normalization to GAPDH, expressed as a fold change from CTRL. The ratio of p-AMPKa1/2 to AMPKa1/2 was determined. Data are presented as mean ± S.E.M. ANOVA followed by the Newman-Keuls test was used to assess statistical significance (ns $p > 0.05$, ** $p \leq 0.01$ vs CTRL; ## $p \leq 0.01$ vs STZ). Measured values for the MO group are not reported here due to data redundancy, the comparison of CTRL vs MO was reported previously in this work in section 5.2.1.1.

Finally, we have examined the insulin receptor beta (IRβ) and insulin receptor substrates 1 and 2 (IRS-1, IRS-2) protein levels by Western blot analysis. While IRβ was significantly down-regulated by streptozotocin (by 50%), IRS-1 and IRS-2 were also down-regulated (by roughly 20% and 40%, respectively) but insignificantly. The FTO inhibitor MO-I-500 had only a negligible impact on levels of IRβ, IRS-1, and IRS-2 (Fig. 37).

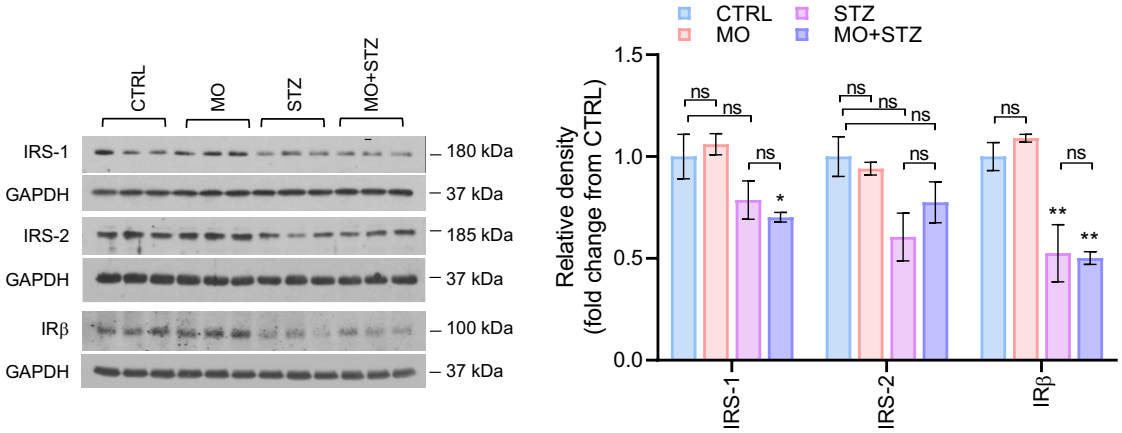

Fig. 37. Effect of streptozotocin and FTO inhibitor MO-I-500 on the expression of selected insulin signaling pathway proteins in CCF-STTG1 cells. Left: Representative immunoblots of insulin receptor beta (IRβ) and insulin receptor substrates 1-2 (IRS-1, IRS-2) from samples treated with vehicle (CTRL), 15 mM streptozotocin (STZ), 10 μM MO-I-500 (MO) or co-treated with 10 μM MO-I-500 and 15 mM streptozotocin (MO+STZ). Right: Quantification of immunoblots by densitometry with normalization to GAPDH, expressed as a fold change from CTRL. Data are presented as mean ± S.E.M. ANOVA followed by Newman-Keuls test was used to assess statistical significance (ns $p > 0.05$, * $p \leq 0.05$ and ** $p \leq 0.01$ vs CTRL). Only selected statistical comparisons are reported in graphs: CTRL vs STZ, CTRL vs MO, CTRL vs MO+STZ, STZ vs MO+STZ.

5.2.3.7 STZ but not FTO inhibition affect tau phosphorylation levels

We used Western blotting to assess levels of total tau and tau phosphorylation at S396 (p-tau). Following STZ treatment, levels of p-tau/tau ratio significantly increased by approximately 2.7-fold, with minimal effect on total tau levels. The FTO inhibitor MO-I-500 did not significantly affect p-tau levels nor did it have any significant effect on STZ-induced tau phosphorylation (Fig. 38).

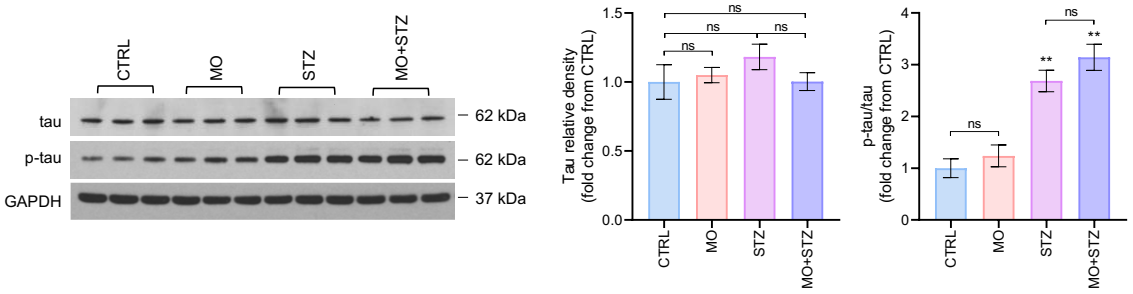

Fig. 38. Effect of streptozotocin and FTO inhibitor MO-I-500 on relative tau expression in CCF-STTG1 cells. Left: Representative immunoblot of phosphorylated (p-) and total tau from samples treated with vehicle (CTRL), 15 mM streptozotocin (STZ), 10 μM MO-I-500 (MO) or co-treated with 10 μM MO-I-500 and 15 mM streptozotocin (MO+STZ). Right: Quantification of immunoblots by densitometry with normalization to GAPDH, expressed as a fold change from CTRL. Data are presented as mean ± S.E.M. ANOVA followed by the Newman-Keuls test was used to assess statistical significance (ns $p > 0.05$, ** $p \leq 0.01$ vs CTRL). Only selected statistical comparisons are reported in graphs: CTRL vs STZ, CTRL vs MO, CTRL vs MO+STZ, STZ vs MO+STZ.

6 Discussion

RNA demethylase FTO, which is responsible for the removal of N6-methyladenosine (m6A) from adenosine bases within RNA, has been closely associated with energy regulation and brain development. Impaired energy homeostasis and neurodevelopment may promote negative effects on central nervous system function and health. According to recent theories, bioenergetic state disruption may play a role in the onset of neurodegenerative disorders like Alzheimer's disease (AD). The role of FTO in model astrocytic and neuronal cells was the main focus of this investigation. The objective was to investigate the effects of FTO inhibition on cell differentiation, energy metabolism, and the expression profile of several proteins vital for neuroenergetics, as well as to determine whether modulation of FTO function affects the tenacity of cells towards streptozotocin, an *in vitro* model of AD pathogenesis.

6.1 Neuronal differentiation

One of the most popular models for studying *in vitro* neural functions and cellular behavior is the SH-SY5Y neuroblastoma cell line. They are a subclone of the parental neuroblastoma cell line SK-N-SH, which comprises both neurons and epithelial cells (Biedler et al., 1973). These cells can be differentiated from a neuroblast-like condition into mature human neurons by a variety of different techniques, including long-term retinoic acid (RA) exposure (Encinas et al., 2000). Here, we show that RA incubation for 6 days caused SH-SY5Y neuroblastoma differentiation that was defined by both the characteristic morphological alterations of mature neurons and their protein expression profiles.

Despite the large number of research using SH-SY5Y cells, there is still disagreement over the phenotype of neuronally differentiated SH-SY5Y cells (Hashemi et al., 2003; Korecka et al., 2013). Therefore, our initial goal was to explore the main proteome alterations that occurred in these cells as a result of our experimental setup and then compare the results with previously available proteomic information about RA-differentiated SH-SY5Y cells. In addition to identifying changes in several proteins already described in the literature, we also discovered other proteins with differential regulation that had not yet been reported. The differentially expressed proteins upon RA treatment participate in several processes that contribute to neuronal differentiation, such as energy metabolism, cytoskeleton control, proteosynthesis, cell signaling, proliferation, and defense mechanisms.

Most of the identified proteins were down-regulated. Upon RA-induced neuronal differentiation, some proteins that we detected to be differently regulated are members of

the hnRNP family. These proteins control the regulation of gene expression and mRNA metabolism. Individual hnRNPs may, in fact, play a part in the differentiation and functioning of brain cells (Folci et al., 2014; Licatalosi et al., 2012; Sinnamon et al., 2012). Interestingly, vimentin, a protein essential for neuritogenesis, is an interacting partner for hnRNPC1/C2 (Kanlaya et al., 2010), which was decreased after RA treatment. Vimentin is highly expressed in neuronal precursors and during cell differentiation, it is gradually replaced with neurofilaments (Yabe et al., 2003). Several hnRNPs were identified to operate via the binding of m6A sites on RNA, which can suggest m6A-dependent mechanisms of regulation of neuronal differentiation (Yang et al., 2018). In accordance with our results, Birkeland also observed alterations (mainly down-regulation) in ribosomal proteins and hnRNPs, particularly hnRNPL, when they used alternate differentiation agents to induce SH-SY5Y neuroblastoma differentiation (Birkeland et al., 2009). After RA-induced differentiation of LAN-5 neuroblastoma cells, Cimmino discovered several differently regulated hnRNPs (Cimmino et al., 2007).

In addition, Cimmino's group noticed similar down-regulation of alpha-enolase in the RA-differentiated neuroblastoma cell line as we did (Cimmino et al., 2007). According to reports, alpha-enolase is up-regulated in a number of cancer cell lines where it promotes anaerobic growth. Additionally, the expression of this enzyme may alter in response to cellular metabolic, developmental, or pathological circumstances. Alpha-enolase expression levels may also change based on the phase of cell differentiation. Its levels decrease during quiescent periods and are up-regulated during cellular proliferation (Ji et al., 2016).

It has been discovered that cancer cells have high levels of the proteins nucleophosmin, stress-induced phosphoprotein 1, and chromobox protein homolog 1, all of which encourage cell growth (Chao et al., 2013; Lee et al., 2015; Wong et al., 2013). Here we found a significant decrease in the expression of these proteins in RA-differentiated cells. In line with our findings, the presence of differentiation-promoting substances was shown to similarly decrease the levels of these proteins (Baharvand et al., 2008; Mattout et al., 2015; Xu et al., 2014). A mutation of nucleophosmin was recently associated with the m6A pathway. In acute myeloid leukemia, mutation of nucleophosmin was accompanied by reduced abundance of m6A mark, caused by a raise of FTO levels (Xiao et al., 2022). Additionally, we found that the multifunctional proteins peroxiredoxin-1 (PRX1) and 14-3-3 protein zeta/delta, which are involved in mitochondrial integrity, apoptosis, cell development, metabolism, and survival processes (Kleppe et al., 2011) were down-regulated. Several studies confirmed changes in PRX1 levels during the development of tumor cells or differentiation of neurons (Kim et al., 2008; Sun et al., 2015;

Yan et al., 2009). Intriguingly, dopaminergic neurons in a number of brain regions express very little peroxiredoxins (Goemaere and Knoops, 2012).

Complement component 1 Q subcomponent-binding protein (C1QBP), the only up-regulated protein we identified, is thought to be a multifunctional protein participating in a variety of processes, including cell growth, apoptosis (McGee et al., 2011), ribosome biogenesis (Yoshikawa et al., 2011), and pre-mRNA splicing (Petersen-Mahrt et al., 1999). It's interesting to note that C1QBP has been linked to tumor cell metabolism and survival, and it has been established that it's critical for the mitochondrial oxidative phosphorylation (OXPHOS) system (Li et al., 2011). This is in line with a work by Hu, who showed that mitochondrial fragmentation is caused by C1QBP knockdown (Hu et al., 2013). Moreover, the metabolism of human cancer cells was switched from OXPHOS to glycolysis by suppressing C1QBP expression. After C1QBP knockdown, cells displayed reduced production of the OXPHOS polypeptides encoded by mitochondrial DNA (Fogal et al., 2010). It is well known that tumor cells typically have higher rates of glucose uptake and glycolysis because they primarily rely on glycolytic pathways rather than OXPHOS (Zheng, 2012). The detected alterations in the glycolytic enzymes alpha-enolase and phosphoglycerate mutase 1 as well as the C1QBP protein in differentiated SH-SY5Y cells may indicate a shift toward mitochondrial energy generation and a reduction in the tumorigenic potential of these cells. Actually, it was previously discovered that differentiated SH-SY5Y cells had a higher rate of OXPHOS and a lesser reliance on glycolysis (Xun et al., 2012). It is conceivable that the m6A pathway may be involved in the proper metabolic reprogramming of differentiating neurons due to emerging evidence implying the involvement of FTO in metabolic pathways.

In fact, the results of our subsequent tests showed that the FTO inhibitor rhein could effectively hinder the differentiation of SH-SY5Y cells caused by RA. Rhein's interference was demonstrated by altered neuronal marker expression and decreased neurite outgrowth. In the present work, we detected decreased abundance of neural progenitor cell marker nestin in RA-differentiated SH-SY5Y cells, but this alteration was reversed by the presence of rhein. The expression of the intermediate filament nestin is cell cycle-dependent (Sunabori et al., 2008). In neuroepithelial stem cells that stopped proliferating and started differentiating, nestin was discovered to be down-regulated (Frederikson and McKay, 1988). Therefore, our findings are indicative of a disrupted differentiation process in rhein-treated cells.

Similarly, we found a rise of MAP2 levels in RA-differentiated cells, but MAP2 protein content in rhein and RA co-treated cells was similar to that seen in controls. A neuronal cytoskeletal protein MAP2 interacts with tubulin and promotes microtubule stability. Inhibition of the binding of MAP2 to microtubules was found to decrease the

number of neurites in hippocampal neurons (Dehmelt et al., 2003) and prevent neurite initiation in cerebellar neurons, supporting the idea that MAP2 promotes neuritogenesis (Caceres et al., 1992). In the current study, we also found lower levels of GAP43 in RA-differentiated cells that were also treated with rhein. GAP43 is a membrane-associated protein that is highly expressed during axonal extension and renewal. It is likely that reduced neurite outgrowth which we observed in RA and rhein co-treated cells is a result of reduced levels of GAP43 and MAP2. However, according to the findings of Shea, levels of GAP43 are dynamically changing during neurite propagation of neuroblastoma cells. Shea observed elevated expression of GAP43 during the initial phase of neuritogenesis followed by a rapid decline to background levels during continued neurite outgrowth (Shea et al., 1991). Importantly, both inhibition of FTO by rhein or silencing of FTO specifically in axons increased m6A levels and were followed by repressed axon elongation, most likely brought on by a reduction in local GAP43 protein translation (Yu et al., 2018). Similarly to this, FTO down-regulation caused the dorsal root ganglion neurons in mice to have a shorter axonal length (Weng et al., 2018). In addition, reduced proliferation and impaired neuronal differentiation were seen due to FTO loss in adult neural stem cells (Cao et al., 2020).

It's interesting to note that Zhang found that rhein can act as a selective competitive antagonist of the retinoid X receptor (Zhang et al., 2011), a nuclear receptor that binds RA. Nonetheless, it was discovered that rhein (Liu et al., 2011)) and the absence of FTO demethylase activity (Zhao et al., 2014a) both affect adipocyte differentiation in a comparable manner, which suggests that rhein's inhibitory action on FTO is a cause of the altered cell differentiation.

Our study on SH-SY5Y cells also showed that FTO inhibitor rhein interfered with the RA-induced reduction of alpha-enolase expression, despite rhein being frequently reported as an anticancer drug having inhibitory effects on glycolysis. Therefore, it can be inferred that under these circumstances, the crucial metabolic shift towards OXPHOS in developing neuroblastoma cells is repressed. In fact, the expression of alpha-enolase was found to be directly regulated by the m6A mark. Increased translation of m6A-modified ENO1 mRNA due to facilitated binding of m6A reader YTHDF1 was detected (Ma et al., 2022).

Surprisingly though, a number of modifications brought on by RA during differentiation were also detected in cells additionally treated with rhein. Levels of two differentiation markers, SYP and NSE, were increased in both RA-treated cells as well as in RA and rhein co-treated cells. Also, although neurite outgrowth was significantly reduced in rhein-treated cells compared to RA-differentiated cells, it was still markedly

higher than in undifferentiated cells. These observations suggest that rhein treatment was not sufficient to completely block the differentiation process.

6.2 Proteomics

Post-transcriptional modification of mRNA in the form of N6-adenosine methylation can regulate gene expression by several mechanisms. It was observed that the translation of m6A-decorated transcripts can be facilitated, for example, by direct binding of initiation factors to m6A sites or interaction with m6A binding proteins (Liu et al., 2020; Meyer et al., 2015). Alternatively, the m6A mark may impact the stability of mRNA and, consequently, its accessibility to the translation machinery (Du et al., 2016; Sang et al., 2022; Y. Xu et al., 2022). All of these processes can markedly affect the cellular protein pool. Therefore, we were curious about studying the differences in the proteome of SH-SY5Y and CCF-STTG1 cells with manipulated FTO function.

We used a 2-DE MS/MS comparative proteomic technique to investigate the effects of the FTO inhibitor rhein on the proteome of both undifferentiated and RA-differentiated SH-SY5Y cells. In samples from SH-SY5Y cells treated with rhein for 24 hours, we discovered a total of 15 down-regulated proteins. Actin beta, tubulin alpha chain, and tubulin beta chain were among the cytoskeletal proteins that were similarly regulated in undifferentiated and RA-differentiated cells after rhein treatment. We have mentioned in the text above that FTO inhibition might interfere with cytoskeleton-linked morphological changes of differentiating neurons. In addition, Iosi observed that rhein treatment of A431 cells caused observable morphological changes as a result of a rearrangement of the cytoskeleton microfilament system below the plasma membrane. These authors noted that rhein-induced cell damage is most likely localized to the cytoskeletal network and mitochondria (Iosi et al., 1993). It was previously suggested by other authors that rhein may prevent the growth of tumor cells by interfering with energy metabolism and mitochondrial function (Du et al., 2013; Legendre et al., 2009; Mao et al., 2017). Here, we noticed that rhein administration to RA-differentiated SH-SY5Y cells caused reduced levels of the stress-70 protein (GRP75; mortalin). Mortalin is a mitochondrial chaperone protein essential for mitochondrial dynamics because it is involved in the quality control of proteins during import. This protein is implicated in the control of cell proliferation and cellular aging, and it also has strong anti-apoptotic activity (Dores-Silva et al., 2015). Mortalin down-regulation was observed to cause mitochondrial fragmentation (Ferré et al., 2021).

Furthermore, we have found that rhein differently regulates a number of metabolically important proteins. In undifferentiated and RA-differentiated cells, we saw

down-regulation of 3-ketoacyl-CoA thiolase and fructose-bisphosphate aldolase A, respectively. The enzyme fructose-bisphosphate aldolase A is essential for glycolysis and gluconeogenesis and helps control cell shape and motility (Kusakabe et al., 1997; Walsh et al., 1989). Together these data indicate that FTO inhibition in SH-SY5Y promotes overall hypometabolism of both mitochondria and glycolysis.

Based on our observations, levels of two peroxiredoxins, PRX6 and PRX3, are significantly lowered after rhein treatment of RA-differentiated cells. Peroxiredoxins are crucial in clearing the built-up hydrogen peroxide (Netto and Antunes, 2016). Multiple neurodegenerative illnesses have been linked to the pathophysiology of oxidative stress brought on by reactive oxygen species (ROS). Cytoplasmic peroxiredoxins are typically up-regulated to fight increased ROS levels under such harmful situations (Kim and Lee, 2021). Yet it has been reported that PRX6 overexpression may expedite the progression of AD (Yun et al., 2013). However, mitochondrial dysfunction may be the result of decreasing protein levels of PRX3, which is localized exclusively in mitochondria (Chang et al., 2004).

The levels of several hnRNPs were altered by RA-induced SH-SY5Y differentiation, as we have previously mentioned. Interestingly, we noticed a change in the expression of some hnRNPs following the treatment of either undifferentiated or RA-differentiated cells with the FTO inhibitor rhein. The hnRNPH and A1 protein level alterations are particularly intriguing since these proteins may control alternative splicing of the insulin receptor pre-mRNA (Paul et al., 2006; Talukdar et al., 2011). Age-related neurodegenerative illnesses and reduced cognitive function were recently revealed to be connected with lower brain insulin levels and altered signaling (Neth and Craft, 2017). HnRNPA1 was also suggested to affect the splicing of the beta-amyloid precursor gene, APP (Donev et al., 2007). To fully comprehend the cause of the observed changes in hnRNPs, more investigation is necessary.

A different approach was used to analyze the proteome of CCF-STTG1 cells. A label-free LC-MS/MS was utilized to compare proteomes of the MO group with controls and the siFTO group with the scramble. As a result of proteomic analysis, 116 proteins were identified differentially regulated as an effect of FTO inhibition by MO-I-500 and 170 proteins due to FTO silencing, with only 12 proteins being detected in both cases. Although the overlap of identified proteins between silencing and pharmacological approach does not appear substantial, interestingly, the GO term for mitochondrion was found to be significantly enriched in both cases, suggesting a common target to be influenced by FTO silencing and FTO inhibition. Furthermore, functional clusters of proteins associated with mitochondria were identified in both conditions. Interestingly, 4 out of 12 overlapping proteins are associated with mitochondrial metabolism and all of these were up-regulated

under both inhibitor and silencing conditions. Together these results indicate that FTO suppression might be able to regulate the bioenergetics of astrocytes possibly via affection of mitochondrial metabolism.

Interestingly, several differentially regulated proteins following FTO inhibition were found to be enriched in functional pathways related to learning, cerebellar development, and apoptotic pathways. The m6A modification was previously found to influence synaptic plasticity (Chang et al., 2017) and gliogenesis during development (Yoon et al., 2017), particularly in the cerebellum (Ma et al., 2018). The above-mentioned GO terms were not, however, enriched in the siFTO group.

6.3 Bioenergetics

FTO has previously been linked to mitochondrial function and energy metabolism. Mitochondrial impairment was seen in myotubes overexpressing FTO. Higher uncoupling protein 1 expression led to mitochondrial uncoupling in adipocytes lacking FTO (Tews et al., 2013). Importantly, the effect of FTO modulation on cellular metabolism appears to be cell-type specific (Pitman et al., 2012). That is particularly relevant for the heavily energy-demanding brain, where different cell types utilize various energy substrates metabolically in very distinct manners. We were therefore curious if FTO inhibition can affect the bioenergetics of neurons or astrocytes and whether it can promote a different effect.

The previously discussed results from proteomic analysis suggested a link between FTO inhibition and mitochondrial metabolism of both SH-SY5Y and CCF-STTG1. Additionally, FTO inhibition seemed to alter the expression of some glycolytic enzymes in SH-SY5Y cells. In fact, other studies have shown that Fto knockdown interferes with the expression of glycolytic genes (Huang et al., 2022) and impairs the glycolytic activity of tumor cells (Liu et al., 2021). However, we found practically no effect of FTO suppression on glycolytic parameters in either differentiated SH-SY5Y cells or CCF-STTG1 cells. The possible discrepancy in our results from SH-SY5Y cells might be resulting from model differences.

On the other hand, we observed different responses of SH-SHY5Y and CCF-STTG1 cells to FTO inhibitor treatment during the investigation of mitochondrial metabolism by assessing oxygen consumption rates. While we observed that treatment of differentiated SH-SY5Y cells with the FTO inhibitor MO-I-500 resulted in reduced basal, ATP-linked, and maximal respiration oxygen consumption, astrocytes seemed to benefit from inhibited FTO and displayed enhanced respiration rates. Rather in contrast to our observations, Chen observed that SH-SY5Y with elevated FTO levels had displayed elevated mitochondria-generated oxidative stress and lower respiratory complex II activity.

Importantly though, Chen utilized undifferentiated SH-SY5Y cells. The different effect of FTO modulation on SH-SY5Y cells based on the differentiation stage was observed by Pitman, who showed that while silencing of FTO increased the ATP pool in undifferentiated SH-SY5Y, differentiated SH-SY5Y had reduced levels of ATP (Pitman et al., 2012). However, we have previously observed impaired respiration following FTO inhibition in undifferentiated cells as well (Cockova, 2017). In the latter work, undifferentiated SH-SY5Y cells displayed reduced respiration spare capacity due to a lower maximal respiration rate.

Our results show for the first time that FTO activity is associated with the mitochondrial metabolism of astrocytes. In contrast to SH-SY5Y cells, basal ATP-linked, and maximal respiration rates in CCF-STTG1 cells were all significantly increased following MO-I-500 treatment. In a follow-up analysis of permeabilized cells for assessment of the function of respiratory chain complexes, we have observed a potent increase in oxygen consumption driven by complex IV activity was observed in cells affected by FTO inhibitor. In accordance with our analysis of respiratory complexes, the Western blot analysis of the relative expression levels of selected OXPHOS subunits showed significant up-regulation of complex I (NDUFB8) and complex IV (MT-CO1) subunits in inhibitor-treated cells compared to controls. Indeed, the latter-mentioned MT-CO1 was also detected among the up-regulated mitochondrial proteins in both MO and siFTO group following label-free LC-MS/MS proteome analysis.

Interestingly, the addition of the FTO inhibitor to healthy astrocytes caused a dramatic increase in mitochondrial mass and was followed by elevated ATP levels. Several authors have described the connection between FTO and mitochondrial biogenesis with the mTOR-PGC-1α pathway being at the forefront of those observations. In our work, we observed increased expression of PGC-1α in astrocytes treated with FTO inhibitor or FTO siRNA, which we speculate might be involved in the detected boost of mitochondrial metabolism. This is in accordance with the work of Wang and colleagues, who showed that muscle cells deprived of FTO had reduced levels of PGC-1α, which was further accompanied by decreased mitochondrial mass and mtDNA content (X. Wang et al., 2017). Another study demonstrated that overexpression of FTO induced up-regulation of PGC-1α by directly affecting the m6A level of PGC-1α transcript (Zhuang et al., 2019). Among other factors, insulin action might be an important contributor to the modified mitochondrial metabolism via mTOR signaling. Li's group has even suggested an association between FTO and AD-related insulin defects (H. Li et al., 2018). Although we observed increased levels of phosphorylated Akt (p-Akt), which is an insulin signaling pathway effector, there was no effect of FTO inhibition on other insulin signaling-involved proteins, such as IRS-1, IRS-2, or IRβ. Therefore, our findings do not point to a significant role for FTO in astrocyte insulin signaling.

6.4 Streptozotocin-caused impairment

In light of emerging hypotheses that associate the onset of AD with disrupted energy metabolism and neuroinflammation, the m6A pathway, and particularly FTO, makes a promising target in the research of new therapeutic strategies. Therefore, in this study we employed streptozotocin, an *in vitro* model of AD pathogenesis, to investigate the involvement of FTO (mostly astrocytic FTO) in STZ-induced harmful conditions.

The experimental model of AD, ICV injection of STZ has been reported to cause molecular and behavioral changes that are similar to abnormalities identified in AD patients. According to Biswas, mouse neuronal N2A cells treated with STZ suffered from beta-amyloid accumulation, tau hyperphosphorylation, glucose hypometabolism, mitochondrial dysfunction, increased rate of apoptosis, and DNA damage, all of which eventually resulted in pronounced cell death (Biswas et al., 2016). In our study, a concentration-dependent detrimental effect of STZ dose on differentiated SH-SY5Y cells was observed. Similarly to neurons, we measured decreasing viability of CCF-STTG1 cells in response to increasing STZ concentration, although greater doses of STZ were required to produce comparable declines in cell viability. We observed that the cytotoxic effects of STZ on CCF-STTG1 cells are accompanied by a diminished energy metabolism, mitochondrial dysfunction, increased ROS, reactivation of astrocytes, and apoptotic and necrotic cell death. In accordance with our results, Biswas has shown that astrocytic cells displayed increased apoptosis and cellular stress in response to STZ (Biswas et al., 2017).

In the latter experiments, we observed that FTO inhibition by MO-I-500 had neither a protective nor stimulatory effect on STZ-induced SH-SY5Y cell death. In contrast to neurons, however, FTO inhibition partially improved the survival ability of the astrocytic cell line CCF-STTG1 which was challenged by the cytotoxic dose of STZ.

Subsequently, we focused on investigating the FTO role in CCF-STTG1 sensitivity to STZ. According to our findings, m6A demethylase FTO is significantly increased in astrocytes that have been exposed to STZ. Furthermore, our research suggested that FTO might be linked to AD pathophysiology in astrocytes. The mitotoxic effects of STZ as well as the closely related energy imbalances, apoptosis, and oxidative stress were all decreased by FTO inhibition.

A growing body of evidence points to a link between aberrant m6A RNA methylation and neurodegenerative disorders like AD (X. Chen et al., 2019; Fu et al., 2019; Han et al., 2020; Huang et al., 2020). A gene variant of the m6A demethylase *FTO* has been identified as a risk factor for AD in genome-wide association studies (Ho et al., 2010; Keller et al., 2011). In the brain and hippocampus of a transgenic AD mouse model, m6A RNA methylation was increased. In AD mice, expression of the m6A methyltransferase

METTL3 was up-regulated while that of the m6A demethylase FTO was down-regulated (Han et al., 2020). Another study described altered *METTL3* expression in AD. Interestingly, *METTL3* expression was decreased in the post-mortem AD brain of humans (Huang et al., 2020). In contrast to both investigations, our study demonstrates that protein levels of FTO are increased whereas METTL3 is unchanged in human astrocytoma cells treated with STZ. The reason for this variation could be due to the employment of different model systems. In neurons obtained from 3xTg AD mice, the role of FTO in connection to AD has been more thoroughly studied. Li and associates manipulated the FTO levels and observed an effect on tau phosphorylation. In their research, tau phosphorylation (Ser 262) levels were decreased by FTO knockdown, whereas FTO overexpression had the reverse impact (H. Li et al., 2018). The phosphorylation of tau in human SH-SY5Y neuroblastoma cells was also decreased by FTO knockdown (Pitman et al., 2013). Employing an astrocytic cell line CCF-STTG1, we found a significant increase in the ratio of phosphorylated tau (Ser 396) to total tau after stimulation with STZ, but no effect was observed in response to FTO inhibition of STZ-challenged cells relative to STZ group.

It has frequently been proposed that glial-mediated neuroinflammation is a significant factor in the pathophysiology of AD. Astrocytes become activated in response to stress, which is followed by a slew of events such as oxidative stress and apoptosis. One of the traits of reactive astrocytes is GFAP up-regulation. We noticed that GFAP expression in astrocytes increased after STZ treatment. Following analysis of apoptosis and ROS production, we discovered that these cells were under oxidative stress and had a lower survival rate. Intriguingly, inhibition of FTO decreased GFAP levels, oxidative stress, and cytotoxic effects of STZ. It has been revealed that the m6A machinery enzymes have a role in the inflammatory process. The methyltransferase METTL3 encouraged the activation of microglia and the production of cytokines with pro-inflammatory activities (Wen et al., 2022). The YTHDF2 protein, which binds to m6A, was proposed to negatively control the inflammatory responses of macrophages (Timper et al., 2020; Yu et al., 2019). Two groups described changed FTO levels in reaction to lipopolysaccharide stimulation (Luo et al., 2021; Zhang et al., 2013), and the loss of FTO was seen to cause a switch of macrophages into pro-inflammatory M1-type macrophages (Gu et al., 2020). Additionally, elevated FTO levels were associated with triggered oxidative stress in renal cells (Zhuang et al., 2019) and dopaminergic neurons (X. Chen et al., 2019). But no research has yet discussed the function of FTO in astrocyte reactivity. Based on our observations, FTO inhibition ameliorated apoptotic signaling induced by STZ. It was shown that m6A pathway proteins can control the expression of apoptotic mediators directly through the regulation of transcript lifetime. For example, *Bcl2* transcripts were shown to be selectively

demethylated by ALKBH5 and FTO, blocking their degradation and therefore increasing *Bcl2* expression (K. Xu et al., 2020).

Both dysregulated ROS and apoptotic responses can originate from compromised astrocyte mitochondrial integrity. Numerous studies have demonstrated that mitochondrial abnormalities play a significant role in neurodegenerative disorders, including Alzheimer's dementia (AD), where they appear to be a late-phase contributor to the pathophysiology of the disease as well as an early feature (Chakravorty et al., 2019). We looked into mitochondrial activity and energy metabolism in order to better understand the impact of STZ and the potential cause of the protective behavior induced by FTO inhibition. In line with prior research, our findings showed that STZ generated a significant mitotoxic impact as evidenced by decreased intracellular ATP levels, decreased mitochondrial membrane potential, and a drop in oxidative phosphorylation. The mitochondrial respiration capacity was likewise decreased in astrocytes treated with STZ, which also showed lower basal respiration rates. On the other hand, pretreatment with an FTO inhibitor was able to partially restore the capacity of the electron transport chain and the potential of the mitochondrial membrane. The rate of oxidative phosphorylation returned to its baseline almost entirely. The depletion of ATP molecules was also generally prevented by FTO inhibition. Observed results showing rescued mitochondrial functioning are in line with our findings of the stimulatory effect of FTO suppression in healthy astrocytes.

We have already suggested that FTO inhibition might be linked to the regulation of mitochondrial biogenesis. Mitochondrial biogenesis is one of the mechanisms involved in defense against excessive ROS. Levels of ROS can be stabilized by a de-novo generation of healthy mitochondria with high antioxidant capability. As we have mentioned before, insulin signaling, which can contribute to the mitochondria biogenesis pathway, does not seem to be particularly affected by FTO inhibition in healthy astrocytes. In addition, we did not observe any effect of FTO inhibition on reduced levels of the insulin receptor and its substrates caused by STZ treatment. On the other hand, levels of phosphorylated AMPK were raised as a result of STZ exposure. In an effort to rewire intracellular signaling to restore energy homeostasis, sensors like the AMPK are usually activated during cellular energy stress. Although AMPK activation has been implicated in the pathophysiology of AD in numerous studies, it is still debatable whether these effects are advantageous or disadvantageous. In the brains of ICV-STZ rats, AMPK activity was discovered to be reduced by several research teams (Du et al., 2015; Wang et al., 2020). However, other researchers presented conflicting findings (Lee et al., 2013). We presume that in our case, starvation or oxidative stress of cells could activate AMPK, but this activation was insufficient to invoke the protective effect against STZ-induced damage. It's interesting to note that pretreating astrocytes with an FTO inhibitor did not result in increased AMPK

phosphorylation, indicating that these cells retained energy balance was retained. All of these findings support the idea that FTO might play a role in regulation of the energy homeostasis of astrocytes and we speculate whether the effect of FTO inhibition on the metabolism of mitochondria can improve the resistance of these cells to metabolic stress conditions.

7 Conclusion

The current study focused on the investigation of FTO functions in the nervous system by using FTO inhibitors and validating approaches by FTO silencing. Previous research has demonstrated a connection between FTO function and the control of neurodevelopment. Indeed, we have shown that FTO inhibition can hinder the differentiation process of SH-SY5Y cells induced by retinoic acid, although not stopping it entirely. As a result of FTO inhibition during the differentiation procedure, we observed an insufficient morphological transformation of cells as well as an altered expression profile of neuronal markers.

By performing an analysis of proteomes of both undifferentiated (UC) and differentiated (DC) SH-SY5Y cells treated with FTO inhibitor rhein, we found a number of proteins to be differentially regulated. These proteins were involved in the regulation of transcription and translation, cytoskeleton structure, cellular metabolism, neural plasticity, and antioxidant defense. With the exception of a few cytoskeletal proteins, the expression profiles of proteins in UC and DC cells treated with rhein were not identical, suggesting that the cellular differentiation stage is critical for the underlying mechanisms induced by FTO inhibitor rhein. Proteomic analysis showed that fructose-bisphosphate aldolase A, an enzyme involved in glycolytic pathway, was down-regulated in differentiated cells following rhein treatment. Though this result implied a potential influence of FTO inhibition on the glycolytic metabolism, we did not observe any notable effects on glycolytic parameters assessed by functional studies. The rate of glycolysis, glycolytic capacity, and glycolytic reserve were unaffected in differentiated SH-SY5Y cells treated with FTO inhibitor or FTO silencing. Down-regulation of mitochondrial proteins (mortalin, peroxiredoxin 3, and 3-ketoacyl-CoA thiolase) which we observed following proteome analysis further suggested that mitochondria might be affected in SH-SY5Y cells after FTO inhibitor treatment. Indeed, our investigation of mitochondrial respiration in differentiated cells showed reduced basal, ATP-linked and maximal respiration after FTO inhibition and similarly after FTO silencing. We have observed a reduction in mitochondrial respiration of undifferentiated SH-SY5Y after rhein treatment in our previous work (Cockova, 2017). Here we showed that FTO inhibition appears to lower respiration in differentiated cells as well.

In order to identify distinctions between different cell types, we looked into how FTO affects the bioenergetics of not only neuronal SH-SY5Y but also astrocytic CCF-STTG1 cells. Similarly to SH-SY5Y, we did not observe any significant differences in glycolysis or glycolytic capacity between controls and CCF-STTG1 cells treated with the FTO inhibitor or silencing. Proteomic analysis of CCF-STTG1 cells with suppressed FTO

function or levels led to the identification of a significant number of mitochondrial proteins suggesting that the mitochondrial compartment is affected, such as was the case in neurons. Consequently, we measured altered respiration of these cells. The effect of FTO suppression on mitochondrial respiration of CCF-STTG1 cells was stimulatory, therefore the opposite trend was noticed in comparison to neurons. Further analysis showed elevated amounts of intracellular ATP, higher levels of OXPHOS subunits NDUFB8 and MT-CO1, and an increase in mitochondrial mass of CCF-STTG1 cells with suppressed FTO. We also found higher levels of mitochondrial biogenesis regulator PGC-1α, suggesting that the overall stimulation of mitochondrial metabolism might be caused to some extent by altered mitochondrial biogenesis.

Finally, we used streptozotocin (STZ) as a bioenergetics-affecting model of Alzheimer's disease (AD). The STZ model we employed led to impaired viability of both neurons and astrocytes. In astrocytes, we further observed STZ-induced astrocyte activation, oxidative stress, and poor energy metabolism. For the first time, we showed that the crucial m6A regulatory enzyme, FTO, is differentially regulated in astrocytes after STZ treatment, pointing to a disruption of m6A signaling in the pathophysiology of the disease. Additionally, we have discovered that tampering with FTO in astrocytes can lessen STZ's harmful effects. When challenged with STZ, cells with inhibited FTO displayed a higher survival rate, reduced oxidative stress, increased ATP pool, and rescued basal respiration. The protective effect of FTO inhibition, therefore, appears to be connected to the changed bioenergetic status of the cells.

In conclusion, our findings are consistent with the hypothesis that FTO regulates bioenergetics in a cell-type-specific manner. The present study supports the evidence that FTO can impact neuronal differentiation and offers new information about the function of FTO in astrocytes and neurodegenerative diseases. The current findings may help clarify the function of the FTO protein in brain energy metabolism and advance research into its potential role in the pathophysiology of AD.

8 References

Aas, A., Isakson, P., Bindesbøll, C., Alemu, E.A., Klungland, A., Simonsen, A., 2017. Nucleocytoplasmic Shuttling of FTO Does Not Affect Starvation-Induced Autophagy. PLoS One 12, e0168182.

Abramov, A.Y., Canevari, L., Duchen, M.R., 2004. β-Amyloid Peptides Induce Mitochondrial Dysfunction and Oxidative Stress in Astrocytes and Death of Neurons through Activation of NADPH Oxidase. The Journal of Neuroscience 24, 565.

Akinlade, O.M., Owoyele, B.V., Soladoye, A.O., 2021. Streptozotocin-induced type 1 and 2 diabetes in rodents: a model for studying diabetic cardiac autonomic neuropathy. Afr Health Sci 21, 719.

Alarcón, C.R., Goodarzi, H., Lee, H., Liu, X., Tavazoie, S., Tavazoie, S.F., 2015. HNRNPA2B1 Is a Mediator of m(6)A-Dependent Nuclear RNA Processing Events. Cell 162, 1299–1308.

Ammer, H., Schulz, R., 1994. Retinoic acid-induced differentiation of human neuroblastoma SH-SY5Y cells is associated with changes in the abundance of G proteins. J Neurochem 62, 1310–1318.

Anders, M., Chelysheva, I., Goebel, I., Trenkner, T., Zhou, J., Mao, Y., Verzini, S., Qian, S.B., Ignatova, Z., 2018. Dynamic m6A methylation facilitates mRNA triaging to stress granules. Life Sci Alliance 1, e201800113.

Arcidiacono, O.A., Krejčí, J., Bártová, E., 2020. The Distinct Function and Localization of METTL3/METTL14 and METTL16 Enzymes in Cardiomyocytes. Int J Mol Sci 21, 1–19.

Arendt, T., Bullmann, T., 2013. Neuronal plasticity in hibernation and the proposed role of the microtubule-associated protein tau as a “master switch” regulating synaptic gain in neuronal networks. Am J Physiol Regul Integr Comp Physiol 305, R478-89.

Arumugam, T., Ghazi, T., Chuturgoon, A.A., 2021. Fumonisin B1 alters global m6A RNA methylation and epigenetically regulates Keap1-Nrf2 signaling in human hepatoma (HepG2) cells. Arch Toxicol 95, 1367–1378.

Baharvand, H., Fathi, A., Gourabi, H., Mollamohammadi, S., Salekdeh, G.H., 2008. Identification of mouse embryonic stem cell-associated proteins. J Proteome Res 7, 412–423.

Bai, L.L., Tang, Q., Zou, Z., Meng, P., Tu, B., Xia, Y., Cheng, S., Zhang, L., Yang, K., Mu, S., et al., 2018. m6A Demethylase FTO Regulates Dopaminergic Neurotransmission Deficits Caused by Arsenite. Toxicol Sci 165, 431–446.

Bassell, G.J., Warren, S.T., 2008. Fragile X syndrome: loss of local mRNA regulation alters synaptic development and function. Neuron 60, 201–214.

Batista, P.J., Molinie, B., Wang, J., Qu, K., Zhang, J., Li, L., Bouley, D.M., Lujan, E., Haddad, B., Daneshvar, K., et al., 2014. m6A RNA modification controls cell fate transition in mammalian embryonic stem cells. Cell Stem Cell 15, 707.

Beach, T.G., McGeer, E.G., 1988. Lamina-specific arrangement of astrocytic gliosis and senile plaques in Alzheimer’s disease visual cortex. Brain Res 463, 357–361.

Bego, T., Čaušević, A., Dujić, T., Malenica, M., Velija-Asimi, Z., Prnjavorac, B., Marc, J., Nekvindová, J., Palička, V., Semiz, S., 2019. Association of FTO Gene Variant (rs8050136) with Type 2 Diabetes and Markers of Obesity, Glycaemic Control and Inflammation. J Med Biochem 38, 153.

Berson, A., Barbash, S., Shaltiel, G., Goll, Y., Hanin, G., Greenberg, D.S., Ketzef, M., Becker, A.J., Friedman, A., Soreq, H., 2012. Cholinergic-associated loss of hnRNP-A/B in Alzheimer’s disease impairs cortical splicing and cognitive function in mice. EMBO Mol Med 4, 730–742.

Berulava, T., Ziehe, M., Klein-Hitpass, L., Mladenov, E., Thomale, J., Rüther, U., Horsthemke, B., 2013. FTO levels affect RNA modification and the transcriptome. Eur J Hum Genet 21, 317–323.

Biedler, J.L., Helson, L., Spengler, B.A., 1973. Morphology and Growth, Tumorigenicity, and Cytogenetics of Human Neuroblastoma Cells in Continuous Culture. Cancer Res 33, 2643–2652.

Birkeland, E., Nygaard, G., Oveland, E., Mjaavatten, O., Ljones, M., Doskeland, S.O., Krakstad, C., Selheim, F., 2009. Epac-induced Alterations in the Proteome of Human SH-SY5Y Neuroblastoma Cells. J Proteomics Bioinform 2, 1–11.

Biswas, J., Goswami, P., Gupta, S., Joshi, N., Nath, C., Singh, S., 2016. Streptozotocin Induced Neurotoxicity Involves Alzheimer's Related Pathological Markers: a Study on N2A Cells. Mol Neurobiol 53, 2794–2806.

Biswas, J., Gupta, S., Verma, D.K., Singh, S., 2017. Streptozotocin alters glucose transport, connexin expression and endoplasmic reticulum functions in neurons and astrocytes. Neuroscience 356, 151–166.

Boissel, S., Reish, O., Proulx, K., Kawagoe-Takaki, H., Sedgwick, B., Yeo, G.S.H., Meyre, D., Golzio, C., Molinari, F., Kadhom, N., et al., 2009. Loss-of-Function Mutation in the Dioxygenase-Encoding FTO Gene Causes Severe Growth Retardation and Multiple Malformations. Am J Hum Genet 85, 106.

Bravard, A., Lefai, E., Meugnier, E., Pesenti, S., Disse, E., Vouillarmet, J., Peretti, N., Rabasa-Lhoret, R., Laville, M., Vidal, H., et al., 2011. FTO is increased in muscle during type 2 diabetes, and its overexpression in myotubes alters insulin signaling, enhances lipogenesis and ROS production, and induces mitochondrial dysfunction. Diabetes 60, 258–268.

Caceres, A., Mautino, J., Kosik, K.S., 1992. Suppression of MAP2 in cultured cerebellar macroneurons inhibits minor neurite formation. Neuron 9, 607–618.

Cagnin, A., Brooks, D.J., Kennedy, A.M., Gunn, R.N., Myers, R., Turkheimer, F.E., Jones, T., Banati, R.B., 2001. In-vivo measurement of activated microglia in dementia. Lancet 358, 461–467.

Cao, Y., Zhuang, Y., Chen, J., Xu, W., Shou, Y., Huang, X., Shu, Q., Li, X., 2020. Dynamic effects of Fto in regulating the proliferation and differentiation of adult neural stem cells of mice. Hum Mol Genet 29, 727–735.

Chai, Z., Gong, J., Zheng, P., Zheng, J., 2020. Inhibition of miR-19a-3p decreases cerebral ischemia/reperfusion injury by targeting IGFBP3 in vivo and in vitro. Biol Res 53, 1–11.

Chakravorty, A., Jetto, C.T., Manjithaya, R., 2019. Dysfunctional Mitochondria and Mitophagy as Drivers of Alzheimer's Disease Pathogenesis. Front Aging Neurosci 11, 311.

Chang, M., Lv, H., Zhang, W., Ma, C., He, X., Zhao, S., Zhang, Z.W., Zeng, Y.X., Song, S., Niu, Y., et al., 2017. Region-specific RNA m6A methylation represents a new layer of control in the gene regulatory network in the mouse brain. Open Biol 7, 170166.

Chang, T.S., Cho, C.S., Park, S., Yu, S., Sang, W.K., Sue, G.R., 2004. Peroxiredoxin III, a mitochondrion-specific peroxidase, regulates apoptotic signaling by mitochondria. J Biol Chem 279, 41975–41984.

Chao, A., Lin, C.Y., Tsai, C.L., Hsueh, S., Lin, Y.Y., Lin, C.T., Chou, H.H., Wang, T.H., Lai, C.H., Wang, H.S., 2013. Estrogen stimulates the proliferation of human endometrial cancer cells by stabilizing nucleophosmin/B23 (NPM/B23). J Mol Med (Berl) 91, 249–259.

Chen, B., Ye, F., Yu, L., Jia, G., Huang, X., Zhang, X., Peng, S., Chen, K., Wang, M., Gong, S., et al., 2012. Development of cell-active N6-methyladenosine RNA demethylase FTO inhibitor. J Am Chem Soc 134, 17963–17971.

Chen, J., Zhang, Y.C., Huang, C., Shen, H., Sun, B., Cheng, X., Zhang, Y.J., Yang, Y.G., Shu, Q., Yang, Y., et al., 2019. m6A Regulates Neurogenesis and Neuronal Development by Modulating Histone Methyltransferase Ezh2. Genomics Proteomics Bioinformatics 17, 154–168.

Chen, J.N., Chen, Y., Wei, Y.Y., Raza, M.A., Zou, Q., Xi, X.Y., Zhu, L., Tang, G.Q., Jiang, Y.Z., Li, X.W., 2019. Regulation of m(6)A RNA Methylation and Its Effect on Myogenic Differentiation in Murine Myoblasts. Molekuliarnaia biologiia 53, 436–445.

Chen, W., Chen, Y., Wu, R., Guo, G., Liu, Y., Zeng, B., Liao, X., Wang, Y., Wang, X., 2022. DHA alleviates diet-induced skeletal muscle fiber remodeling via FTO/m6A/DDIT4/PGC1α signaling. BMC Biol 20, 1–19.

Chen, X., Yu, C., Guo, M., Zheng, X., Ali, S., Huang, H., Zhang, L., Wang, S., Huang, Y., Qie, S., et al., 2019. Down-Regulation of m6A mRNA Methylation Is Involved in Dopaminergic Neuronal Death. ACS Chem Neurosci 10, 2355–2363.

Cheng, Y., Luo, H., Izzo, F., Pickering, B.F., Nguyen, D., Myers, R., Schurer, A., Gourkanti, S., Brüning, J.C., Vu, L.P., et al., 2019. m6A RNA Methylation Maintains Hematopoietic Stem Cell Identity and Symmetric Commitment. Cell Rep 28, 1703-1716.e6.

Cheng, Z., Luo, C., Guo, Z., 2020. LncRNA-XIST/microRNA-126 sponge mediates cell proliferation and glucose metabolism through the IRS1/PI3K/Akt pathway in glioma. J Cell Biochem 121, 2170–2183.

Cheung, M.K., Gulati, P., O'Rahilly, S., Yeo, G.S.H., 2013. FTO expression is regulated by availability of essential amino acids. Int J Obes 37, 744–747.

Choi, J., Ieong, K.W., Demirci, H., Chen, J., Petrov, A., Prabhakar, A., O'Leary, S.E., Dominissini, D., Rechavi, G., Soltis, S.M., et al., 2016. N6-methyladenosine in mRNA disrupts tRNA selection and translation elongation dynamics. Nat Struct Mol Biol 23, 110.

Chokkalla, A.K., Mehta, S.L., Kim, T.H., Chelluboina, B., Kim, J., Vemuganti, R., 2019. Transient Focal Ischemia Significantly Alters the m6A Epitranscriptomic Tagging of RNAs in the Brain. Stroke 50, 2912–2921.

Christofi, T., Zaravinos, A., 2019. RNA editing in the forefront of epitranscriptomics and human health. J Transl Med 17, 319.

Church, C., Moir, L., McMurray, F., Girard, C., Banks, G.T., Teboul, L., Wells, S., Brüning, J.C., Nolan, P.M., Ashcroft, F.M., et al., 2010. Overexpression of Fto leads to increased food intake and results in obesity. Nat Genet 42, 1086–1092.

Cimmino, F., Spano, D., Capasso, M., Zambrano, N., Russo, R., Zollo, M., Iolascon, A., 2007. Comparative proteomic expression profile in all-trans retinoic acid differentiated neuroblastoma cell line. J Proteome Res 6, 2550–2564.

Cockova, Z., 2017. Modulation of RNA demethylase FTO function in SH-SY5Y cells: the effect on insulin signaling and mitochondrial respiration [Diploma thesis]. Charles University, Department of Physiology, Prague.

Cockova, Z., Honc, O., Telensky, P., Olsen, M.J., Novotny, J., 2021. Streptozotocin-Induced Astrocyte Mitochondrial Dysfunction Is Ameliorated by FTO Inhibitor MO-I-500. ACS Chem Neurosci 12, 3818–3828.

Coots, R.A., Liu, X.M., Mao, Y., Dong, L., Zhou, J., Wan, J., Zhang, X., Qian, S.B., 2017. m6A Facilitates eIF4F-Independent mRNA Translation. Mol Cell 68, 504-514.e7.

Cui, Q., Shi, H., Ye, P., Li, L., Qu, Q., Sun, Guoqiang, Sun, Guihua, Lu, Z., Huang, Y., Yang, C.G., et al., 2017. m6A RNA Methylation Regulates the Self-Renewal and Tumorigenesis of Glioblastoma Stem Cells. Cell Rep 18, 2622–2634.

Dehmelt, L., Smart, F.M., Ozer, R.S., Halpain, S., 2003. The role of microtubule-associated protein 2c in the reorganization of microtubules and lamellipodia during neurite initiation. J Neurosci 23, 9479–9490.

Demetrius, L.A., Magistretti, P.J., Pellerin, L., 2015. Alzheimer's disease: The amyloid hypothesis and the Inverse Warburg effect. Front Physiol 6, 522.

Deng, J., Chen, S., Wang, F., Zhao, H., Xie, Z., Xu, Z., Zhang, Q., Liang, P., Zhai, X., Cheng, Y., 2016. Effects of hnRNP A2/B1 Knockdown on Inhibition of Glioblastoma Cell Invasion, Growth and Survival. Mol Neurobiol 53, 1132–1144.

Dermentzaki, G., Lotti, F., 2020. New Insights on the Role of N6-Methyladenosine RNA Methylation in the Physiology and Pathology of the Nervous System. Front Mol Biosci 7, 229.

Desrosiers, R., Friderici, K., Rottman, F., 1974. Identification of Methylated Nucleosides in Messenger RNA from Novikoff Hepatoma Cells. Proc Natl Acad Sci U S A 71, 3971.

Ding, L., Wu, H., Wang, Y., Li, Y., Liang, Z., Xia, X., Zheng, J.C., 2022. m6A Reader Igf2bp1 Regulates the Inflammatory Responses of Microglia by Stabilizing Gbp11 and Cp mRNAs. Front Immunol 13, 872252.

Dominissini, D., Moshitch-Moshkovitz, S., Schwartz, S., Salmon-Divon, M., Ungar, L., Osenberg, S., Cesarkas, K., Jacob-Hirsch, J., Amariglio, N., Kupiec, M., et al., 2012. Topology of the human and mouse m6A RNA methylomes revealed by m6A-seq. Nature 485, 201–206.

Donev, R., Newall, A., Thome, J., Sheer, D., 2007. A Role for SC35 and hnRNPA1 in the Determination of Amyloid Precursor Protein Isoforms. Mol Psychiatry 12, 681.

Dores-Silva, P.R., Barbosa, L.R.S., Ramos, C.H.I., Borges, J.C., 2015. Human Mitochondrial Hsp70 (Mortalin): Shedding Light on ATPase Activity, Interaction with Adenosine Nucleotides, Solution Structure and Domain Organization. PLoS One 10, e0117170.

Du, H., Zhao, Y., He, J., Zhang, Y., Xi, H., Liu, M., Ma, J., Wu, L., 2016. YTHDF2 destabilizes m6A-containing RNA through direct recruitment of the CCR4–NOT deadenylase complex. Nat Commun 7, 12626.

Du, L.L., Chai, D.M., Zhao, L.N., Li, X.H., Zhang, F.C., Zhang, H.B., Liu, L. bin, Wu, K., Liu, R., Wang, J.Z., et al., 2015. AMPK activation ameliorates Alzheimer's disease-like pathology and spatial memory impairment in a streptozotocin-induced Alzheimer's disease model in rats. J Alzheimers Dis 43, 775–784.

Du, Q., Bian, X.L., Xu, X. le, Zhu, B., Yu, B., Zhai, Q., 2013. Role of mitochondrial permeability transition in human hepatocellular carcinoma Hep-G2 cell death induced by rhein. Fitoterapia 91, 68–73.

Edens, B.M., Vissers, C., Su, J., Arumugam, S., Xu, Z., Shi, H., Miller, N., Rojas Ringeling, F., Ming, G. li, He, C., et al., 2019. FMRP Modulates Neural Differentiation through m6A-Dependent mRNA Nuclear Export. Cell Rep 28, 845-854.e5.

Edupuganti, R.R., Geiger, S., Lindeboom, R.G.H., Shi, H., Hsu, P.J., Lu, Z., Wang, S.Y., Baltissen, M.P.A., Jansen, P.W.T.C., Rossa, M., et al., 2017. N6-methyladenosine (m6A) recruits and repels proteins to regulate mRNA homeostasis. Nat Struct Mol Biol 24, 870.

Encinas, M., Iglesias, M., Liu, Y., Wang, H., Muhaisen, A., Ceña, V., Gallego, C., Comella, J.X., 2000. Sequential treatment of SH-SY5Y cells with retinoic acid and brain-derived neurotrophic factor gives rise to fully differentiated, neurotrophic factor-dependent, human neuron-like cells. J Neurochem 75, 991–1003.

Engel, M., Eggert, C., Kaplick, P.M., Eder, M., Röh, S., Tietze, L., Namendorf, C., Arloth, J., Weber, P., Rex-Haffner, M., et al., 2018. The Role of m6A/m-RNA Methylation in Stress Response Regulation. Neuron 99, 389.

Fan, H.Q., He, W., Xu, K.F., Wang, Z.X., Xu, X.Y., Chen, H., 2015. FTO Inhibits Insulin Secretion and Promotes NF-κB Activation through Positively Regulating ROS Production in Pancreatic β cells. PLoS One 10, e0127705.

Fanti, Z., De-Miguel, F.F., Martinez-Perez, M.E., 2008. A method for semiautomatic tracing and morphological measuring of neurite outgrowth from DIC sequences. Annu Int Conf IEEE Eng Med Biol Soc 2008, 1196–1199.

Feng, Z., Li, Q., Meng, R., Yi, B., Xu, Q., 2018. METTL3 regulates alternative splicing of MyD88 upon the lipopolysaccharide-induced inflammatory response in human dental pulp cells. J Cell Mol Med 22, 2558–2568.

Ferré, C.A., Thouard, A., Bétourné, A., le Dorze, A.L., Belenguer, P., Miquel, M.C., Peyrin, J.M., Gonzalez-Dunia, D., Szelechowski, M., 2021. HSPA9/Mortalin mediates axo-protection and modulates mitochondrial dynamics in neurons. Sci Rep 11, 1–12.

Fischer, J., Koch, L., Emmerling, C., Vierkotten, J., Peters, T., Brüning, J.C., Rüther, U., 2009. Inactivation of the Fto gene protects from obesity. Nature 458, 894–898.

Flamand, M.N., Meyer, K.D., 2022. m6A and YTHDF proteins contribute to the localization of select neuronal mRNAs. Nucleic Acids Res 50, 4464.

Fogal, V., Richardson, A.D., Karmali, P.P., Scheffler, I.E., Smith, J.W., Ruoslahti, E., 2010. Mitochondrial p32 protein is a critical regulator of tumor metabolism via maintenance of oxidative phosphorylation. Mol Cell Biol 30, 1303–1318.

Folci, A., Mapelli, L., Sassone, J., Prestori, F., D'Angelo, E., Bassani, S., Passafaro, M., 2014. Loss of hnRNP K impairs synaptic plasticity in hippocampal neurons. J Neurosci 34, 9088–9095.

Fountoulakis, M., Takács, M.F., Berndt, P., Langen, H., Takács, B., 1999. Enrichment of low abundance proteins of Escherichia coli by hydroxyapatite chromatography. Electrophoresis 20, 2181–2195.

Frayling, T.M., Timpson, N.J., Weedon, M.N., Zeggini, E., Freathy, R.M., Lindgren, C.M., Perry, J.R.B., Elliott, K.S., Lango, H., Rayner, N.W., et al., 2007. A common variant in the FTO gene is associated with body mass index and predisposes to childhood and adult obesity. Science 316, 889–894.

Frederikson, K., McKay, R.D.G., 1988. Proliferation and differentiation of rat neuroepithelial precursor cells in vivo. J Neurosci 8, 1144–1151.

Fredriksson, R., Hägglund, M., Olszewski, P.K., Stephansson, O., Jacobsson, J.A., Olszewska, A.M., Levine, A.S., Lindblom, J., Schiöth, H.B., 2008. The obesity gene, FTO, is of ancient origin, up-regulated during food deprivation and expressed in neurons of feeding-related nuclei of the brain. Endocrinology 149, 2062–2071.

Fu, L., Guerrero, C.R., Zhong, N., Amato, N.J., Liu, Y., Liu, S., Cai, Q., Ji, D., Jin, S.G., Niedernhofer, L.J., et al., 2014. Tet-mediated formation of 5-hydroxymethylcytosine in RNA. J Am Chem Soc 136, 11582–11585.

Fu, Y., Zorman, B., Sumazin, P., Sanna, P.P., Repunte-Canonigo, V., 2019. Epitranscriptomics: Correlation of N6-methyladenosine RNA methylation and pathway dysregulation in the hippocampus of HIV transgenic rats. PLoS One 14, e0203566.

Furman, J.L., Sama, D.M., Gant, J.C., Beckett, T.L., Murphy, M.P., Bachstetter, A.D., van Eldik, L.J., Norris, C.M., 2012. Targeting Astrocytes Ameliorates Neurologic Changes in a Mouse Model of Alzheimer's Disease. The Journal of Neuroscience 32, 16129.

Fustin, J.M., Doi, M., Yamaguchi, Y., Hida, H., Nishimura, S., Yoshida, M., Isagawa, T., Morioka, M.S., Kakeya, H., Manabe, I., et al., 2013. RNA-methylation-dependent RNA processing controls the speed of the circadian clock. Cell 155, 793.

Gao, G., Duan, Y., Chang, F., Zhang, T., Huang, X., Yu, C., 2022. METTL14 promotes apoptosis of spinal cord neurons by inducing EEF1A2 m6A methylation in spinal cord injury. Cell Death Discov 8, 1–14.

Gao, X., Shin, Y.H., Li, M., Wang, F., Tong, Q., Zhang, P., 2010. The fat mass and obesity associated gene FTO functions in the brain to regulate postnatal growth in mice. PLoS One 5, e14005.

Garone, C., D'Souza, A.R., Dallabona, C., Lodi, T., Rebelo-Guiomar, P., Rorbach, J., Donati, M.A., Procopio, E., Montomoli, M., Guerrini, R., et al., 2017. Defective mitochondrial rRNA methyltransferase MRM2 causes MELAS-like clinical syndrome. Hum Mol Genet 26, 4257–4266.

Gerken, T., Girard, C.A., Tung, Y.C.L., Webby, C.J., Saudek, V., Hewitson, K.S., Yeo, G.S.H., McDonough, M.A., Cunliffe, S., McNeill, L.A., et al., 2007. The obesity-associated FTO gene encodes a 2-oxoglutarate-dependent nucleic acid demethylase. Science 318, 1469–1472.

Geuens, T., Bouhy, D., Timmerman, V., 2016. The hnRNP family: insights into their role in health and disease. Hum Genet 135, 851–867.

Goemaere, J., Knoops, B., 2012. Peroxiredoxin distribution in the mouse brain with emphasis on neuronal populations affected in neurodegenerative disorders. J Comp Neurol 520, 258–280.

González-Reyes, R.E., Nava-Mesa, M.O., Vargas-Sánchez, K., Ariza-Salamanca, D., Mora-Muñoz, L., 2017. Involvement of Astrocytes in Alzheimer's Disease from a Neuroinflammatory and Oxidative Stress Perspective. Front Mol Neurosci 10, 427.

Grieb, P., 2016. Intracerebroventricular Streptozotocin Injections as a Model of Alzheimer's Disease: in Search of a Relevant Mechanism. Mol Neurobiol 53, 1741–1752.

Gu, X., Zhang, Y., Li, D., Cai, H., Cai, L., Xu, Q., 2020. N6-methyladenosine demethylase FTO promotes M1 and M2 macrophage activation. Cell Signal 69, 109553.

Gulati, P., Avezov, E., Ma, M., Antrobus, R., Lehner, P., O'Rahilly, S., Yeo, G.S.H., 2014. Fat mass and obesity-related (FTO) shuttles between the nucleus and cytoplasm. Biosci Rep 34, 621–628.

Gulati, P., Cheung, M.K., Antrobus, R., Church, C.D., Harding, H.P., Tung, Y.C.L., Rimmington, D., Ma, M., Ron, D., Lehner, P.J., et al., 2013. Role for the obesity-related FTO gene in the cellular sensing of amino acids. Proc Natl Acad Sci U S A 110, 2557–2562.

Han, M., Liu, Z., Xu, Y., Liu, X., Wang, D., Li, F., Wang, Y., Bi, J., 2020. Abnormality of m6A mRNA Methylation Is Involved in Alzheimer's Disease. Front Neurosci 14, 98.

Hardy, J.A., Higgins, G.A., 1992. Alzheimer's disease: the amyloid cascade hypothesis. Science 256, 184–185.

Harris, F.M., Tesseur, I., Brecht, W.J., Xu, Q., Mullendorff, K., Chang, S., Wyss-Coray, T., Mahley, R.W., Huang, Y., 2004. Astroglial regulation of apolipoprotein E expression in neuronal cells. Implications for Alzheimer's disease. J Biol Chem 279, 3862–3868.

Hashemi, S.H., Li, J.Y., Ahlman, H., Dahlström, A., 2003. SSR2(a) receptor expression and adrenergic/cholinergic characteristics in differentiated SH-SY5Y cells. Neurochem Res 28, 449–460.

Hashioka, S., Wu, Z., Klegeris, A., 2021. Glia-Driven Neuroinflammation and Systemic Inflammation in Alzheimer's Disease. Curr Neuropharmacol 19, 908.

Haussmann, I.U., Bodi, Z., Sanchez-Moran, E., Mongan, N.P., Archer, N., Fray, R.G., Soller, M., 2016. m6A potentiates Sxl alternative pre-mRNA splicing for robust Drosophila sex determination. Nature 540, 301–304.

Heneka, M.T., Carson, M.J., Khoury, J. el, Landreth, G.E., Brosseron, F., Feinstein, D.L., Jacobs, A.H., Wyss-Coray, T., Vitorica, J., Ransohoff, R.M., et al., 2015. Neuroinflammation in Alzheimer's disease. Lancet Neurol 14, 388–405.

Hernández-Caballero, M.E., Sierra-Ramírez, J.A., 2015. Single nucleotide polymorphisms of the FTO gene and cancer risk: an overview. Mol Biol Rep 42, 699–704.

Hess, M.E., Hess, S., Meyer, K.D., Verhagen, L.A.W., Koch, L., Brönneke, H.S., Dietrich, M.O., Jordan, S.D., Saletore, Y., Elemento, O., et al., 2013. The fat mass and obesity associated gene (Fto) regulates activity of the dopaminergic midbrain circuitry. Nat Neurosci 16, 1042–1048.

Hirayama, M., Wei, F.Y., Chujo, T., Oki, S., Yakita, M., Kobayashi, D., Araki, N., Takahashi, N., Yoshida, R., Nakayama, H., et al., 2020. FTO Demethylates Cyclin D1 mRNA and Controls Cell-Cycle Progression. Cell Rep 31, 107464.

Ho, A.J., Stein, J.L., Hua, X., Lee, S., Hibar, D.P., Leow, A.D., Dinov, I.D., Toga, A.W., Saykin, A.J., Shen, L., et al., 2010. A commonly carried allele of the obesity-related FTO gene is associated with reduced brain volume in the healthy elderly. Proc Natl Acad Sci U S A 107, 8404–8409.

Hu, M.J., Crawford, S.A., Henstridge, D.C., Ng, I.H.W., Boey, E.J.H., Xu, Y., Febbraio, M.A., Jans, D.A., Bogoyevitch, M.A., 2013. p32 protein levels are integral to mitochondrial and endoplasmic reticulum morphology, cell metabolism and survival. Biochem J 453, 381–391.

Hu, Y., Chen, J., Wang, Y., Sun, J., Huang, P., Feng, J., Liu, T., Sun, X., 2022. Fat mass and obesity-associated protein alleviates Aβ1-40 induced retinal pigment epithelial cells degeneration via PKA/CREB signaling pathway. Cell Biol Int Online ahead of print.

Huang, H., Camats-Perna, J., Medeiros, R., Anggono, V., Widagdo, J., 2020. Altered Expression of the m6A Methyltransferase METTL3 in Alzheimer's Disease. eNeuro 7, 1–10.

Huang, H., Weng, H., Sun, W., Qin, X., Shi, H., Wu, H., Zhao, B.S., Mesquita, A., Liu, C., Yuan, C.L., et al., 2018. Recognition of RNA N6-methyladenosine by IGF2BP Proteins Enhances mRNA Stability and Translation. Nat Cell Biol 20, 285.

Huang, J., Sun, W., Wang, Z., Lv, C., Zhang, T., Zhang, D., Dong, W., Shao, L., He, L., Ji, X., et al., 2022. FTO suppresses glycolysis and growth of papillary thyroid cancer via decreasing stability of APOE mRNA in an N6-methyladenosine-dependent manner. J Exp Clin Cancer Res 41, 42.

Huang, T., Gao, Q., Feng, T., Zheng, Y., Guo, J., Zeng, W., 2019. FTO knockout causes chromosome instability and G2/M arrest in mouse GC-1 cells. Front Genet 10, 732.

Huang, Y., Su, R., Sheng, Y., Dong, L., Dong, Z., Xu, H., Ni, T., Zhang, Z.S., Zhang, T., Li, C., et al., 2019. Small-Molecule Targeting of Oncogenic FTO Demethylase in Acute Myeloid Leukemia. Cancer Cell 35, 677-691.e10.

Huang, Y., Yan, J., Li, Q., Li, J., Gong, S., Zhou, H., Gan, J., Jiang, H., Jia, G.F., Luo, C., et al., 2015. Meclofenamic acid selectively inhibits FTO demethylation of m6A over ALKBH5. Nucleic Acids Res 43, 373–384.

Huff, S., Tiwari, S.K., Gonzalez, G.M., Wang, Y., Rana, T.M., 2021. m6A-RNA Demethylase FTO Inhibitors Impair Self-Renewal in Glioblastoma Stem Cells. ACS Chem Biol 16, 324–333.

Iliff, J.J., Chen, M.J., Plog, B.A., Zeppenfeld, D.M., Soltero, M., Yang, L., Singh, I., Deane, R., Nedergaard, M., 2014. Impairment of glymphatic pathway function promotes tau pathology after traumatic brain injury. J Neurosci 34, 16180–16193.

Iliff, J.J., Wang, M., Liao, Y., Plogg, B.A., Peng, W., Gundersen, G.A., Benveniste, H., Vates, G.E., Deane, R., Goldman, S.A., et al., 2012. A paravascular pathway facilitates CSF flow through the brain parenchyma and the clearance of interstitial solutes, including amyloid β. Sci Transl Med 4, 147ra111.

Iosi, F., Santini, M.T., Malorni, W., 1993. Membrane and cytoskeleton are intracellular targets of rhein in A431 cells. Anticancer Res 13, 545–554.

Janelidze, S., Mattsson, N., Stomrud, E., Lindberg, O., Palmqvist, S., Zetterberg, H., Blennow, K., Hansson, O., 2018. CSF biomarkers of neuroinflammation and cerebrovascular dysfunction in early Alzheimer disease. Neurology 91, e867–e877.

Ji, H., Wang, J., Guo, J., Li, Y., Lian, S., Guo, W., Yang, H., Kong, F., Zhen, L., Guo, L., et al., 2016. Progress in the biological function of alpha-enolase. Animal Nutrition 2, 12.

Jia, G., Fu, Y., Zhao, X., Dai, Q., Zheng, G., Yang, Y., Yi, C., Lindahl, T., Pan, T., Yang, Y.G., et al., 2011. N6-Methyladenosine in Nuclear RNA is a Major Substrate of the Obesity-Associated FTO. Nat Chem Biol 7, 885.

Jin, D., Guo, J., Wu, Y., Du, J., Yang, L., Wang, X., Di, W., Hu, B., An, J., Kong, L., et al., 2019. m6A mRNA methylation initiated by METTL3 directly promotes YAP translation and increases YAP activity by regulating the MALAT1-miR-1914-3p-YAP axis to induce NSCLC drug resistance and metastasis. J Hematol Oncol 12, 135.

Jo, S., Yarishkin, O., Hwang, Y.J., Chun, Y.E., Park, M., Woo, D.H., Bae, J.Y., Kim, T., Lee, J., Chun, H., et al., 2014. GABA from reactive astrocytes impairs memory in mouse models of Alzheimer's disease. Nat Med 20, 886.

Kang, H., Zhang, Z., Yu, L., Li, Y., Liang, M., Zhou, L., 2018. FTO reduces mitochondria and promotes hepatic fat accumulation through RNA demethylation. J Cell Biochem 119, 5676–5685.

Kanlaya, R., Pattanakitsakul, S.N., Sinchaikul, S., Chen, S.T., Thongboonkerd, V., 2010. Vimentin interacts with heterogeneous nuclear ribonucleoproteins and dengue nonstructural protein 1 and is important for viral replication and release. Mol Biosyst 6, 795–806.

Karra, E., O'Daly, O.G., Choudhury, A.I., Yousseif, A., Millership, S., Neary, M.T., Scott, W.R., Chandarana, K., Manning, S., Hess, M.E., et al., 2013. A link between FTO, ghrelin, and impaired brain food-cue responsivity. J Clin Invest 123, 3539.

Ke, S., Pandya-Jones, A., Saito, Y., Fak, J.J., Vågbø, C.B., Geula, S., Hanna, J.H., Black, D.L., Darnell, J.E., Darnell, R.B., 2017. m6A mRNA modifications are deposited in nascent pre-mRNA and are not required for splicing but do specify cytoplasmic turnover. Genes Dev 31, 990–1006.

Keller, L., Xu, W., Wang, H.X., Winblad, B., Fratiglioni, L., Graff, C., 2011. The obesity related gene, FTO, interacts with APOE, and is associated with Alzheimer's disease risk: a prospective cohort study. J Alzheimers Dis 23, 461–469.

Kim, J., Lee, G., 2021. Metabolic Control of m6A RNA Modification. Metabolites 11, 1–11.

Kim, S.Y., Kim, T.J., Lee, K.Y., 2008. A novel function of peroxiredoxin 1 (Prx-1) in apoptosis signal-regulating kinase 1 (ASK1)-mediated signaling pathway. FEBS Lett 582, 1913–1918.

Kleppe, R., Martinez, A., Døskeland, S.O., Haavik, J., 2011. The 14-3-3 proteins in regulation of cellular metabolism. Semin Cell Dev Biol 22, 713–719.

Koh, C.W.Q., Goh, Y.T., Goh, W.S.S., 2019. Atlas of quantitative single-base-resolution N6-methyl-adenine methylomes. Nat Commun 10, 1–15.

Kolisnyk, B., Al-Onaizi, M., Soreq, L., Barbash, S., Bekenstein, U., Haberman, N., Hanin, G., Kish, M.T., Souza Da Silva, J., Fahnestock, M., et al., 2017. Cholinergic Surveillance over Hippocampal RNA Metabolism and Alzheimer's-Like Pathology. Cereb Cortex 27, 3553–3567.

Koranda, J.L., Dore, L., Shi, H., Patel, M.J., Vaasjo, L.O., Rao, M.N., Chen, K., Lu, Z., Yi, Y., Chi, W., et al., 2018. Mettl14 Is Essential for Epitranscriptomic Regulation of Striatal Function and Learning. Neuron 99, 283-292.e5.

Korb, E., Finkbeiner, S., 2011. Arc in synaptic plasticity: from gene to behavior. Trends Neurosci 34, 591.

Korecka, J.A., van Kesteren, R.E., Blaas, E., Spitzer, S.O., Kamstra, J.H., Smit, A.B., Swaab, D.F., Verhaagen, J., Bossers, K., 2013. Phenotypic characterization of retinoic acid differentiated SH-SY5Y cells by transcriptional profiling. PLoS One 8, e63862.

Krüger, N., Biwer, L.A., Good, M.E., Ruddiman, C.A., Wolpe, A.G., DeLalio, L.J., Murphy, S., Macal, E.H., Ragolia, L., Serbulea, V., et al., 2020. Loss of endothelial FTO antagonizes obesity-induced metabolic and vascular dysfunction. Circ Res 126, 232–242.

Kumar, N., Gowda, C., Nawalpuri, B., Ramakrishna, S., Jhaveri, V., Muddashetty, R.S., 2022. NMDAR mediated dynamic changes in m6A inversely correlates with neuronal translation. bioRxiv 2022.06.01.494458.

Kumar, S., Mohapatra, T., 2021. Deciphering Epitranscriptome: Modification of mRNA Bases Provides a New Perspective for Post-transcriptional Regulation of Gene Expression. Front Cell Dev Biol 9, 550.

Kusakabe, T., Motoki, K., Hori, K., 1997. Mode of interactions of human aldolase isozymes with cytoskeletons. Arch Biochem Biophys 344, 184–193.

Kwon, H.S., Koh, S.H., 2020. Neuroinflammation in neurodegenerative disorders: the roles of microglia and astrocytes. Transl Neurodegener 9, 1–12.

Lane, C.A., Hardy, J., Schott, J.M., 2018. Alzheimer's disease. Eur J Neurol 25, 59–70.

Lee, C.-W., Shih, Y.-H., Wu, S.-Y., Yang, T., Lin, C., Kuo, Y.-M., 2013. Hypoglycemia induces tau hyperphosphorylation. Curr Alzheimer Res 10, 298–308.

Lee, I., 2015. Betaine is a positive regulator of mitochondrial respiration. Biochem Biophys Res Commun 456, 621–625.

Lee, Y.-H., Liu, X., Qiu, F., O'Connor, T.R., Yen, Y., Ann, D.K., 2015. HP1β is a biomarker for breast cancer prognosis and PARP inhibitor therapy. PLoS One 10, e0121207.

Legendre, F., Heuze, A., Boukerrouche, K., Leclercq, S., Boumediene, K., Galera, P., Domagala, F., Pujol, J.P., Ficheux, H., 2009. Rhein, the metabolite of diacerhein, reduces the proliferation of osteoarthritic chondrocytes and synoviocytes without inducing apoptosis. Scand J Rheumatol 38, 104–111.

Li, A., Chen, Y.S., Ping, X.L., Yang, X., Xiao, W., Yang, Y., Sun, H.Y., Zhu, Q., Baidya, P., Wang, X., et al., 2017. Cytoplasmic m6A reader YTHDF3 promotes mRNA translation. Cell Res 27, 444.

Li, F., Yi, Y., Miao, Y., Long, W., Long, T., Chen, S., Cheng, W., Zou, C., Zheng, Y., Wu, X., et al., 2019. N6-methyladenosine Modulates Nonsense-mediated mRNA Decay in Human Glioblastoma. Cancer Res 79, 5785.

Li, H., Ren, Y., Mao, K., Hua, F., Yang, Y., Wei, N., Yue, C., Li, D., Zhang, H., 2018. FTO is involved in Alzheimer's disease by targeting TSC1-mTOR-Tau signaling. Biochem Biophys Res Commun 498, 234–239.

Li, L., Zang, L., Zhang, F., Chen, J., Shen, H., Shu, L., Liang, F., Feng, C., Chen, D., Tao, H., et al., 2017. Fat mass and obesity-associated (FTO) protein regulates adult neurogenesis. Hum Mol Genet 26, 2398.

Li, M., Zhao, X., Wang, W., Shi, H., Pan, Q., Lu, Z., Perez, S.P., Suganthan, R., He, C., Bjørås, M., et al., 2018. Ythdf2-mediated m6A mRNA clearance modulates neural development in mice. Genome Biol 19, 69.

Li, N., Zhang, D., Cao, S., Qiao, M., Zhang, P., Zhao, Q., Shen, Y., Huang, X., Song, L., 2021. The effects of folic acid on RNA m6A methylation in hippocampus as well as learning and memory ability of rats with acute lead exposure. J Funct Foods 76, 104276.

Li, Q., Huang, Y., Liu, X., Gan, J., Chen, H., Yang, C.G., 2016. Rhein Inhibits AlkB Repair Enzymes and Sensitizes Cells to Methylated DNA Damage. J Biol Chem 291, 11083–11093.

Li, Q., Wen, S., Ye, W., Zhao, S., Liu, X., 2021. The potential roles of m6A modification in regulating the inflammatory response in microglia. J Neuroinflammation 18, 149.

Li, W., Jiang, M., Zhao, S., Liu, H., Zhang, X., Wilson, J.X., Huang, G., 2015. Folic Acid Inhibits Amyloid β-Peptide Production through Modulating DNA Methyltransferase Activity in N2a-APP Cells. Int J Mol Sci 16, 25002–25013.

Li, Y., Su, R., Deng, X., Chen, Y., Chen, J., 2022. FTO in cancer: functions, molecular mechanisms, and therapeutic implications. Trends Cancer 8, 598–614.

Li, Y., Wan, O.W., Xie, W., Chung, K.K.K., 2011. p32 regulates mitochondrial morphology and dynamics through parkin. Neuroscience 199, 346–358.

Lian, H., Yang, L., Cole, A., Sun, L., Chiang, A.C.A., Fowler, S.W., Shim, D.J., Rodriguez-Rivera, J., Taglialatela, G., Jankowsky, J.L., et al., 2015. NFκB-activated astroglial release of complement C3 compromises neuronal morphology and function associated with Alzheimer's disease. Neuron 85, 101–115.

Licatalosi, D.D., Yano, M., Fak, J.J., Mele, A., Grabinski, S.E., Zhang, C., Darnell, R.B., 2012. Ptbp2 represses adult-specific splicing to regulate the generation of neuronal precursors in the embryonic brain. Genes Dev 26, 1626–1642.

Lim, J.W., Lee, J., Pae, A.N., 2020. Mitochondrial dysfunction and Alzheimer's disease: prospects for therapeutic intervention. BMB Rep 53, 47.

Lin, L., Hales, C.M., Garber, K., Jin, P., 2014. Fat mass and obesity-associated (FTO) protein interacts with CaMKII and modulates the activity of CREB signaling pathway. Hum Mol Genet 23, 3299–3306.

Liu, N., Parisien, M., Dai, Q., Zheng, G., He, C., Pan, T., 2013. Probing N6-methyladenosine RNA modification status at single nucleotide resolution in mRNA and long noncoding RNA. RNA 19, 1848.

Liu, Q., Zhang, X.L., Tao, R.Y., Niu, Y.J., Chen, X.G., Tian, J.Y., Ye, F., 2011. Rhein, an inhibitor of adipocyte differentiation and adipogenesis. J Asian Nat Prod Res 13, 714–723.

Liu, S.J., Cai, T.H., Fang, C.L., Lin, S.Z., Yang, W.Q., Wei, Y., Zhou, F., Liu, L., Luo, Y., Guo, Z.Y., et al., 2022. Long-term exercise training down-regulates m6A RNA demethylase FTO expression in the hippocampus and hypothalamus: an effective intervention for epigenetic modification. BMC Neurosci 23, 54.

Liu, T., Wei, Q., Jin, J., Luo, Q., Liu, Y., Yang, Y., Cheng, C., Li, Lanfang, Pi, J., Si, Y., et al., 2020. The m6A reader YTHDF1 promotes ovarian cancer progression via augmenting EIF3C translation. Nucleic Acids Res 48, 3816.

Liu, Y., Liang, G., Xu, H., Dong, W., Dong, Z., Qiu, Z., Zhang, Z., Li, F., Huang, Y., Li, Y., et al., 2021. Tumors exploit FTO-mediated regulation of glycolytic metabolism to evade immune surveillance. Cell Metab 33, 1221-1233.e11.

Liu, Y., Wang, R., Zhang, L., Li, J., Lou, K., Shi, B., 2017. The lipid metabolism gene FTO influences breast cancer cell energy metabolism via the PI3K/AKT signaling pathway. Oncol Lett 13, 4685–4690.

Luo, J., Wang, F., Sun, F., Yue, T., Zhou, Q., Yang, C., Rong, S., Yang, P., Xiong, F., Yu, Q., et al., 2021. Targeted Inhibition of FTO Demethylase Protects Mice Against LPS-Induced Septic Shock by Suppressing NLRP3 Inflammasome. Front Immunol 12, 663295.

Lv, Z., Xu, T., Li, R., Zheng, D., Li, Y., Li, W., Yang, Y., Hao, Y., 2022. Downregulation of m6A Methyltransferase in the Hippocampus of Tyrobp–/– Mice and Implications for Learning and Memory Deficits. Front Neurosci 16, 739201.

Ma, C., Chang, M., Lv, H., Zhang, Z.W., Zhang, W., He, X., Wu, G., Zhao, S., Zhang, Y., Wang, D., et al., 2018. RNA m6A methylation participates in regulation of postnatal development of the mouse cerebellum. Genome Biol 19, 68.

Ma, L., Xue, X., Zhang, X., Yu, K., Xu, X., Tian, X., Miao, Y., Meng, F., Liu, X., Guo, S., et al., 2022. The essential roles of m6A RNA modification to stimulate ENO1-dependent glycolysis and tumorigenesis in lung adenocarcinoma. J Exp Clin Cancer Res 41, 36.

Mao, Y., Zhang, M., Yang, J., Sun, H., Wang, D., Zhang, X., Yu, F., Li, J., 2017. The UCP2-related mitochondrial pathway participates in rhein-induced apoptosis in HK-2 cells. Toxicol Res (Camb) 6, 297–304.

Mattout, A., Aaronson, Y., Sailaja, B.S., Raghu Ram, E. v., Harikumar, A., Mallm, J.P., Sim, K.H., Nissim-Rafinia, M., Supper, E., Singh, P.B., et al., 2015. Heterochromatin Protein 1β (HP1β) has distinct functions and distinct nuclear distribution in pluripotent versus differentiated cells. Genome Biol 16, 1–21.

Mauer, J., Luo, X., Blanjoie, A., Jiao, X., Grozhik, A. v., Patil, D.P., Linder, B., Pickering, B.F., Vasseur, J.J., Chen, Q., et al., 2017. Reversible methylation of m6Am in the 5' cap controls mRNA stability. Nature 541, 371–375.

McGee, A.M., Douglas, D.L., Liang, Y., Hyder, S.M., Baines, C.P., 2011. The mitochondrial protein C1qbp promotes cell proliferation, migration and resistance to cell death. Cell Cycle 10, 4119–4127.

McMurray, F., Church, C.D., Larder, R., Nicholson, G., Wells, S., Teboul, L., Tung, Y.C.L., Rimmington, D., Bosch, F., Jimenez, V., et al., 2013. Adult onset global loss of the fto gene alters body composition and metabolism in the mouse. PLoS Genet 9, e1003166.

McTaggart, J.S., Lee, S., Iberl, M., Church, C., Cox, R.D., Ashcroft, F.M., 2011. FTO Is Expressed in Neurones throughout the Brain and Its Expression Is Unaltered by Fasting. PLoS One 6, 27968.

Melka, M.G., Gillis, J., Bernard, M., Abrahamowicz, M., Chakravarty, M.M., Leonard, G.T., Perron, M., Richer, L., Veillette, S., Banaschewski, T., et al., 2013. FTO, obesity and the adolescent brain. Hum Mol Genet 22, 1050–1058.

Merkurjev, D., Hong, W.T., Iida, K., Oomoto, I., Goldie, B.J., Yamaguti, H., Ohara, T., Kawaguchi, S.Y., Hirano, T., Martin, K.C., et al., 2018. Synaptic N6-methyladenosine (m6A) epitranscriptome reveals functional partitioning of localized transcripts. Nat Neurosci 21, 1004–1014.

Metodiev, M.D., Lesko, N., Park, C.B., Cámara, Y., Shi, Y., Wibom, R., Hultenby, K., Gustafsson, C.M., Larsson, N.G., 2009. Methylation of 12S rRNA is necessary for in vivo stability of the small subunit of the mammalian mitochondrial ribosome. Cell Metab 9, 386–397.

Meyer, K.D., Patil, D.P., Zhou, J., Zinoviev, A., Skabkin, M.A., Elemento, O., Pestova, T. v., Qian, S.B., Jaffrey, S.R., 2015. 5' UTR m(6)A Promotes Cap-Independent Translation. Cell 163, 999–1010.

Meyer, K.D., Saletore, Y., Zumbo, P., Elemento, O., Mason, C.E., Jaffrey, S.R., 2012. Comprehensive Analysis of mRNA Methylation Reveals Enrichment in 3' UTRs and Near Stop Codons. Cell 149, 1635.

Mizuno, T., Lew, P.S., 2021. Regulation of Activating Transcription Factor 4 (ATF4) Expression by Fat Mass and Obesity-Associated (FTO) in Mouse Hepatocyte Cells. Acta Endocrinol (Buchar) 17, 26–32.

Morena, F., Argentati, C., Bazzucchi, M., Emiliani, C., Martino, S., 2018. Above the Epitranscriptome: RNA Modifications and Stem Cell Identity. Genes (Basel) 9, 329.

Mosmann, T., 1983. Rapid colorimetric assay for cellular growth and survival: application to proliferation and cytotoxicity assays. J Immunol Methods 65, 55–63.

Müller, T.A., Struble, S.L., Meek, K., Hausinger, R.P., 2018. Characterization of human AlkB homolog 1 produced in mammalian cells and demonstration of mitochondrial dysfunction in ALKBH1-deficient cells. Biochem Biophys Res Commun 495, 98–103.

Neth, B.J., Craft, S., 2017. Insulin Resistance and Alzheimer's Disease: Bioenergetic Linkages. Front Aging Neurosci 9, 345.

Netto, L.E.S., Antunes, F., 2016. The Roles of Peroxiredoxin and Thioredoxin in Hydrogen Peroxide Sensing and in Signal Transduction. Mol Cells 39, 65–71.

Ofengand, J., 2002. Ribosomal RNA pseudouridines and pseudouridine synthases. FEBS Lett 514, 17–25.

Olszewski, P.K., Fredriksson, R., Olszewska, A.M., Stephansson, O., Alsiö, J., Radomska, K.J., Levine, A.S., Schiöth, H.B., 2009. Hypothalamic FTO is associated with the regulation of energy intake not feeding reward. BMC Neurosci 10, 129.

Park, J., Won, J., Seo, J., Yeo, H.-G., Kim, K., Kim, Y.G., Jeon, C.-Y., Kam, M.K., Kim, Y.-H., Huh, J.-W., et al., 2020. Streptozotocin Induces Alzheimer's Disease-Like Pathology in Hippocampal Neuronal Cells via CDK5/Drp1-Mediated Mitochondrial Fragmentation. Front Cell Neurosci 14, 235.

Parks, J.K., Smith, T.S., Trimmer, P.A., Bennett, J.P., Davis Parker, W.J., 2001. Neurotoxic Aβ peptides increase oxidative stress in vivo through NMDA-receptor and nitric-oxide-synthase mechanisms, and inhibit complex IV activity and induce a mitochondrial permeability transition in vitro. J Neurochem 76, 1050–1056.

Patil, D.P., Chen, C.K., Pickering, B.F., Chow, A., Jackson, C., Guttman, M., Jaffrey, S.R., 2016. m(6)A RNA methylation promotes XIST-mediated transcriptional repression. Nature 537, 369–373.

Paul, S., Dansithong, W., Kim, D., Rossi, J., Webster, N.J.G., Comai, L., Reddy, S., 2006. Interaction of muscleblind, CUG-BP1 and hnRNP H proteins in DM1-associated aberrant IR splicing. EMBO J 25, 4271–4283.

Pendleton, K.E., Chen, B., Liu, K., Hunter, O. v., Xie, Y., Tu, B.P., Conrad, N.K., 2017. The U6 snRNA m6A Methyltransferase METTL16 Regulates SAM Synthetase Intron Retention. Cell 169, 824-835.e14.

Peng, S., Xiao, W., Ju, D., Sun, B., Hou, N., Liu, Q., Wang, Yanli, Zhao, H., Gao, C., Zhang, S., et al., 2019. Identification of entacapone as a chemical inhibitor of FTO mediating metabolic regulation through FOXO1. Sci Transl Med 11, eaau7116.

Perry, R.P., Kelley, D.E., 1974. Existence of methylated messenger RNA in mouse L cells. Cell 1, 37–42.

Peters, T., Ausmeier, K., Rüther, U., 1999. Cloning of Fatso (Fto), a novel gene deleted by the Fused toes (Ft) mouse mutation. Mamm Genome 10, 983–986.

Petersen-Mahrt, S.K., Estmer, C., Öhrmalm, C., Matthews, D.A., Russell, W.C., Akusjärvi, G., 1999. The splicing factor-associated protein, p32, regulates RNA splicing by inhibiting ASF/SF2 RNA binding and phosphorylation. EMBO J 18, 1014.

Piaceri, I., Nacmias, B., Sorbi, S., 2013. Genetics of familial and sporadic Alzheimer's disease. Frontiers in Bioscience - Elite 5 E, 167–177.

Ping, X.L., Sun, B.F., Wang, L., Xiao, W., Yang, X., Wang, W.J., Adhikari, S., Shi, Y., Lv, Y., Chen, Y.S., et al., 2014. Mammalian WTAP is a regulatory subunit of the RNA N6-methyladenosine methyltransferase. Cell Res 24, 177–189.

Pitman, R.T., Fong, J.T., Billman, P., Puri, N., 2012. Knockdown of the fat mass and obesity gene disrupts cellular energy balance in a cell-type specific manner. PLoS One 7, e38444.

Pitman, R.T., Fong, J.T., Stone, A.L., Devito, J.T., Puri, N., 2013. FTO Knockdown Decreases Phosphorylation of Tau in Neuronal Cells; A Potential Model Implicating the Association of FTO with Alzheimer 's Disease. J Alzheimers Dis Parkinsonism 3, 1–4.

Poritsanos, N.J., Lew, P.S., Fischer, J., Mobbs, C. v., Nagy, J.I., Wong, D., Rüther, U., Mizuno, T.M., 2011. Impaired hypothalamic Fto expression in response to fasting and glucose in obese mice. Nutr Diabetes 1, e19–e19.

Qi, Z., Wang, S., Li, J., Wen, Y., Cui, R., Zhang, K., Liu, Y., Yang, X., Zhang, L., Xu, B., et al., 2022. Protective role of mRNA demethylase FTO on axon guidance molecules of nigro-striatal projection system in manganese-induced parkinsonism. J Hazard Mater 426, 128099.

Relier, S., Ripoll, J., Guillorit, H., Amalric, A., Achour, C., Boissière, F., Vialaret, J., Attina, A., Debart, F., Choquet, A., et al., 2021. FTO-mediated cytoplasmic m6Am demethylation adjusts stem-like properties in colorectal cancer cell. Nat Commun 12, 1–13.

Richter, J.D., Bassell, G.J., Klann, E., 2015. Dysregulation and restoration of translational homeostasis in fragile X syndrome. Nat Rev Neurosci 16, 595–605.

Rivera, M., Cohen-Woods, S., Kapur, K., Breen, G., Ng, M.Y., Butler, A.W., Craddock, N., Gill, M., Korszun, A., Maier, W., et al., 2012. Depressive disorder moderates the effect of the FTO gene on body mass index. Mol Psychiatry 17, 604–611.

Roundtree, I.A., Luo, G.Z., Zhang, Z., Wang, X., Zhou, T., Cui, Y., Sha, J., Huang, X., Guerrero, L., Xie, P., et al., 2017. YTHDC1 mediates nuclear export of N6-methyladenosine methylated mRNAs. Elife 6, e31311.

Rowles, J., Wong, M., Powers, R., Olsen, M., 2012. FTO, RNA epigenetics and epilepsy. Epigenetics 7, 1094.

Ruud, J., Alber, J., Tokarska, A., Engström Ruud, L., Nolte, H., Biglari, N., Lippert, R., Lautenschlager, Ä., Cieślak, P.E., Szumiec, Ł., et al., 2019. The Fat Mass and Obesity-Associated Protein (FTO) Regulates Locomotor Responses to Novelty via D2R Medium Spiny Neurons. Cell Rep 27, 3182-3198.e9.

Salditt-Georgieff, M., Jelinek, W., Darnell, J.E., Furuichi, Y., Morgan, M., Shatkin, A., 1976. Methyl labeling of HeLa cell hnRNA: a comparison with mRNA. Cell 7, 227–237.

Sami Saribas, A., Cicalese, S., Ahooyi, T.M., Khalili, K., Amini, S., Sariyer, I.K., 2017. HIV-1 Nef is released in extracellular vesicles derived from astrocytes: evidence for Nef-mediated neurotoxicity. Cell Death Dis 8, e2542.

Sang, L., Wu, X., Yan, T., Naren, D., Liu, X., Zheng, X., Zhang, N., Wang, H., Li, Y., Gong, Y., 2022. The m6A RNA methyltransferase METTL3/METTL14 promotes leukemogenesis through the mdm2/p53 pathway in acute myeloid leukemia. J Cancer 13, 1019–1030.

Schwartz, S., Agarwala, S.D., Mumbach, M.R., Jovanovic, M., Mertins, P., Shishkin, A., Tabach, Y., Mikkelsen, T.S., Satija, R., Ruvkun, G., et al., 2013. High-resolution mapping reveals a conserved, widespread, dynamic meiotically regulated mRNA methylation program. Cell 155, 1409.

Seo, K.W., Kleiner, R.E., 2021. Mechanisms of epitranscriptomic gene regulation. Biopolymers 112, e23403.

Sevgi, M., Rigoux, L., Kühn, A.B., Mauer, J., Schilbach, L., Hess, M.E., Gruendler, T.O.J., Ullsperger, M., Stephan, K.E., Brüning, J.C., et al., 2015. An Obesity-Predisposing Variant of the FTO Gene Regulates D2R-Dependent Reward Learning. J Neurosci 35, 12584–12592.

Shafik, A.M., Zhang, F., Guo, Z., Dai, Q., Pajdzik, K., Li, Y., Kang, Y., Yao, B., Wu, H., He, C., et al., 2021. N6-methyladenosine dynamics in neurodevelopment and aging, and its potential role in Alzheimer's disease. Genome Biol 22, 17.

Shang, R., Pu, M., Li, Y., Wang, D., 2017. FOXM1 regulates glycolysis in hepatocellular carcinoma by transactivating glucose transporter 1 expression. Oncol Rep 37, 2261–2269.

Shea, T.B., Perrone-Bizzozero, N.I., Beermann, M.L., Benowitz, L.I., 1991. Phospholipid-mediated delivery of anti-GAP-43 antibodies into neuroblastoma cells prevents neuritogenesis. The Journal of Neuroscience 11, 1685.

Shen, F., Huang, W., Huang, J.T., Xiong, J., Yang, Y., Wu, K., Jia, G.F., Chen, J., Feng, Y.Q., Yuan, B.F., et al., 2015. Decreased N(6)-methyladenosine in peripheral blood RNA from diabetic patients is associated with FTO expression rather than ALKBH5. J Clin Endocrinol Metab 100, E148–E154.

Shi, H., Wang, X., Lu, Z., Zhao, B.S., Ma, H., Hsu, P.J., Liu, C., He, C., 2017. YTHDF3 facilitates translation and decay of N6-methyladenosine-modified RNA. Cell Res 27, 315–328.

Shi, H., Zhang, X., Weng, Y.L., Lu, Zongyang, Liu, Y., Lu, Zhike, Li, J., Hao, P., Zhang, Y., Zhang, F., et al., 2018. m6A facilitates hippocampus-dependent learning and memory through YTHDF1. Nature 563, 249–253.

Shi, W., Yang, F., Dai, R., Sun, Y., Chu, Y., Liao, S., Hao, B., 2021. METTL3-Mediated N6-Methyladenosine Modification Is Involved in the Dysregulation of NRIP1 Expression in Down Syndrome. Front Cell Dev Biol 9, 621374.

Shi, Y., Fan, S., Wu, M., Zuo, Z., Li, X., Jiang, L., Shen, Q., Xu, P., Zeng, L., Zhou, Y., et al., 2019. YTHDF1 links hypoxia adaptation and non-small cell lung cancer progression. Nat Commun 10, 4892.

Singh, B., Kinne, H.E., Milligan, R.D., Washburn, L.J., Olsen, M., Lucci, A., 2016. Important Role of FTO in the Survival of Rare Panresistant Triple-Negative Inflammatory Breast Cancer Cells Facing a Severe Metabolic Challenge. PLoS One 11, e0159072.

Singhal, N.K., Sternbach, S., Fleming, S., Alkhayer, K., Shelestak, J., Popescu, D., Weaver, A., Clements, R., Wasek, B., Bottiglieri, T., et al., 2020. Betaine restores epigenetic control and supports neuronal mitochondria in the cuprizone mouse model of multiple sclerosis. Epigenetics 15, 871–886.

Sinnamon, J.R., Waddell, C.B., Nik, S., Chen, E.I., Czaplinski, K., 2012. Hnrpab regulates neural development and neuron cell survival after glutamate stimulation. RNA 18, 704.

Smemo, S., Tena, J.J., Kim, K.H., Gamazon, E.R., Sakabe, N.J., Gómez-Marín, C., Aneas, I., Credidio, F.L., Sobreira, D.R., Wasserman, N.F., et al., 2014. Obesity-associated variants within FTO form long-range functional connections with IRX3. Nature 507, 371–375.

Stratigopoulos, G., Burnett, L.C., Rausch, R., Gill, R., Penn, D.B., Skowronski, A.A., LeDuc, C.A., Lanzano, A.J., Zhang, P., Storm, D.R., et al., 2016. Hypomorphism of Fto and Rpgrip1l causes obesity in mice. J Clin Invest 126, 1897–1910.

Su, R., Dong, L., Li, C., Nachtergaele, S., Wunderlich, M., Qing, Y., Deng, X., Wang, Y., Weng, X., Hu, C., et al., 2018. R-2HG Exhibits Anti-tumor Activity by Targeting FTO/m6A/MYC/CEBPA Signaling. Cell 172, 90-105.e23.

Su, R., Dong, L., Li, Y., Gao, M., Han, L., Wunderlich, M., Deng, X., Li, H., Huang, Y., Gao, L., et al., 2020. Targeting FTO Suppresses Cancer Stem Cell Maintenance and Immune Evasion. Cancer Cell 38, 79-96.e11.

Sun, Y.L., Cai, J.Q., Liu, F., Bi, X.Y., Zhou, L.P., Zhao, X.H., 2015. Aberrant expression of peroxiredoxin 1 and its clinical implications in liver cancer. World J Gastroenterol 21, 10840.

Sunabori, T., Tokunaga, A., Nagai, T., Sawamoto, K., Okabe, M., Miyawaki, A., Matsuzaki, Y., Miyata, T., Okano, H., 2008. Cell-cycle-specific nestin expression coordinates with morphological changes in embryonic cortical neural progenitors. J Cell Sci 121, 1204–1212.

Swerdlow, R.H., Khan, S.M., 2004. A “mitochondrial cascade hypothesis” for sporadic Alzheimer’s disease. Med Hypotheses 63, 8–20.

Talukdar, I., Sen, S., Urbano, R., Thompson, J., Yates, J.R., Webster, N.J.G., 2011. hnRNP A1 and hnRNP F modulate the alternative splicing of exon 11 of the insulin receptor gene. PLoS One 6, e27869.

Tanabe, C., Hotoda, N., Sasagawa, N., Sehara-Fujisawa, A., Maruyama, K., Ishiura, S., 2007. ADAM19 is tightly associated with constitutive Alzheimer's disease APP alpha-secretase in A172 cells. Biochem Biophys Res Commun 352, 111–117.

Tang, C., Klukovich, R., Peng, H., Wang, Z., Yu, T., Zhang, Y., Zheng, H., Klungland, A., Yan, W., 2017. ALKBH5-dependent m6A demethylation controls splicing and stability of long 3'-UTR mRNAs in male germ cells. Proc Natl Acad Sci U S A 115, E325–E333.

Tews, D., Fischer-Posovszky, P., Fromme, T., Klingenspor, M., Fischer, J., Rüther, U., Marienfeld, R., Barth, T.F., Möller, P., Debatin, K.M., et al., 2013. FTO deficiency induces UCP-1 expression and mitochondrial uncoupling in adipocytes. Endocrinology 154, 3141–3151.

Thorsell, A., Heilig, M., 2002. Diverse functions of neuropeptide Y revealed using genetically modified animals. Neuropeptides 36, 182–193.

Timper, K., del Río-Martín, A., Cremer, A.L., Bremser, S., Alber, J., Giavalisco, P., Varela, L., Heilinger, C., Nolte, H., Trifunovic, A., et al., 2020. GLP-1 Receptor Signaling in Astrocytes Regulates Fatty Acid Oxidation, Mitochondrial Integrity, and Function. Cell Metab 31, 1189-1205.e13.

Timpson, N.J., Harbord, R., Smith, G.D., Zacho, J., Tybjærg-Hansen, A., Nordestgaard, B.G., 2009. Does greater adiposity increase blood pressure and hypertension risk?: Mendelian randomization using the FTO/MC4R genotype. Hypertension 54, 84–90.

Toh, J.D.W., Crossley, S.W.M., Bruemmer, K.J., Ge, E.J., He, D., Iovan, D.A., Chang, C.J., 2020. Distinct RNA N-demethylation pathways catalyzed by nonheme iron ALKBH5 and FTO enzymes enable regulation of formaldehyde release rates. Proc Natl Acad Sci U S A 117, 25284–25292.

Trixl, L., Amort, T., Wille, A., Zinni, M., Ebner, S., Hechenberger, C., Eichin, F., Gabriel, H., Schoberleitner, I., Huang, A., et al., 2018. RNA cytosine methyltransferase Nsun3 regulates embryonic stem cell differentiation by promoting mitochondrial activity. Cellular and Molecular Life Sciences 75, 1483–1497.

Tung, Y.C.L., Ayuso, E., Shan, X., Bosch, F., O'Rahilly, S., Coll, A.P., Yeo, G.S.H., 2010. Hypothalamic-specific manipulation of Fto, the ortholog of the human obesity gene FTO, affects food intake in rats. PLoS One 5, e8771.

Ujcikova, H., Eckhardt, A., Kagan, D., Roubalova, L., Svoboda, P., 2014. Proteomic analysis of post-nuclear supernatant fraction and percoll-purified membranes prepared from brain cortex of rats exposed to increasing doses of morphine. Proteome Sci 12, 11.

Ujcikova, H., Vosahlikova, M., Roubalova, L., Svoboda, P., 2016. Proteomic analysis of protein composition of rat forebrain cortex exposed to morphine for 10days; comparison with animals exposed to morphine and subsequently nurtured for 20days in the absence of this drug. J Proteomics 145, 11–23.

van der Hoeven, F., Schimmang, T., Volkmann, A., Mattei, M.G., Kyewski, B., Rüther, U., 1994. Programmed cell death is affected in the novel mouse mutant Fused toes (Ft). Development 120, 2601–2607.

Vujovic, P., Stamenkovic, S., Jasnic, N., Lakic, I., Djurasevic, S.F., Cvijic, G., Djordjevic, J., 2013. Fasting Induced Cytoplasmic Fto expression in Some Neurons of Rat Hypothalamus. PLoS One 8, 63694.

Walsh, J.L., Keith, T.J., Knull, H.R., 1989. Glycolytic enzyme interactions with tubulin and microtubules. Biochim Biophys Acta 999, 64–70.

Walters, B.J., Mercaldo, V., Gillon, C.J., Yip, M., Neve, R.L., Boyce, F.M., Frankland, P.W., Josselyn, S.A., 2017. The Role of The RNA Demethylase FTO (Fat Mass and Obesity-Associated) and mRNA Methylation in Hippocampal Memory Formation. Neuropsychopharmacology 42, 1502–1510.

Wang, D.C., Chen, S.S., Lee, Y.C., Chen, T.J., 2006. Amyloid-beta at sublethal level impairs BDNF-induced arc expression in cortical neurons. Neurosci Lett 398, 78–82.

Wang, H., Dong, S., Xu, H., Qian, J., Yang, J., 2012. Genetic variants in FTO associated with metabolic syndrome: A meta- and gene-based analysis. Mol Biol Rep 39, 5691–5698.

Wang, Jian, Ishfaq, M., Xu, L., Xia, C., Chen, C., Li, J., 2019. METTL3/m6A/miRNA-873-5p Attenuated Oxidative Stress and Apoptosis in Colistin-Induced Kidney Injury by Modulating Keap1/Nrf2 Pathway. Front Pharmacol 10, 517.

Wang, Jinghua, Yan, S., Lu, H., Wang, S., Xu, D., 2019. METTL3 Attenuates LPS-Induced Inflammatory Response in Macrophages via NF-κB Signaling Pathway. Mediators Inflamm 2019, 3120391.

Wang, L., Shi, F.X., Li, N., Cao, Y., Lei, Y., Wang, J.Z., Tian, Q., Zhou, X.W., 2020. AMPK Ameliorates Tau Acetylation and Memory Impairment Through Sirt1. Mol Neurobiol 57, 5011–5025.

Wang, T., Hong, T., Huang, Y., Su, H., Wu, F., Chen, Y., Wei, L., Huang, W., Hua, X., Xia, Y., et al., 2015. Fluorescein Derivatives as Bifunctional Molecules for the Simultaneous Inhibiting and Labeling of FTO Protein. J Am Chem Soc 137, 13736–13739.

Wang, X., Huang, N., Yang, M., Wei, D., Tai, H., Han, X., Gong, H., Zhou, J., Qin, J., Wei, X., et al., 2017. FTO is required for myogenesis by positively regulating mTOR-PGC-1α pathway-mediated mitochondria biogenesis. Cell Death Dis 8, e2702.

Wang, Xiao, Zhao, B.S., Roundtree, I.A., Lu, Z., Han, D., Ma, H., Weng, X., Chen, K., Shi, H., He, C., 2015. N6-methyladenosine Modulates Messenger RNA Translation Efficiency. Cell 161, 1388.

Wang, Xinxia, Zhu, L., Chen, J., Wang, Y., 2015. mRNA m6A methylation downregulates adipogenesis in porcine adipocytes. Biochem Biophys Res Commun 459, 201–207.

Wang, Y., Li, Y., Toth, J.I., Petroski, M.D., Zhang, Z., Zhao, J.C., 2014. N6-methyladenosine modification destabilizes developmental regulators in embryonic stem cells. Nat Cell Biol 16, 191.

Wang, Y., Li, Y., Yue, M., Wang, J., Kumar, S., Wechsler-Reya, R.J., Zhang, Z., Ogawa, Y., Kellis, M., Duester, G., et al., 2018. N6-methyladenosine RNA modification regulates embryonic neural stem cell self-renewal through histone modifications. Nat Neurosci 21, 195–206.

Wang, Y., Rao, K., Yuan, L., Everaert, N., Buyse, J., Grossmann, R., Zhao, R., 2012. Chicken FTO gene: tissue-specific expression, brain distribution, breed difference and effect of fasting. Comp Biochem Physiol A Mol Integr Physiol 163, 246–252.

Wang, Y., Yun, Y., Wu, B., Wen, L., Wen, M., Yang, H., Zhao, L., Liu, W., Huang, S., Wen, N., et al., 2016. FOXM1 promotes reprogramming of glucose metabolism in epithelial ovarian cancer cells via activation of GLUT1 and HK2 transcription. Oncotarget 7, 47985–47997.

Wang, Z., Tang, K., Zhang, D., Wan, Y., Wen, Y., Lu, Q., Wang, L., 2017. High-throughput m6A-seq reveals RNA m6A methylation patterns in the chloroplast and mitochondria transcriptomes of Arabidopsis thaliana. PLoS One 12, e0185612.

Warda, A.S., Kretschmer, J., Hackert, P., Lenz, C., Urlaub, H., Höbartner, C., Sloan, K.E., Bohnsack, M.T., 2017. Human METTL16 is a N 6-methyladenosine (m6A) methyltransferase that targets pre-mRNAs and various non-coding RNAs. EMBO Rep 18, 2004–2014.

Wei, C.M., Gershowitz, A., Moss, B., 1975. Methylated nucleotides block 5' terminus of HeLa cell messenger RNA. Cell 4, 379–386.

Wei, G., Almeida, M., Pintacuda, G., Coker, H., Bowness, J.S., Ule, J., Brockdorff, N., 2021. Acute depletion of METTL3 implicates N6-methyladenosine in alternative intron/exon inclusion in the nascent transcriptome. Genome Res 31, 1395–1408.

Wei, J., Liu, F., Lu, Z., Fei, Q., Ai, Y., He, P.C., Shi, H., Cui, X., Su, R., Klungland, A., et al., 2018. Differential m6A, m6Am, and m1A Demethylation Mediated by FTO in the Cell Nucleus and Cytoplasm. Mol Cell 71, 973-985.e5.

Wen, L., Sun, W., Xia, D., Wang, Y., Li, J., Yang, S., 2022. The m6A methyltransferase METTL3 promotes LPS-induced microglia inflammation through TRAF6/NF-κB pathway. Neuroreport 33, 243–251.

Weng, Y.L., Wang, Xu, An, R., Cassin, J., Vissers, C., Liu, Yuanyuan, Liu, Yajing, Xu, T., Wang, Xinyuan, Wong, S.Z.H., et al., 2018. Epitranscriptomic m6A Regulation of Axon Regeneration in the Adult Mammalian Nervous System. Neuron 97, 313-325.e6.

Widagdo, J., Wong, J.J.L., Anggono, V., 2022. The m6A-epitranscriptome in brain plasticity, learning and memory. Semin Cell Dev Biol 125, 110–121.

Widagdo, J., Zhao, Q.Y., Kempen, M.J., Tan, M.C., Ratnu, V.S., Wei, W., Leighton, L., Spadaro, P.A., Edson, J., Anggono, V., et al., 2016. Experience-Dependent Accumulation of N6-Methyladenosine in the Prefrontal Cortex Is Associated with Memory Processes in Mice. J Neurosci 36, 6771–6777.

Wong, J.C.T., Hasan, M.R., Rahman, M., Yu, A.C., Chan, S.K., Schaeffer, D.F., Kennecke, H.F., Lim, H.J., Owen, D., Tai, I.T., 2013. Nucleophosmin 1, upregulated in adenomas and cancers of the colon, inhibits p53-mediated cellular senescence. Int J Cancer 133, 1567–1577.

Wu, J., Petralia, R.S., Kurushima, H., Patel, H., Jung, M.Y., Volk, L., Chowdhury, S., Shepherd, J.D., Dehoff, M., Li, Y., et al., 2011. Arc/Arg3.1 Regulates an Endosomal Pathway Essential for Activity-Dependent β-Amyloid Generation. Cell 147, 615–628.

Wu, R., Li, A., Sun, B., Sun, J.G., Zhang, J., Zhang, T., Chen, Y., Xiao, Y., Gao, Y., Zhang, Q., et al., 2019. A novel m6A reader Prrc2a controls oligodendroglial specification and myelination. Cell Res 29, 23.

Wu, W., Feng, J., Jiang, D., Zhou, X., Jiang, Q., Cai, M., Wang, X., Shan, T., Wang, Y., 2017. AMPK regulates lipid accumulation in skeletal muscle cells through FTO-dependent demethylation of N6-methyladenosine. Sci Rep 7, 41606.

Xiao, Q., Lei, L., Ren, J., Peng, M., Jing, Y., Jiang, X., Huang, J., Tao, Y., Lin, C., Yang, J., et al., 2022. Mutant NPM1-Regulated FTO-Mediated m6A Demethylation Promotes Leukemic Cell Survival via PDGFRB/ERK Signaling Axis. Front Oncol 12, 269.

Xiao, W., Adhikari, S., Dahal, U., Chen, Y.S., Hao, Y.J., Sun, B.F., Sun, H.Y., Li, A., Ping, X.L., Lai, W.Y., et al., 2016. Nuclear m(6)A Reader YTHDC1 Regulates mRNA Splicing. Mol Cell 61, 507–519.

Xie, W., Ma, L.L., Xu, Y.Q., Wang, B.H., Li, S.M., 2019. METTL3 inhibits hepatic insulin sensitivity via N6-methyladenosine modification of Fasn mRNA and promoting fatty acid metabolism. Biochem Biophys Res Commun 518, 120–126.

Xu, C., Huang, H., Zhang, M., Zhang, P., Li, Z., Liu, X., Fang, M., 2022. Methyltransferase-Like 3 Rescues the Amyloid-beta protein-Induced Reduction of Activity-Regulated Cytoskeleton Associated Protein Expression via YTHDF1-Dependent N6-Methyladenosine Modification. Front Aging Neurosci 14, 890134.

Xu, D.H., Liu, F., Li, X., Chen, X.F., Jing, G.J., Wu, F.Y., Shi, S.L., Li, Q.F., 2014. Regulatory role of nucleophosmin during the differentiation of human liver cancer cells. Int J Oncol 45, 264–272.

Xu, H., Dzhashiashvili, Y., Shah, A., Kunjamma, R.B., Weng, Y. lan, Elbaz, B., Fei, Q., Jones, J.S., Li, Y.I., Zhuang, X., et al., 2020. m6A mRNA methylation is essential for oligodendrocyte maturation and CNS myelination. Neuron 105, 293.

Xu, K., Mo, Y., Li, D., Yu, Q., Wang, L., Lin, F., Kong, C., Balelang, M.F., Zhang, A., Chen, S., et al., 2020. N6-methyladenosine demethylases Alkbh5/Fto regulate cerebral ischemia-reperfusion injury. Ther Adv Chronic Dis 11, 2040622320916024.

Xu, Y., Zhou, Z., Kang, X., Pan, L., Liu, C., Liang, X., Chu, J., Dong, S., Li, Y., Liu, Q., et al., 2022. Mettl3-mediated mRNA m6A modification controls postnatal liver development by modulating the transcription factor Hnf4a. Nat Commun 13, 1–17.

Xun, Z., Lee, D.Y., Lim, J., Canaria, C.A., Barnebey, A., Yanonne, S.M., McMurray, C.T., 2012. Retinoic acid-induced differentiation increases the rate of oxygen consumption and enhances the spare respiratory capacity of mitochondria in SH-SY5Y cells. Mech Ageing Dev 133, 176–185.

Yabe, J.T., Chan, W.K.H., Wang, F.S., Pimenta, A., Ortiz, D.D., Shea, T.B., 2003. Regulation of the transition from vimentin to neurofilaments during neuronal differentiation. Cell Motil Cytoskeleton 56, 193–205.

Yadav, P.K., Rajasekharan, R., 2018. The m6A methyltransferase Ime4 and mitochondrial functions in yeast. Curr Genet 64, 353–357.

Yan, Y., Sabharwal, P., Rao, M., Sockanathan, S., 2009. The antioxidant enzyme Prdx1 controls neuronal differentiation by thiol-redox-dependent activation of GDE2. Cell 138, 1209–1221.

Yang, H., An, J.J., Sun, C., Xu, B., 2016. Regulation of Energy Balance via BDNF Expressed in Nonparaventricular Hypothalamic Neurons. Molecular Endocrinology 30, 494.

Yang, Y., Hsu, P.J., Chen, Y.S., Yang, Y.G., 2018. Dynamic transcriptomic m6A decoration: writers, erasers, readers and functions in RNA metabolism. Cell Res 28, 616–624.

Yang, Y., Huang, G., Jiang, X., Li, X., Sun, K., Shi, Y., Yang, Z., Zhu, X., 2022. Loss of Wtap results in cerebellar ataxia and degeneration of Purkinje cells. Journal of Genetics and Genomics 49, 847–858.

Yang, Y., Shen, F., Huang, W., Qin, S., Huang, J.T., Sergi, C., Yuan, B.F., Liu, S.M., 2019. Glucose Is Involved in the Dynamic Regulation of m6A in Patients With Type 2 Diabetes. J Clin Endocrinol Metab 104, 665–673.

Yates, S.C., Zafar, A., Hubbard, P., Nagy, S., Durant, S., Bicknell, R., Wilcock, G., Christie, S., Esiri, M.M., Smith, A.D., et al., 2014. Dysfunction of the mTOR pathway is a risk factor for Alzheimer's disease. Acta Neuropathol Commun 2, 1–15.

Yi, D., Wang, Q., Zhao, Y., Song, Y., You, H., Wang, J., Liu, R., Shi, Z., Chen, X., Luo, Q., 2021. Alteration of N6 -Methyladenosine mRNA Methylation in a Rat Model of Cerebral Ischemia–Reperfusion Injury. Front Neurosci 15, 164.

Yoon, K.J., Ringeling, F.R., Vissers, C., Jacob, F., Pokrass, M., Jimenez-Cyrus, D., Su, Y., Kim, N.S., Zhu, Y., Zheng, L., et al., 2017. Temporal Control of Mammalian Cortical Neurogenesis by m6A Methylation. Cell 171, 877-889.e17.

Yoshikawa, H., Komatsu, W., Hayano, T., Miura, Y., Homma, K., Izumikawa, K., Ishikawa, H., Miyazawa, N., Tachikawa, H., Yamauchi, Y., et al., 2011. Splicing factor 2-associated protein p32 participates in ribosome biogenesis by regulating the binding of Nop52 and fibrillarin to preribosome particles. Mol Cell Proteomics 10, M110.006148.

Yu, J., Chen, M., Huang, H., Zhu, Junda, Song, H., Zhu, Jian, Park, J., Ji, S.J., 2018. Dynamic m6A modification regulates local translation of mRNA in axons. Nucleic Acids Res 46, 1412–1423.

Yu, J., She, Y., Ji, S.J., 2021. m6A Modification in Mammalian Nervous System Development, Functions, Disorders, and Injuries. Front Cell Dev Biol 9, 1343.

Yu, R., Li, Q., Feng, Z., Cai, L., Xu, Q., 2019. m6A Reader YTHDF2 Regulates LPS-Induced Inflammatory Response. Int J Mol Sci 20, 1323.

Yu, Y.T., Meier, U.T., 2014. RNA-guided isomerization of uridine to pseudouridine--pseudouridylation. RNA Biol 11, 1483–1494.

Yun, H.M., Jin, P., Han, J.Y., Lee, M.S., Han, S.B., Oh, K.W., Hong, S.H., Jung, E.Y., Hong, J.T., 2013. Acceleration of the development of Alzheimer's disease in amyloid beta-infused peroxiredoxin 6 overexpression transgenic mice. Mol Neurobiol 48, 941–951.

Zhang, F., Kang, Y., Wang, M., Li, Y., Xu, T., Yang, W., Song, H., Wu, H., Shu, Q., Jin, P., 2018. Fragile X mental retardation protein modulates the stability of its m6A-marked messenger RNA targets. Hum Mol Genet 27, 3936–3950.

Zhang, H., Chen, L., Chen, J., Jiang, H., Shen, X., 2011. Structural basis for retinoic X receptor repression on the tetramer. J Biol Chem 286, 24593–24598.

Zhang, L., Qi, Y., Aluo, Z., Liu, S., Zhang, Z., Zhou, L., 2019. Betaine increases mitochondrial content and improves hepatic lipid metabolism. Food Funct 10, 216–223.

Zhang, S., Zhao, B.S., Zhou, A., Lin, K., Zheng, S., Lu, Z., Chen, Y., Sulman, E.P., Xie, K., Bögler, O., et al., 2017. The m6A Demethylase ALKBH5 Maintains Tumorigenicity of Glioblastoma Stem-Like Cells by Sustaining FOXM1 Expression and Cell Proliferation Program. Cancer Cell 31, 591.

Zhang, Y., Guo, F., Ni, Y., Zhao, R., 2013. LPS-induced inflammation in the chicken is associated with CCAAT/enhancer binding protein beta-mediated fat mass and obesity associated gene down-regulation in the liver but not hypothalamus. BMC Vet Res 9, 257.

Zhang, Y., Guo, F., Zhao, R., 2016. Hepatic expression of FTO and fatty acid metabolic genes changes in response to lipopolysaccharide with alterations in m6A modification of relevant mRNAs in the chicken. Br Poult Sci 57, 628–635.

Zhang, Z., Wang, M., Xie, D., Huang, Z., Zhang, L., Yang, Y., Ma, D., Li, W., Zhou, Q., Yang, Y.G., et al., 2018. METTL3-mediated N6-methyladenosine mRNA modification enhances long-term memory consolidation. Cell Res 28, 1050–1061.

Zhang, Z., Chen, L.Q., Zhao, Y.L., Yang, C.G., Roundtree, I.A., Zhang, Zijie, Ren, J., Xie, W., He, C., Luo, G.Z., 2019. Single-base mapping of m6A by an antibody-independent method. Sci Adv 5, eaax0250.

Zhao, F., Xu, Y., Gao, S., Qin, L., Austria, Q., Siedlak, S.L., Pajdzik, K., Dai, Q., He, C., Wang, W., et al., 2021. METTL3-dependent RNA m6A dysregulation contributes to neurodegeneration in Alzheimer's disease through aberrant cell cycle events. Mol Neurodegener 16, 70.

Zhao, T., Li, X., Sun, D., Zhang, Z., 2019. Oxidative stress: One potential factor for arsenite-induced increase of N6-methyladenosine in human keratinocytes. Environ Toxicol Pharmacol 69, 95–103.

Zhao, X., Yang, Y., Sun, B.F., Shi, Y., Yang, X., Xiao, W., Hao, Y.J., Ping, X.L., Chen, Y.S., Wang, W.J., et al., 2014a. FTO-dependent demethylation of N6-methyladenosine regulates mRNA splicing and is required for adipogenesis. Cell Res 24, 1403–1419.

Zhao, X., Yang, Y., Sun, B.F., Zhao, Y.L., Yang, Y.G., 2014b. FTO and obesity: Mechanisms of association. Curr Diab Rep 14, 1–9.

Zheng, G., Cox, T., Tribbey, L., Wang, G.Z., Iacoban, P., Booher, M.E., Gabriel, G.J., Zhou, L., Bae, N., Rowles, J., et al., 2014. Synthesis of a FTO inhibitor with anticonvulsant activity. ACS Chem Neurosci 5, 658–665.

Zheng, G., Dahl, J.A., Niu, Y., Fedorcsak, P., Huang, C.M., Li, C.J., Vågbø, C.B., Shi, Y., Wang, W.L., Song, S.H., et al., 2013. ALKBH5 Is a Mammalian RNA Demethylase that Impacts RNA Metabolism and Mouse Fertility. Mol Cell 49, 18.

Zheng, J., 2012. Energy metabolism of cancer: Glycolysis versus oxidative phosphorylation (Review). Oncol Lett 4, 1151–1157.

Zheng, L., Tang, X., Lu, M., Sun, S., Xie, S., Cai, J., Zan, J., 2020. microRNA-421-3p prevents inflammatory response in cerebral ischemia/reperfusion injury through targeting m6A Reader YTHDF1 to inhibit p65 mRNA translation. Int Immunopharmacol 88, 106937.

Zhou, J., Wan, J., Shu, X.E., Mao, Y., Liu, X.M., Yuan, X., Zhang, X., Hess, M.E., Brüning, J.C., Qian, S.B., 2018. N6-Methyladenosine Guides mRNA Alternative Translation during Integrated Stress Response. Mol Cell 69, 636.

Zhou, K.I., Pan, T., 2016. Structures of the m6A methyltransferase complex: two subunits with distinct but coordinated roles. Mol Cell 63, 183.

Zhou, X., Chen, Jingqing, Chen, Jin, Wu, W., Wang, X., Wang, Y., 2015. The beneficial effects of betaine on dysfunctional adipose tissue and N6-methyladenosine mRNA methylation requires the AMP-activated protein kinase α1 subunit. J Nutr Biochem 26, 1678–1684.

Zhu, Y., Shen, J., Gao, L., Feng, Y., 2016. Estrogen promotes fat mass and obesity-associated protein nuclear localization and enhances endometrial cancer cell proliferation via the mTOR signaling pathway. Oncol Rep 35, 2391–2397.

Zhuang, Changshui, Zhuang, Chengle, Luo, X., Huang, X., Yao, L., Li, J., Li, Y., Xiong, T., Ye, J., Zhang, F., et al., 2019. N6-methyladenosine demethylase FTO suppresses clear cell renal cell carcinoma through a novel FTO-PGC-1α signalling axis. J Cell Mol Med 23, 2163–2173.